Modeling and Simulation of the Dual Stage Pressure Retarded Osmosis Systems

by

Roghayeh Soltani
B.Sc., Iran University of Science and Technology, 2005
M.Sc., Sharif University of Technology, 2010

A Dissertation Submitted in Partial Fulfillment of the
Requirements for the Degree of

DOCTOR OF PHILOSOPHY

in the Department of Mechanical Engineering

Modeling and Simulation of the Dual Stage Pressure Retarded Osmosis Systems

by

Roghayeh Soltani
B.Sc., Iran University of Science and Technology, 2005
M.Sc., Sharif University of Technology, 2010

Supervisory Committee

Dr. H. Struchtrup, Supervisor
(Department of Mechanical Engineering)

Dr. P. Wild, Departmental Member
(Department of Mechanical Engineering)

Dr. T. Fyles, Outside Member
(Department of Chemistry)

Supervisory Committee

Dr. H. Struchtrup, Supervisor
(Department of Mechanical Engineering)

Dr. P. Wild, Departmental Member
(Department of Mechanical Engineering)

Dr. T. Fyles, Outside Member
(Department of Chemistry)

ABSTRACT

Utilization of renewable energy sources, as an approach to reduce greenhouse gas (GHG) emissions, have been globally popular in the last few decades. Among renewable energy sources, pressure retarded osmosis (PRO) has been scrutinized by scientists since the mid 70's. However, even today, the existing river-sea PRO systems can only marginally meet the generally approved criterion of 5 W/m^2 power density, a threshold for an economically feasible PRO system. As an approach to increase the performance of PRO systems, multi-staging of PRO modules are investigated.

A mathematical model of the scaled up PRO process is proposed with consideration for internal and external concentration polarization, reverse salt flux, and spatial variations along the membrane. A thermodynamic model is also developed with consideration for entropy generation and losses in the process. It predicts the percentile of each work loss source compared to the net work in the system. Several configurations of dual stage PRO system are presented and compared to single stage PRO. The comparison is based on three proposed target functions of power density (PD), specific energy (SE), and work per drawn freshwater (W_{drawn}). Applied hydraulic pressures and flow rates of draw and feed solutions are optimized for maximizing the target functions. The results indicate that overall performance of the system could be improved by up to 8 % with a dual stage PRO in the case of SE. The system

performance is not improved by depressurizing the draw solution before the second module in cases of SE and W_{drawn}. The thermodynamic analysis demonstrate the contribution of each work loss and justify the reason of diminishing the net work over the losses. The effect of membrane area and membrane characteristics on the SE target function is also investigated. The distribution of membrane area in each module depends on the selected configuration and inlet draw solution. In the dual stage systems, the SE value increases up to 14% by improving the membrane characteristics. Reducing the salt rejection coefficient (B) is the most effective membrane characteristic in our configurations. Replacing seawater with RO brine in draw solution results in a significant improvement in SE values.

Contents

Supervisory Committee ii

Abstract iii

Table of Contents v

List of Tables viii

List of Figures ix

Acknowledgements xiii

1 Introduction 1

1.1 Background . . . 1
1.2 Research needs and motivation . . . 2
1.3 Objective and scope . . . 3
1.4 Contribution . . . 4

2 Literature Review 6

2.1 Salinity gradient energy (SGE) . . . 6
2.2 Osmotic processes . . . 9
2.2.1 PRO process . . . 10
2.3 Basic concepts of PRO . . . 11
2.3.1 Water and salt fluxes across the membrane . . . 11
2.3.2 Concentration polarization . . . 12
2.4 PRO models . . . 14
2.4.1 Loeb model . . . 15
2.4.2 Lee model . . . 15
2.4.3 Achilli model . . . 16
2.4.4 Yip model . . . 16

2.4.5 Bui model 16
2.5 Thermodynamic limits of the PRO process 17
2.6 PRO membranes 18
2.6.1 Flat sheet membranes 19
2.6.2 Hollow fiber membranes 22
2.7 Membrane fouling and scaling 23
2.8 PRO configurations 24
2.8.1 RO-PRO hybrid systems 25
2.8.2 MD-PRO hybrid systems 27
2.8.3 FO-PRO hybrid systems 28
2.8.4 Dual stage PRO systems 29

3 Methodology **37**
3.1 General 37
3.2 Mass balances of water and solutes in membrane 41
3.2.1 Mass transfer in the feed side 42
3.2.2 Mass transfer in the draw side 44
3.3 Momentum balance 45
3.4 Mass transfer and frictional pressure drop 47
3.5 PRO modeling 49
3.6 Quantifying the system performance 50
3.7 Target functions for optimization 52
3.8 Thermodynamic analysis of PRO system 53
3.9 Optimization of PRO modules 56
3.9.1 Arrangement of membrane module 56
3.9.2 Membrane characteristics 57
3.9.3 Draw and feed solution sources 57

4 Results and Discussions **59**
4.1 Variations along the membrane length in PRO 59
4.2 Single stage versus dual stage PRO System 63
4.2.1 Power Density (PD) 63
4.2.2 Specific Energy (SE) 64
4.2.3 Work per Fresh Water Drawn (W_{drawn}) 65
4.3 Thermodynamic Analysis of the PRO Systems 67

4.4 Internal Performance of Modules for Single and Dual Stage Systems . 69
4.5 Effect of membrane area on PRO performance 72
4.6 Effect of the membrane characteristics on PRO performance 75
4.7 Effect of the draw solution source on PRO performance 80

5 Conclusions and recommendations **83**
5.1 Mathematical model of PRO system 83
5.2 Dual stage PRO system configurations 84
5.3 Optimizing PRO modules 85
5.3.1 Effect of membrane area 85
5.3.2 Effect of membrane characteristics 86
5.3.3 Effect of draw solution 86
5.4 Implication and future directions 86

Bibliography **88**

List of Tables

Table 2.1 Experimental results using flat sheet membranes under different operating conditions. 21
Table 2.2 Experimental results using flat sheet membranes under different operating conditions. 23

Table 3.1 Parameters used in PRO model 49
Table 3.2 Proposed membrane characteristics 57

Table 4.1 Optimization results for single and dual stage modules for maximum power density (PD) 64
Table 4.2 Optimization results for single and dual- stage modules for maximum specific energy (SE) 65
Table 4.3 Optimization results for single and dual stage modules for maximum work per drawn water (W_{drawn}) 66
Table 4.4 Thermodynamic analysis for single and dual stage modules for net work and losses percentages for PD 68
Table 4.5 Thermodynamic analysis for single and dual stage modules for net work and losses percentages for SE 68
Table 4.6 Thermodynamic analysis for single and dual stage modules for net work and losses percentages for W_{drawn} 69
Table 4.7 Optimization results for single and dual stage modules for maximum specific energy (SE) with optimum membrane length . . . 74
Table 4.8 Proposed membrane characteristics 76
Table 4.9 Optimization results for single and dual stage modules for maximum specific energy (SE) with improved membrane characteristics 77
Table 4.10 Optimization results for single and dual stage modules for maximum specific energy (SE) with RO brine as a draw solution source 81

List of Figures

Figure 2.1 A schematic classification of SGE technologies based on the type of process 7
Figure 2.2 Representation of solvent flow in FO, PRO, RO, and Equilibrium processes [44]. 9
Figure 2.3 A schematic of Statcraft PRO power plant [47]. 11
Figure 2.4 A schematic of salt concentration profile in a membrane module [51]. 12
Figure 2.5 An illustration of water flux (J_w) (a) and power density (b) against hydraulic pressure in the PRO process to investigate the effects of ECP, ICP and reverse salt flux [56] 14
Figure 2.6 Maximum extractable work, unutilized energy and frictional losses [64] 18
Figure 2.7 Flat sheet membranes used as laboratory scale module (a), and rolled as spiral wound module (b) [83, 84]. 20
Figure 2.8 SEM images of cross section of PAN membrane support (a) before and (b) after being pressurized at 15 bar for 120 min [56] . 21
Figure 2.9 A schematic of geometry and structure of an inner-selective TFC-PRO hollow fiber membrane [93] 22
Figure 2.10SEM images of cross section and surface morphology of hollow fiber membrane [95] 23

Figure 2.11A schematic of an RO-PRO system. V_f is the volume flow of the RO feed solution, and V_c is the concentrated brine waste stream exiting from RO subsystem. $V_{p,RO}$ and $V_{p,PRO}$ are freshwater permeate in RO and PRO subsystems, respectively. In PRO subsystem $V_{ds,en}$ is the draw solution stream and $V_{f,en}$ is the feed solution stream. $V_{f,ex}$ and $V_{ds,ex}$ are exiting concentrated feed and diluted draw solutions from PRO subsystem, respectively. ERD and PX denote energy recovery device and pressure exchanger, respectively. [120]. 26
Figure 2.12A schematic of stand-alone salinity power driven RO desalination system. HP: Hydro pump, BP: Booster pump, HT: Hydro turbine, ERD: Energy recovery device, SW: Seawater, PW: Pure water, CW: Concentrated water, BW: Brackish water [121]. . . 27
Figure 2.13A schematic of the hybrid MD-PRO system for harvesting low-grade heat energy [123]. The system includes of a thermal separation and power generation components. Thermal separation consists a membrane distillation (MD) module and a heat exchanger (HX). Power generation component consists a pressure retarded osmosis (PRO) module, a pressure exchange (PX), and a turbine (TB). The numbers represent the streams. The H (in red) stands for an ideal constant temperature heat source, whereas the C1 and C2 (in blue) represent ideal constant-temperature heat sinks. The P and F in the MD module stand for the permeate (distillate) and feed channels, respectively. The F and D in the PRO module stand for the feed and draw solutions, respectively . . . 28
Figure 2.14A schematic of the hybrid MVMD-R-PRO system [125]. 29
Figure 2.15A schematic of the hybrid FO-PRO system [125]. 30
Figure 2.16schematic diagram of the four possible configurations of dual stage PRO system proposed by [25]. 31
Figure 2.17The illustration of thermodynamic analysis of dual stage PRO system that are a) operated at their optimal C-PRO b) operated at the condition to obtain the total optimum C-PRO [129]. . . 32

Figure 2.18Schematic diagram of two proposed design for dual stage PRO system [130]. P_w: Power, Q_{ds-in}: Draw solution flow rate, Q_R: Recycle flow to PX, V_1: Permeate flow rate in first stage, V_2: Permeate flow rate in second stage, Q_{f-in}: Feed flow rate. . . . 33
Figure 2.19Schematic diagram of a closed-loop a) single stage b) dual stage PRO system [133]. 34
Figure 2.20Schematic diagram of dual stage RO subsystem with a) single stage PRO subsystem b) dual stage PRO subsystem [135]. Darker colors correspond to more concentrated solutions and arrow thickness represents the approximate flow rate. Q_{sw} and Q_{DR} are the seawater flow and the diluted draw solution flows, respectively. Q_D and Q_F are the PRO entering draw and feed solution flows, respectively. Q_{FR} is the PRO feed solution bleed flow. Q_R^1 and Q_R^2 are the rejected flow of the RO first and second stages, respectively. Q_P^1 and Q_P^2 are the permeate flow of the RO first and second stages, respectively. Q_{ad} is the added seawater and Q_t is the flow that goes to turbine. 35
Figure 2.21Schematic diagram of dual stage hybrid RO-PRO with dual stage RO and dual stage PRO subsystems connected in series [136]. . 36

Figure 3.1 Schematic of single and dual stages PRO systems with the same membrane area: (a) Single stage with P-T; (b) dual stage with P-T; (c) single stage with PX; (d) dual stage with 1PX; (e) dual stage PRO with $Q_{D,in}$ back to PX before the HT1; (f) dual stage with 2PX; (g) dual stage system with 1HT 39
Figure 3.2 Volumetric slice of the draw channel with thickness of Δx, height of the channel (H) and width of the channel (Z) 42
Figure 3.3 A schematic of salt concentration profile in a membrane module. 43
Figure 3.4 The geometric parameters of a non-woven spacer 48

Figure 4.1 (a) and (b) Salt concentration of draw and feed solutions (c_D, c_F); (c) and (d) Osmotic pressure of draw and feed solutions (π_D, π_F); (e) and (f) Hydraulic pressure of draw and feed solutions (P_D, P_F) in the case of optimal power production in single stage PRO systems with PX (configuration (c)) for the counter-current flow. 60

Figure 4.2 (a) and (b) Permeated water (J_{wr}) and reverse salt flux (J_s); (c) and (d) Volumetric flow rate of draw and feed solutions (Q_D, Q_F) in the case of optimal power production in single stage PRO systems with PX (configuration (c)) for the counter-current flow. 62

Figure 4.3 Osmotic pressure of draw and feed solutions (a) and (b)(π_D,π_F); (c) and (d) volumetric flow rate of draw and feed solutions (Q_D,Q_F); (e) permeated water flux (J_{wr}) and (f) reverse salt flux (J_s), for single stage PRO configuration (C) (green solid line), dual stage configuration (e) (blue solid line for module 1, and red solid line for module 2) and dual stage 1HT configuration (g) (blue dashed line for module 1, and black dashed line for module 2) optimized for specific energy (SE). 71

Figure 4.4 Fresh water permeation flux through the membrane in single stage PRO with various membrane area of 5 (green line), 15 (blue line), 30 (red line), and 40 (yellow line) m^2 73

Figure 4.5 The effect of membrane length on specific energy of single and dual stage PRO configurations 75

Figure 4.6 The variation of water permeation flux (J_{wr}) along the membrane module for dual stage PRO configuration (e) with optimized membrane distribution of L_1=9 and L_2=6 m (solid line) and equally distributed membrane of L_1=L_2=7.5 m (dashed line). 76

Figure 4.7 Contour plot of SE values changing with water and salt permeation coefficient (A and B) in membranes in dual stage configuration (e) 78

ACKNOWLEDGEMENTS

My deepest gratitude goes to:

My supervisor, Prof. Henning Struchtrup, for his invaluable direction and continuous guidance in this arduous journey. He taught me how to get to the roots of seemingly unsolvable questions. He showed me not to fear failure since, failure is a way toward a deeper understanding of the problem.

My beloved parents Bahman and Soraya. Maman, baba, your unconditional love has been my light through the darkest moments and your belief in me has been my courage to pursue my dreams. I'd like to thank my brother Saeed for his lifetime support and encouragement.

My colleagues and friends Dr. Behnam Rahimi, Dr. Alireza Mohammadzadeh, Dr. Arash Kanani, and Alexander Beckmann for their suggestions and help. It has been enriching to walk alongside each of you.

My friends Parnyian Tayebi, Dr. Sahar Sam, Jimmy Li, Dr. Sara Salem, Pedram Darban, Amin Ebrahimi nejad, Panan Xu and all the others I forgot to mention. I thank each and every of you for lending me your shoulders to lean on and for giving me the warmth of your friendship.

The Natural Sciences and Engineering Research Council (NSERC) of Canada for their financial support.

You are not a drop in the ocean. You are the entire ocean in a drop.
Rumi

Chapter 1

Introduction

1.1 Background

To meet increasing global energy demands and mitigate climate change, alternative energy sources and new technologies are needed to harvest energy from sustainable and environmental friendly energy sources [1]. Alternative renewable energy sources to traditional fossil fuels are solar, wind, biomass and hydro power. However, due to high installation cost, discontinuous energy generation, and uneven distribution, the energy sources and energy storage remain as major challenges for today society [2].

Salinity gradient energy (SGE) can generate energy from mixing two solutions with different salinities [3, 4]. It can harvest energy from different solutions and can also be helpful to regain some part of the energy consumed for reusing and desalinating water.

Pressure Retarded Osmosis (PRO) is the most developed SGE as a renewable source of power [5]. This form of power is released when two solutions with different salt concentrations are mixed in a membrane module at appropriate pressures. That is, wherever rivers meet oceans there is a potential for power generation all over the world. The worldwide capacity for PRO to generate power has been estimated to be 2TW, which is almost 13 % of the global power consumption [6]. In PRO, a hydraulic pressure is applied to the concentrated solution (draw solution) at one side of a semi-permeable membrane and the other side is the diluted solution with low concentration (feed solution). The chemical potential difference of the solutions drives freshwater to permeate through the membrane from feed solution into the pressurized draw solution. The process continues as long as the difference in the hydraulic pressure is less than

the difference in the osmotic pressures between the solutions. The expanding volume of the pressurized draw solution is then depressurized by a turbine to generate power.

The concept of PRO was fist introduced by Norman [7] in 1974 and developed by Loeb [8, 9, 10, 11]. The concept attracted increasing interest for 20 years from 1970's and over the past decades from 2000's due to oil crisis and the advances in membrane and energy recovery devices [12]. In 2009 a pilot scale PRO power plant was built by the Norwegian company Statkraft. However, they shut it down due to lack of efficiency in the system [13].

In 2016, Straub et al. [14] and O'Toole et al. [15] criticized the viability of power generation from river-sea PRO power plants in terms of net work per inlet flow rates of draw and feed solutions (specific energy, SE), and the net work per drawn fresh water, respectively. They stated that the net positive extractible energy is hard to achieve or even impossible with today's available technology. Therefore the upfront challenge is to improve the efficiency of the PRO system. It is estimated that for a PRO power plant to be commercially viable, the power density of the process needs to exceed 5 W/m^2 of membrane [16]. To increase the power output, some studies have been conducted considering:

- Utilization of high salinity sources such as the Dead Sea [17] and Great Salt Lake [18] instead of seawater as draw solution.

- Development of the membranes that allow high power densities. Recently, membranes are specifically developed for PRO and the improvements are promising, especially in laboratory scale [19, 20]. However, the commercially fabrication and performance of these membranes in full scale PRO power plant is unclear due to the additional limitations and losses in the large scale PRO.

- Utilization of PRO as a part of hybrid systems, such as osmotic heat engine [21], forward osmosis (FO) [22], for energy recovery from reverse osmosis (RO) [23], and for energy storage via a closed loop RO-PRO cycle [24].

1.2 Research needs and motivation

To improve the system performance, new configurations of PRO toward even utilization of membrane can be proposed. Improvement of PRO processes must rely on good understanding of the interplay of all processes within. Optimization of design

and operating parameters is necessary in order to achieve the best efficiency of the system.

Dual stage PRO systems are among the recent proposed PRO configurations that can reduce the irreversibile losses of the system [25, 26]. In general, dual stage systems may utilize the advantages of:

1. Reducing the impact of reverse salt flux and concentration polarization which is accumulation of salt within the support or boundary layers of the membrane by introducing low concentrated freshwater to the second module. It increases the osmotic pressure difference and causes additional water permeation through the membrane.

2. Flexibility in selection of membrane type for each module based on the design and the selected draw and feed solutions.

3. Flexibility to have different module configurations.

The single stage system uses the membrane unevenly, with most fresh water drawn early close to the inflow, and only little drawn further downstream. As freshwater permeates through the membrane the osmotic pressure difference between draw and feed solutions ($\Delta\pi$) drops due to dilution of the draw solution while the applied hydraulic pressure difference (ΔP) remains roughly constant. The difference of osmotic and hydraulic pressures ($\Delta\pi - \Delta P$) is the driving force for fresh water permeation which drops along the membrane. Therefore, if the applied pressure difference drops accordingly with osmotic pressure drop, ($\Delta\pi - \Delta P$) remains more consistent and results in more even water permeation along the membrane. Reducing applied pressure can be achieved by multi staging the PRO system and depressurising the draw solution after each module. From thermodynamic perspective, reducing hydraulic pressure after each module reduces entropy generation and increases the power output. This idea encouraged us to propose new configurations and models for dual stage PRO system including depressurizing the draw solution after the first module by means of a hydro turbine.

1.3 Objective and scope

In an attempt to increase the efficiency of PRO systems, the main objectives of this investigation are:

1. To develop a model of the water and salt flux for a PRO flat sheet membrane that includes all the limitation factors of the PRO process, such as the concentration polarization, the salt leakage and pressure drop along the membrane module. The model will be applied to a large-scale PRO membrane.

2. To propose new dual stage PRO configurations and to compare them with standard single and dual stage PRO configurations in an effort to reduce the entropy generation and to increase the power output.

3. To study the effect of the operating conditions such as flow rate and hydraulic pressures of inlet solutions on the performance of the PRO in realistic conditions. The operational conditions are optimized to find the maximum proposed target functions of (a) work per membrane area (PD), (b) work per inlet draw and feed solutions (SE), and (c) work per amount of fresh water drawn through the membrane (W_{drawn}).

4. To conduct a thermodynamic analysis in PRO that investigates the source of losses in the systems and the contribution of each loss compared to the net work.

5. To study the parameters affecting the system efficiency such as membrane area, and draw solution concentration and to suggest solutions for better PRO membranes.

1.4 Contribution

This dissertation contributes to the area of harnessing energy from pressure retarded osmosis systems trying to improve the efficiency of the system performance.

The performance of proposed configurations showed up to 8% improvement from single stage to dual stage PRO system in SE. It means that depressurizing the draw solution after the first module is beneficial for SE target function. However, depressurizing the dual stage PRO did not benefit the system performance in terms of PD and W_{drawn} and the system tended to eliminate pressure difference between the modules. Thermodynamic analysis confirmed that in cases of PD and W_{drawn}, even though the net power output improves, the associated irreversible losses are increasing accordingly.

Further studies toward decreasing the losses in the system show that the membrane area and distribution of membranes for each module can be optimized in case of SE. Investigating the effect of membrane characteristics shows improvements up to 14% in the dual stage PRO from single stage configuration which means the proposed configurations are promising for future improved membranes. With RO brine-Freshwater pair, the dual stage system improved up to 7% compared to single stage PRO.

This document contains 5 chapters as follows:

- The first chapter (the current one) contains a brief introduction presenting a brief discussion of the PRO process, the motivation, and the objectives of the study.
- The second chapter presents a review about PRO processes, models, membranes, and configurations.
- The third chapter deals with the development of a model for PRO system performance. The model is also used to study the effect of the operating conditions on the water flux and, subsequently, on the power output. The new configurations of dual stage PRO systems are also proposed in this chapter.
- The fourth chapter contains the discussions about the effect of selected configurations on system performance, and thermodynamic analysis. The model is also used to study the effect of the membrane area, membrane characteristics, and draw solution concentration and their impact on power output.
- the fifth chapter contains the main outcomes of the study and the implications for future directions.

Chapter 2

Literature Review

2.1 Salinity gradient energy (SGE)

The global trend to reduce usage of fossil fuels highlights the need for clean and renewable energy as the consumption of energy will grow up to 50% between 2010 to 2035 [27, 28]. The best known renewable energy sources are solar, wind, biomass, and hydro energy. Another-less known-renewable energy source is salinity gradient energy (SGE) that can generate power from mixing of two solutions with different salinities such as river and seawater [3, 4]. SGE has the theoretical potential of between 1.4 and 2.7 TW energy generation [29, 30]. However, in practice due to process efficiencies and practical limits, only part of this potential can be recovered and the technical estimated power generation ranges from 0.2 to 1 TW [29, 30].

Salinity gradient energy is CO_2 emission free and unlike other renewable sources of energy (e.g. solar, wind, tidal, etc.) is suitable for continues power production. The energy is generated from the controlled mixing of two solutions with different salinity levels. The salinity difference causes the difference in chemical potentials which results in various osmotic pressures. Therefore, this osmotic pressure is proportional to the salt concentration of each solution.

Several parameters may affect the SGE power generation like salinity source, temperature,and average flow rates [31]. Figure 2.1 shows a simple SGE classification scheme based on the type of process with related technologies. As illustrated in Figure 2.1, the main SGE processes are osmotic process, ionic exchange, direct mixing, captive mixing, adsorption/desorption, and vapor pressure difference. In this study, we will concentrate on osmotic processes.

Osmotic processes are based on the solvent transport through a semipermeable membrane which separates two solutions with salinity gradient. Pressure Retarded Osmosis (PRO) is the power generation technology, using the osmotic pressure difference between two solutions with different salt concentration. The freshwater will transfer through the membrane due to the chemical potential difference between the fresh and salty water streams. If a hydraulic pressure lower than the osmotic pressure is applied to the saltwater side, the water transport will be partly retarded. The pressurized volume of transported water can run a hydraulic turbine to generate energy [9, 8]. This approach will be discussed in detail in section 2.2. Other SGE methods are described as below:

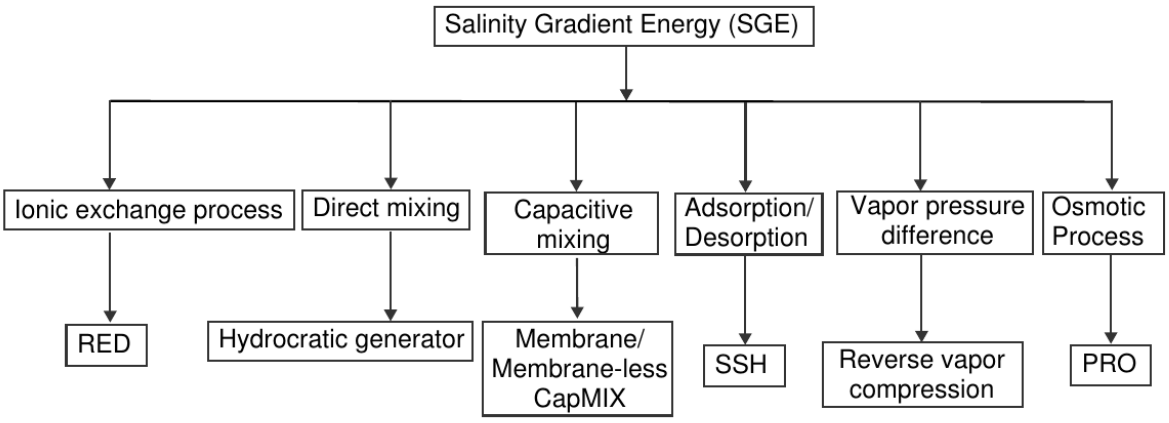

Figure 2.1: A schematic classification of SGE technologies based on the type of process

In **ionic exchange** processes the transport of ions (i.e. cations and anions) is the mechanism responsible for the concentration change of the two solutions with different salinity. The main available technology for this process is Reverse ElectroDialysis (RED). RED uses ion exchange membranes for the controlled mixing of the ions between the fresh and salty water solutions [32, 33].

In **direct mixing** both the ions and solvent are able to transport from one solution to another and can be mixed directly without the use of any membrane. The related technology is Hydrocratic Generator (HG) which is a vertical tube with a series of openings submerged in seawater. HG can exploit the natural direct mixing of freshwater in a large volume of saltwater along with utilizing hydraulic head and buoyancy for power production [34, 35].

In **captive mixing (CapMIX)**, two electrodes dipped in the feed solution are

charged when the solution has high salinity and discharged when the solution has low salinity. When loaded by a current, the anions and cations in solution are captured by electrodes forming an interface electric double layer (EDL). When discharged, ions transfer in opposite direction due to a loss of mixing free energy (ΔG) that happens from transferring from the high concentration to the low concentration solution [36, 37]. Therefore, the sequences of a cycle in the CapMIX cell are:

(A) The cell is charged by an external device. The ions charge the electrodes and cause a current.

(B) The circuit is opened. The solution in the cell is substituted with the low-salinity feed solution.

(C) The cell is discharged through a load. the electrical current flows in the opposite direction with respect to step A.

(D) The circuit is opened. The liquid in the cell is substituted with the high-salinity feed solution.

The most common technologies are Membrane-less externally charged CapMIX, Membrane-less chemically charged CapMIX, and Membrane-based CapMIX [38].

In **adsorption/desorption** an adsorbent material removes the solvent from one solution and subsequently discharges it into the other one by desorption. Swelling and Shrinking of Hydrogels (SSH) is a recent technology [39] based on extracting work from expansion and contraction of polymeric hydrogels by alternating exposure to solutions with high and low salt concentrations. The hydrogels swell while exposed to fresh water. If an external load less than swelling pressure applies to the hydrogel chamber, hydrogels can do work against a load due to their expanding volume. Subsequently, the hydrogels in contact with seawater can dehydrate and shrink by releasing the water captured in the previous step. With this swelling/shrinking cyclic process, a continues energy can be extracted.

Vapour pressure difference is based on the difference in vapor pressure between the low and the high salinity solutions. Reverse Vapor Compression (RVC) is the related technology that does not need a membrane. If the fresh and salty water evaporate in separate chambers under vacuum conditions, the freshwater will have higher vapor pressure than the salty one. In a natural manner, the high pressure vapor flows toward the low pressure vapor. The generated vapor flow then can run the turbine and produce power [40, 41].

2.2 Osmotic processes

The osmotic pressure (π) is the minimum pressure to be applied to the draw solution to prevent both solutions to pass through the membrane. By considering both feed and draw solutions as incompressible liquids and sufficiently diluted, the van't Hoff equation can be used to approximate the osmotic pressure as [42]

$$\pi = ic\bar{R}T, \tag{2.1}$$

where i is the van't Hoff factor which represents the degree of dissociation, c is the molar concentration of salt, $\bar{R}$ is the universal gas constant, and T is the thermodynamic temperature of the solution. In the draw solution, 1 litre of seawater typically consists of 35 g NaCl which dissociates into Na^+ and Cl^- ions ($i = 2$), and 993 g of fresh water. Hence, the molar concentration of salt in the draw solution is $c_D = 600\ \frac{mol}{m^3}$. At a temperature of 298 K, the osmotic pressure of the draw solution is π_D =29.7 bar [43].

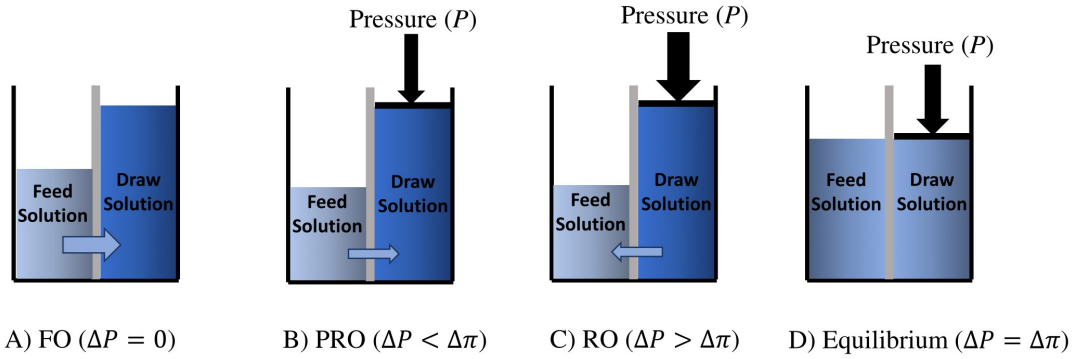

Figure 2.2: Representation of solvent flow in FO, PRO, RO, and Equilibrium processes [44].

When two solutions are separated by a semipermeable membrane, four possible osmotic phenomena may happen as described schematically in Figure 2.2. Forward osmosis (FO) occurs when the osmotic pressure difference between the feed and draw solution is positive and freshwater can permeate to the draw side through the membrane, spontaneously. Here both solutions are at the same hydrostatic pressure. When the applied hydraulic pressure difference(ΔP) is $0 < \Delta P < \Delta\pi$, again freshwater permeates to the draw side but with the lower flux. This process is called Pressure Retarded Osmosis (PRO) and is represented in Figure 2.2(B). This phenomenon can be used as an energy source since the added volume of permeated water to the draw

side is at elevated pressure and can be used to generate continues energy. If the applied hydraulic pressure is increased further to reach the osmotic pressure value $\Delta P{=}\Delta\pi$, both solutions are in thermodynamic equilibrium as illustrated in Figure 2.2(D). If the hydraulic pressure exceeds the osmotic pressure $\Delta P > \Delta\pi$ the reverse flow of freshwater occurs from the draw side to the feed side which is called Reverse osmosis (RO) (Figure 2.2(C)). Nowadays, most modern desalination plants are based on RO technology.

Other than applications like desalination, food preservation, and medicine, osmotic process can be considered as a renewable energy source candidate [5]. Osmotic power can be produced by mixing to solutions by means of a semi permeable membrane. The solution having a lower salt concentration is referred as the feed solution, while the other with high salinity is known as the draw solution. When draw and feed solutions enter the module, one on each side of the semipermeable membrane at different pressures, there is a driving force for freshwater to permeate from the feed (diluted water) to the pressurized draw solution (concentrated water). The process is continued as long as the difference in the hydraulic pressure is less than the difference in the osmotic pressures.

2.2.1 PRO process

To harness osmotic energy, hydraulic pressure can be applied to the draw solution to retard water flux across the membrane and secure constant energy generation in the module. This process is known as pressure retarded osmosis (PRO) [7]. As discussed in section 2.2, the hydraulic pressure must not exceed the osmotic pressure difference in the system which is the driving force of water permeation. Osmotic pressure is related to the difference in salt concentration of the draw and feed solutions. Therefore, the higher the salt concentration difference, the higher the osmotic pressure is. Various sources of the draw solution with higher salt concentrations like the Dead Sea [11], the brine of desalination plants [4], and salt lakes [45] are considered for PRO systems. A pilot scale power plant, harvesting PRO energy from seawater was developed in Norway by Statkraft in 2009. The schematic of this power plant is illustrated in Figure 2.3. However, mainly due to the inefficiency of the membrane causing low generation of power per membrane area (0.5 Wm^{-2}) [13], but also due to low osmotic pressure driving force of the chosen draw and feed solution sources [46], this power plant was shut down in 2012.

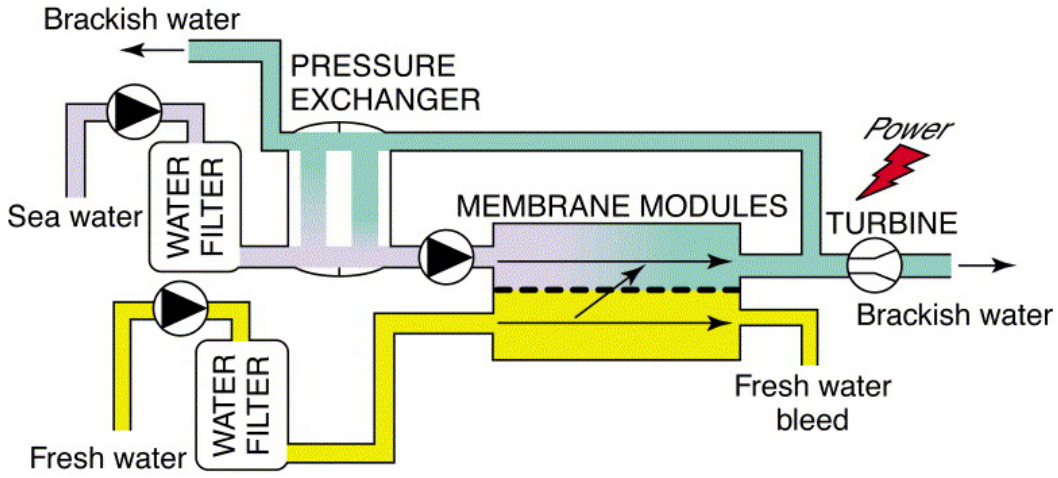

Figure 2.3: A schematic of Statcraft PRO power plant [47].

In order for a PRO power plant to be commercially feasible, it is estimated that the power density needs to be above 5 Wm^{-2} [16]. Recently, there have been improvements in membranes and their parameters, especially in laboratory scale power plants [48]. Other factors also affect the power density such as operating condition, pressure drop along the membrane, and PRO configuration. As the system scales up, the mentioned factors play a vital role and become more significant to investigate.

2.3 Basic concepts of PRO

2.3.1 Water and salt fluxes across the membrane

In an ideal semipermeable membrane, freshwater can permeate through the membrane, but all the other solutes and ions are supposed to be fully rejected. In this case, the water flux (J_{wr}) passing through the membrane is generally described by Baker [49]

$$J_{wr} = A(\Delta\pi - \Delta P) = A(\pi_D - \pi_F - \Delta P), \tag{2.2}$$

where A is the water permeability, π_D and π_F are bulk osmotic pressures in draw and feed solutions, respectively, and $\Delta\pi = \pi_D$ - π_F. ΔP is the applied hydraulic pressure difference between the two flows. Equation 2.2 is only valid in an ideal system, where the membrane is perfectly selective and the concentrations at the surface of the membrane are equal to the bulk concentrations. In a realistic membrane solutes and ions can also pass through the membrane mostly from the draw solution to

the feed solution. Salt permeation through the membrane reduces the water flux. Therefore, the following need to be considered in order to modify Eq. (2.2):

1. Reverse salt flux (RSF);
2. Internal concentration polarization (ICP); and
3. External concentration polarization (ECP).

RSF occurs due to non-selective behaviour of membranes. Hence, salt permeates from the draw solution to the feed solution in the opposite direction of water permeation. RSF is described by [50]

$$J_s = B(c_{D,m} - c_{F,m}), \tag{2.3}$$

where J_s is the reverse salt flux, B is the salt permeability coefficient, and $c_{D,m}$ and $c_{F,m}$ are the solute concentration right at the membrane in draw and feed sides, respectively. A schematic of salt concentration profile through the membrane is shown in Figure 2.4.

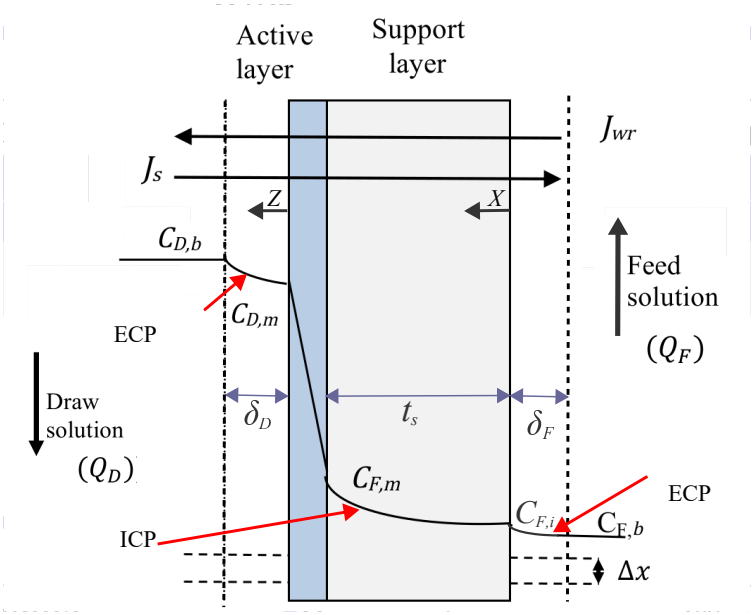

Figure 2.4: A schematic of salt concentration profile in a membrane module [51].

2.3.2 Concentration polarization

Concentration polarization refers to concentration gradient across the membrane due to accumulation or depletion of solutes near the interface [52]. As a result, the effective

osmotic pressure difference can drastically reduce due to less effective concentration gradient across the membrane. The membranes operated in PRO are mostly asymmetric with a thin dense active layer and a relatively thick porous support layer. Therefore, concentration polarization occurs externally on the active layer (depletion of solutes) and internally in the support layer (accumulation of solutes) [53, 54]. Both internal and external concentration polarization ultimately leads to a drop in water permeate flux and power density.

2.3.2.1 Internal concentration polarization (ICP)

In PRO systems, if active layer is facing the draw solution, permeated freshwater flows from the feed side through the support and active layer, respectively. The salt permeates from draw solution across the active and support layer to the feed solution due to the imperfection of the active layer. The support layer is protected from sheer and mixing that develops in the bulk solution and the salt diffuses along the membrane to reach to the feed side. Therefore, a salt gradient in the thick support layer happens that results in internal concentration polarization (ICP)(see Figure 2.4). The resulted unstirred boundary layer increases π_F, thus reduces the transmembrane driving force [55, 52].

2.3.2.2 External concentration polarization (ECP)

a. Concentrative ECP

As a result of the imperfect membrane and reverse salt flux, the salty water permeates through the membrane from the feed side to the draw side. Concentrative ECP occurs due to the accumulation of salt at the surface of the support layer [54]. Without perfect mixing, the concentration of salt will vary from the feed bulk resulting in the concentrative ECP and causes the increase of the feed concentration ($c_{F,i} \rightarrow c_{F,b}$)(see Figure 2.4).

b. Dilutive ECP

In PRO system, significant ECP happens in the draw solution side where the fresh water coming through the membrane needs to be mixed with more concentrated draw solution. The driving force for fresh water is the osmotic pressure at the membrane, where the fresh water arrives. Without perfect mixing in the draw channel, the local osmotic pressure, and hence the driving force, will drastically decrease, and energy extraction in the process will drop ($c_{D,b} \rightarrow c_{D,m}$)(see Figure 2.4).

The effect of ECP, ICP, and RSF on water flux (J_w) and power density is demonstrated in Figure 2.5. According to this evaluation, the most substantial change is observed when ICP is neglected indicating that ICP has the most influence on power reduction of PRO processes [56].

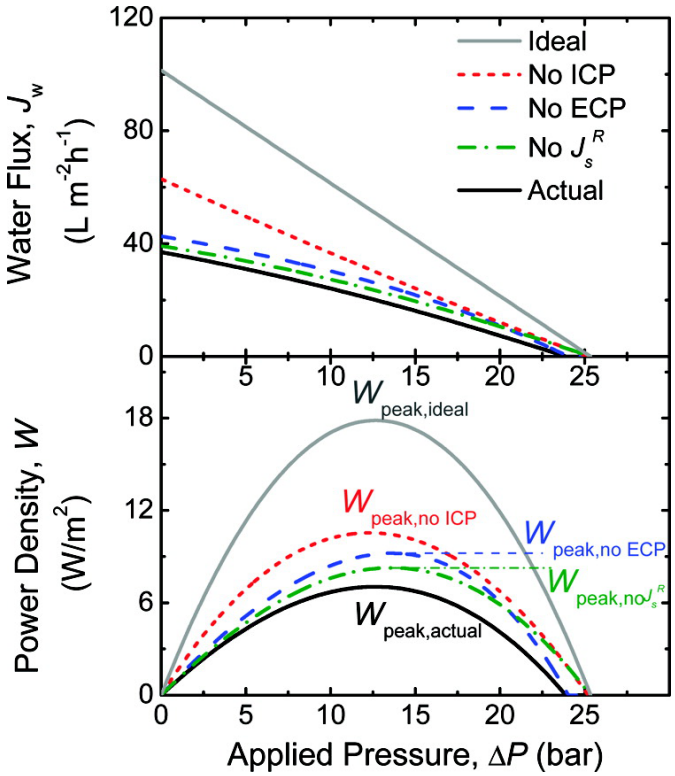

Figure 2.5: An illustration of water flux (J_w) (a) and power density (b) against hydraulic pressure in the PRO process to investigate the effects of ECP, ICP and reverse salt flux [56]

Due to the combined effects of ICP, reverse salt flux, and ECP, the effective osmotic pressure driving force is lower than in the ideal system. Therefore, Eq. (2.2) needs to be rewritten considering all destructive parameters. To develop the most accurate equations some models have been suggested that will be discussed in section 2.4.

2.4 PRO models

Since the inception of the PRO system, the development of mathematical models has been a fundamental factor in the development of the PRO process. These models

are continuously improved by better understanding of the process such as the effect of concentration polarization, reverse salt flux, and membrane fouling. Furthermore, the various types of membranes like spiral wound and hollow fiber membranes need to be specified in the presented models. This section summarizes the most important models developed for water and salt flux across a flat sheet membrane in the PRO system.

2.4.1 Loeb model

The first PRO model was developed by Sidney Loeb [10]. He considered the support layer as a boundary layer in which water flux is a function of the concentrations and the concentration gradients. Loeb assumed that concentration is proportional to the osmotic pressure and that the transportation of water in the support layer is only by diffusion. He neglected the salt flux and external concentration polarization. The water flux expression is

$$J_{wr} = A(\pi_{Draw} - \pi_{Feed} \exp(\frac{\Delta X}{D_{sp}}) - \Delta P), \tag{2.4}$$

where π_{Draw} and π_{Feed} are the osmotic pressures of the draw and feed bulks, respectively, ΔX is the thickness of the membrane, and D_{sp} is the diffusion coefficient in the support.

2.4.2 Lee model

This model is developed by Lee et al. [57] as the first one to consider concentration polarization for PRO. It assumes that the ratio of salt concentrations is equal to the ratio of osmotic pressures and neglects the ECP effect. Considering the effect of ICP applied for the model, the expression was

$$J_{wr} = A\Big[\frac{\pi_{D,b} - \pi_{F,b} \exp(\frac{J_{wr}S}{D})}{1 + \frac{B}{J_{wr}}[\exp(\frac{J_{wr}S}{D}) - 1]} - \Delta P\Big], \tag{2.5}$$

where $\pi_{D,b}$ and $\pi_{F,b}$ are the bulk osmotic pressure of the draw and solutions, respectively. B is the salt permeability, D is the diffusion coefficient of the solute in the porous support and S is the structural parameter as effective diffusion coefficient, i.e., $S = \frac{t_s \tau}{\varepsilon}$, where t_s is the thickness of the support layer, ε is porosity, and τ is tortuosity. The effect of the ICP corresponds to the term $\exp(\frac{J_{wr}S}{D})$ in the water flux

equation. The reverse salt flux J_s is expressed by

$$J_s = \frac{B}{J_{wr}}\Big[\exp(\frac{J_{wr}S}{D}) - 1\Big]. \tag{2.6}$$

2.4.3 Achilli model

Achilli et al. [58] expanded Lee model by considering external concentration polarization. Development of the model utilizes the ECP modules developed by McCutcheon and Elimelech [54]. Assuming $\frac{c_{F,b}}{c_{D,m}} = \frac{\pi_{F,b}}{\pi_{D,m}}$, Eq. (2.5) becomes

$$J_{wr} = A\Big[\frac{\pi_{D,b}\exp(\frac{-J_{wr}}{k}) - \pi_{F,b}\exp(\frac{J_{wr}S}{D})}{1 + \frac{B}{J_{wr}}[\exp(\frac{J_{wr}S}{D}) - 1]} - \Delta P\Big], \tag{2.7}$$

where k is the mass transfer coefficient in the draw solution.

2.4.4 Yip model

Achilli model ignores the effect of draw solute loss on ECP and the effect of reverse salt flux. Yip et al. [59] improved the previous model incorporating the effect of ECP and reverse salt permeation. Assuming the linear relationship between the osmotic pressure and salt concentration, the effective water and salt flux are

$$J_{wr} = A\left[\frac{\pi_{D,b}\exp(\frac{-J_{wr}}{k}) - \pi_{F,b}\exp(\frac{J_{wr}S}{D})}{1 + \frac{B}{J_{wr}}[\exp(\frac{J_{wr}S}{D}) - \exp(\frac{-J_{wr}}{k})]} - \Delta P\right], \tag{2.8}$$

$$J_s = B\left[\frac{c_{D,b}\exp(\frac{-J_{wr}}{k}) - c_{F,b}\exp(\frac{J_{wr}S}{D})}{1 + \frac{B}{J_{wr}}[\exp(\frac{J_{wr}S}{D}) - \exp(\frac{-J_{wr}}{k})]}\right], \tag{2.9}$$

where $\pi_{D,b}$ and $\pi_{F,b}$ are the osmotic pressures of the draw and feed bulks, respectively, and k is the mass transfer coefficient in the draw water solution. The effect of the ECP corresponds to the term $exp(\frac{-J_{wr}}{k})$ in the Eqs. (2.8 and 2.9).

2.4.5 Bui model

Yip model ignores the effect of concentrative ECP at the feed side and assumes the equal mass transfer coefficient for draw and feed solutions ($k_D = k_F$). Incorporating these factors, Bui et al. [51] developed the Yip model. The resulting water and salt

flux equations are improving the accuracy of the model predictions as

$$J_{wr} = A\left[\frac{\pi_{D,b}\exp(\frac{-J_{wr}}{k_D}) - \pi_{F,b}\exp(\frac{J_{wr}S}{D} + \frac{J_{wr}}{k_F})}{1 + \frac{B}{J_{wr}}[\exp(\frac{J_{wr}S}{D} + \frac{J_{wr}}{k_F}) - \exp(\frac{-J_{wr}}{k})]} - \Delta P\right], \tag{2.10}$$

$$J_s = B\left[\frac{c_{D,b}\exp(\frac{-J_{wr}}{k_D}) - c_{F,b}\exp(\frac{J_{wr}S}{D} + \frac{J_{wr}}{k_F})}{1 + \frac{B}{J_{wr}}[\exp(\frac{J_{wr}S}{D} + \frac{J_{wr}}{k_F}) - \exp(\frac{-J_{wr}}{k_D})]}\right], \tag{2.11}$$

where k_D and k_F are the mass transfer coefficient in draw and feed solutions, respectively. The term $\exp(\frac{J_{wr}}{k_F})$ condenses the effect of concentrative ECP.

There are some other suggested models developed based on convection-diffusion theory [60] or considering the effect of fouling layer on the mass transport equations [61]. Some models have been modified for hollow fiber membranes to consider the spatial parameters with the change of geometry for the membrane [62, 63].

2.5 Thermodynamic limits of the PRO process

Mass transfer characterizes the movement of the water through the membrane and the related power output. However, thermodynamics explains the ratio of the total transported water to the total power generation. The theoretical maximum power extractable in PRO can be harvested by a reversible mixing process and is equal to the Gibbs free energy of mixing [64]. Assuming ideal solutions, the Gibbs free energy per volume of total feed and draw solution can be written in the simple form [65, 66]

$$\frac{\Delta G}{\nu RT} = c_M \ln(\gamma_M c_M) - \phi c_F \ln(\gamma_F c_F) - (1-\phi)c_D \ln(\gamma_D c_D), \tag{2.12}$$

where c_M, c_F and c_D are the mixed, feed and draw solution molar concentrations, respectively and γ_M,γ_F, and γ_D are the activity coefficients in the corresponding solutions. For dilute solutions, assuming ideal behavior, the activity coefficient can be approximated as unity [67]. ν is the van't Hoff factor for strong electrolytes ($\nu = 2$ for NaCl) and ϕ is the ratio of the volume of the feed solution to the total volume of feed and draw solutions. R is the ideal gas constant and T is the absolute temperature.

Maximum Gibbs free energy of mixing for seawater draw solutions is 0.26 $\mathrm{kWhm^{-3}}$ and for the hypersaline Dead Sea is 2.52 $\mathrm{kWhm^{-3}}$ [65]. However, full-scale PRO systems will operate under constant pressure and the osmotic pressure of feed and draw solutions will vary along the membrane module. The mixing stops when the osmotic

pressure drops to the hydraulic pressure value. Figure 4.3 illustrates the actual energy extracted by a PRO system along with the frictional losses to overcome the hydraulic resistance of the membrane, and unutilized energy due to the application of system irreversibilities since the real operating conditions are far from the thermodynamic equilibrium [65, 25].

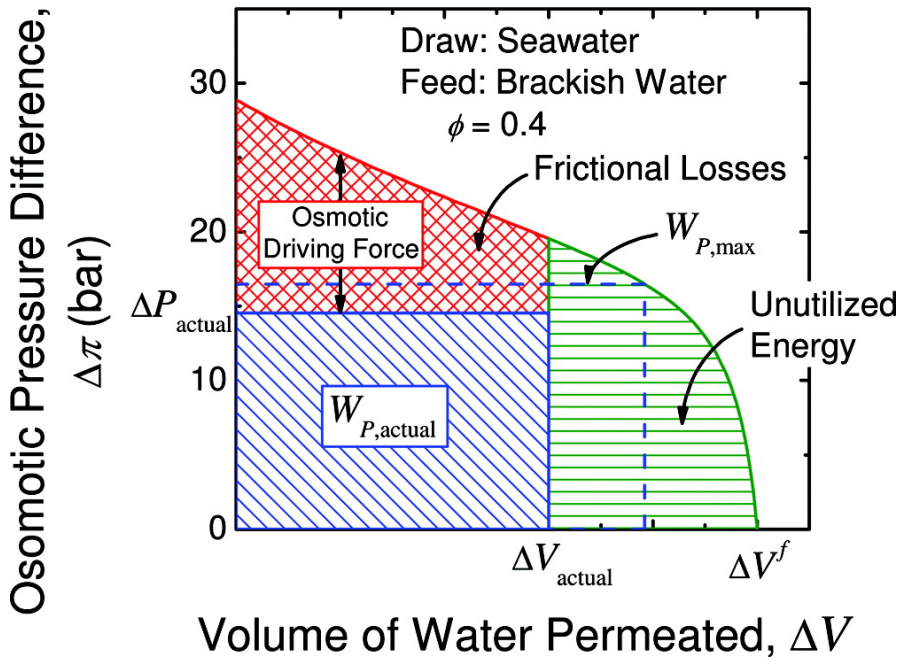

Figure 2.6: Maximum extractable work, unutilized energy and frictional losses [64]

Other than the membrane losses, there are some other losses in system operation, related to the pretreatment of the draw and feed solutions and hydraulic losses in pump, turbine, and pressure exchanger. A detailed thermodynamic analysis for PRO systems will be conducted in chapter 3.

2.6 PRO membranes

As discussed earlier, the membrane plays an important role in the PRO system. To have high power density in a PRO process, the membrane should promote the fresh water passing, reject the salt passage, and have low support layer structural parameter (S). The mechanical stability is another factor in membrane selection since it needs to withstand the high applied hydraulic pressure difference. The early membranes used in PRO were the same for RO which had proper mechanical stability, but they

were as thick as 150-250 μm to withstand high pressures of 100 bar of a RO process. The thickness retards the diffusion of ions through the membrane and increases ICP. This reduces the osmotic pressure difference and accordingly the power density to less than 1.22 Wm^{-2} [68], far from the estimated power of 5 Wm^{-2} viable for economical PRO. The reason was attributed to the severe ICP occurring inside the thick and hydrophobic membrane substances [57].

Due to similarities of required characteristics between FO and PRO, some FO membranes were tested at the next steps. The main FO membrane was the asymmetric cellulose triacetate (CTA) based flat sheet membrane produced by Hydration Technology Innovations (HTI, Albany, OR). The results were mostly below 5 Wm^{-2} due to intrinsic low water permeability and high salt permeability [30, 69]. Most of the other FO membranes failed under PRO operation because of their poor mechanical behavior. As they were not supposed to operate at high pressures like PRO, they were compacted, deformed or even torn [70, 71, 72]. In order to improve PRO membrane functionality, developed membranes should have:

- The best combination possible of a membrane having high water permeability (A) and reasonably low salt rejection (B) to achieve high J_{wr} and low J_s.
- Low structural parameter to minimize ICP effects.
- Hydrophobicity to enhance flux and reduce membrane fouling.
- High mechanical strength to withstand applied hydraulic pressure.

PRO membranes can be classified by their preparation method and their configuration. Two main PRO configurations are flat sheet membranes and hollow fiber membranes.

2.6.1 Flat sheet membranes

Flat sheet membrane developments for PRO started with improvements of CTA-RO membranes. These membranes have the advantages of hydrophilicity, proper mechanical strength and relatively high tolerance to chlorine [73]. Hydrophilicity of CTA membranes improves wetting of the membrane which promotes water flux, reduces membrane fouling, and decrease the ICP effect. Improvement of CTA membranes by HTI and their primary promising laboratory scale results [74] led the Statkraft to use

them for their PRO power plant. However, in practice, Statkraft obtained power densities of less than 1.5 Wm^{-2} using these CTA flat sheet membranes [30]. This value is far below the estimated 5 Wm^{-2} to make a PRO process commercially feasible. Another option for PRO membranes is thin film composite (TFC) membrane. TFC membranes usually consist of an asymmetric porous support and a top selective skin joined together to form a membrane. This combination optimizes the system performance since the microporous support provides the mechanical strength, while the selective layer performs the separation. Despite CTA membrane, TFC membranes can tolerate a wide range of pH but they have a low tolerance to oxidants and chlorine chemicals [75].

To improve the TFC membranes and make them specialized for the PRO system, different aspects were used on polyamide active layer and support layer. At the active layer, some treatments were done during the reaction or as a post-treatment to make optimized water permeability with a slight decrease in salt rejection. Consequently, the water flux and power density were increased [76, 77]. At the support layer, mechanical strength and structural parameters were modified by making thin woven support [78, 79] or electrospun nanofiber substrates [80, 81].

However, to improve the mixing and reduction of ECP effects as well as to maintain the channel geometry, channel spacers are needed in flat sheet modules. These spacers will cause pressure drop in the feed solution and induce shadow effects which will decrease the effective length of the membrane [82]. Flat sheet membranes can be

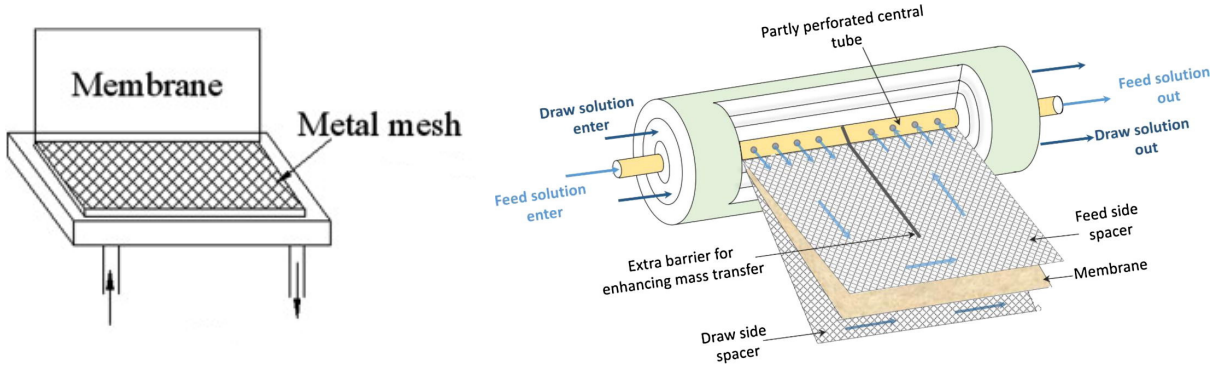

(a) (b)

Figure 2.7: Flat sheet membranes used as laboratory scale module (a), and rolled as spiral wound module (b) [83, 84].

used in a parallel stacked module as Figure 2.7(a)[83] or spiral wound module that has multiple flat sheet leafs rolled as Figure 2.7(b)[84]. The first module is usually

used for lab scale experiments and the latter is suitable for industrial applications since it saves more space. SEM image of the cross section of a thin film polyacrylonitrile (PAN) membrane support layer before and after applying hydraulic pressure is shown is Figure 2.8(a,b) [85]. It consists of a finger-like macroporous structure with many straight big pores. This structure is drastically damaged after being under hydraulic pressure of 15 bar for 120 min indicated by the reduction of the support layer thickness from 250 to 195 μm and some collapsed porous structure.

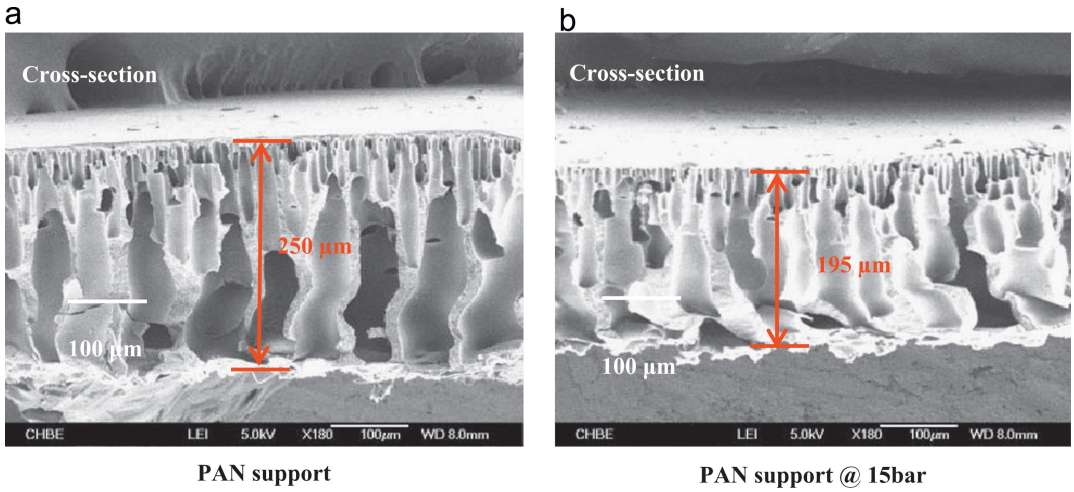

Figure 2.8: SEM images of cross section of PAN membrane support (a) before and (b) after being pressurized at 15 bar for 120 min [56]

The performance of some flat sheet membranes are summarized in Table 2.1.

Table 2.1: Experimental results using flat sheet membranes under different operating conditions.

Membrane	Feed solution concentration	Draw solution concentration	Pressure (bar)	Power density (Wm^{-2})	References
CTA	DI water	1 M	9.7	5.1	[58]
CA	0.1 M	1 M	13	3.8	[86]
CTA	0.5 M	1 M	9.3	0.73	[87]
Matrimid TFC	DI water	1 M	15	9	[85]
PAN TFC	DI water	0.6 M	10	2.6	[77]
SiO_2/PAN	80 mM	1.06 M	24	15.2	[81]
PAN-mTFC	DI water	0.6 M	8.3	6.2	[88]
TFC	DI water	3 M	48	60	[89]
PEG-CA	DI water	0.6 M	-	2.7-3.1	[90]
TR-TFC	DI water	0.6 M	15	17.2	[91]

2.6.2 Hollow fiber membranes

Hollow fiber (HF) membranes are tubular membranes with a fiber diameter of less than 500 μm. Compared to flat sheet membranes, hollow fiber configuration has the advantages of a self-supporting structure, no need to the spacers, high surface area and ease of fabrication [92]. In addition to the importance of careful selection of the materials, the microstructure of the fiber needs to be highly porous with small, uniformly sized, interconnected pores [93]. The fiber dimension and the wall thickness can influence the strength and performance of the membrane [68]. The hollow fiber membranes tailored for PRO applications may have inner- or outer-selective configurations (active layer at inner or outer side of the fiber, respectively). Most studies are focused on inner- selective HF membranes since synthesizing a uniform selective layer is more difficult in outer-selective HF membranes. However, outer-selective HF membranes show less pressure drop along the membrane and provide more active surface area [68]. A developed TFC- hollow fiber membrane could reach to the maximum power density of 24 Wm^{-2} with a synthetic seawater brine (0.1 M NaCl) as the draw solution and deionized water as the feed solution at the applied hydraulic pressure of 20 bar [94].

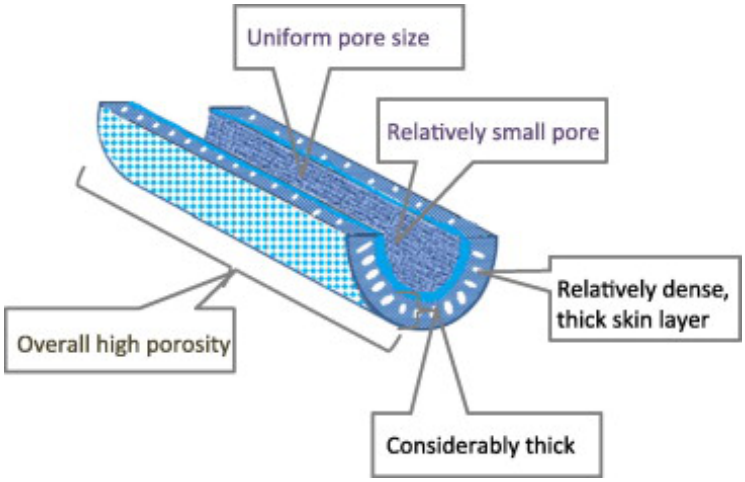

Figure 2.9: A schematic of geometry and structure of an inner-selective TFC-PRO hollow fiber membrane [93]

.

A schematic of an inner-selective hollow fiber membrane is illustrated in Figure 2.9. A relatively dense cushion layer followed by a highly porous support layer is desired in these membranes to redistribute the stresses and to reduce ICP, respectively [95]. SEM image of cross section and surface morphology of a hollow fiber membrane is

shown is Figure 2.10 [95].The performance of some hollow fiber membranes in the PRO system are summarized in table 2.2.

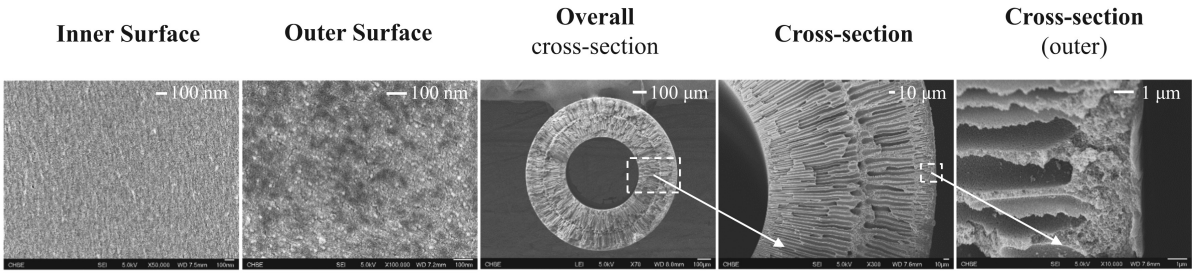

Figure 2.10: SEM images of cross section and surface morphology of hollow fiber membrane [95]

.

With current membranes, the characteristics of A value in the range of 3-6 (Lm^{-2} $h^{-1}bar^{-1}$) , B value less than 1 ($Lm^{-2}h^{-1}$), and S value less than 300 μm with proper mechanical strength are available in laboratory scale. The maximum power density obtained for seawater and freshwater pair is 10 Wm^{-2} [96].

Table 2.2: Experimental results using flat sheet membranes under different operating conditions.

Membrane	Feed solution concentration	Draw solution concentration	Pressure (bar)	Power density (Wm^{-2})	References
PES-TFC	0.04 M	1 M	5.1	6.2	[55]
PEI-TFC	0.001 M	1 M	15	20.9	[96]
Matrimid TFC	DI water	1 M	15	16.5	[94]
PES TFC	DI water	0.6 M	6	1.62	[97]
P84 TFC	DI water	1 M	21	12	[98]
Modified PES-TFC	DI water	1 M	20	24.3	[99]
TFC-PES	DI water	1 M	20	27	[100]
TFC	DI water	1 M	22	10.05	[95]
TFC	DI water	0.6 M	15	11.1-20.8	[19]
PAH/GA	wastewater	1 M	13	4.3	[101]
TFC-PES	DI water	1.2 M	30	38	[20]

2.7 Membrane fouling and scaling

Membrane fouling is caused by the deposition of impurities and particulates on the surface or within the membrane pores due to convective or diffusive transport. This

phenomenon blocks the passage of freshwater flow, reduces the effective membrane area and decreases the permeability of the membrane. It also increases pressure loss along the membrane module [102], affects the membrane durability and increases the maintenance cost. Natural organic matter (NOM), aquatic microorganisms, inorganic compounds, and colloids are the main sources of fouling. In PRO, the support layer faces the feed solution, therefore fouling happens both on active and support layer [103, 104]. Fouling on the active layer is relatively mild due to the permeation flux of fresh water draws away the foulants. However, with the permeation of the water through the membrane, solutes and other foulants can penetrate into the porous support layer, accumulate and block the pores, leading to increased ICP.

To control or reduce membrane fouling, appropriate methods must be applied based on the type of the foulants. Physical cleaning of the surface such as flushing and membrane backwashing can control the fouling in PRO [105, 106]. Chemical cleaning is another method that can be applied choosing suitable cleaning agent and considering the pH, temperature, flow rate and cleaning time [107, 108]. Pretreatment of the draw and feed solutions is also an effective method to reduce the amount of foulants before entering the module. Ultrafiltration system and a multimedia sand filter are the common ways of pretreatment.

Surface modification and coating of membranes can improve fouling resistance against various types of foulants [109, 110, 111, 112]. Anti-biofouling of feed spacers can reduce the fouling effects without affecting the membrane permeability [113]. Membrane scaling is another phenomenon that hinders mass transport through the membrane due to the formation of a thin layer of supersaturated salts on the membrane surface [102]. The reverse solute diffusion in PRO (e.g. Ca^{2+} or Mg^{2+}, and $SO4^{2-}$) from the draw solution lead to the gypsum clogging in the support layer and eventually making an external thin layer of crystallized gypsum [99].

2.8 PRO configurations

The standard PRO system configuration utilizes the mixing of river water and seawater pressurized by a pressure exchanger (PX) as shown in Figure 2.3 [11]. This configuration, even with optimized membranes, is limited by low salinity gradient of river and seawater. Maximum theoretical energy of a river-sea PRO system per feed solution inlet is found to be 0.77 $kWhm^{-3}$ [114]. This value after considering the pretreatment and all the other losses could be approximately 0.15 $kWhm^{-3}$ per inlet

draw and feed solution [15]. To improve the energy output some other configurations including higher salinity gradient sources have been suggested.

2.8.1 RO-PRO hybrid systems

In the past few years, PRO was considered as a part of a hybrid system, mostly to recover energy from other osmotic processes such as reverse osmosis (RO) [115, 116]. The byproduct of desalination systems, which is concentrated brine, can be used in the PRO system to create some of the required power for desalination [117]. In an RO-PRO system, the high salinity solution is pressurized to enter the RO for the desalination process. The concentrated brine exiting from RO enters the PRO subsystem having higher salinity as draw solution. The feed solution can be from a wastewater treatment plant. The volumized draw solution exiting from the PRO subsystem can be used to recover some of the energy consumption of the RO subsystem. Other than reducing the energy consumption of the RO system, the PRO process can minimize the environmental impact of the marine ecology. The diluted brine exiting from the PRO subsystem is almost close to the salinity of seawater. The RO brine prepared for the PRO is pretreated and easily available from the commercial RO systems. In 2010, Japan launched Mega-ton water system project in which they used RO brine and treated sewage as the draw and feed solutions, respectively. They used Toyobo hollow fiber membrane to regenerate with the potential of 13.3 Wm^{-3} power density and reduced the energy consumption of RO subsystem by 30% [118, 119].

A pilot scaled RO-PRO system modeled and experimented using spiral-wound TFC PRO membrane module [114, 120]. As shown in the Figure 2.11, the RO brine exiting from the RO subsystem enters an Energy Recovery Device (ERD) subsystem to reduce the pressure suitable for entering the PRO subsystem as the draw solution. The exiting flow from the PRO process enters a pressure exchanger to exchange the pressure of the diluted draw solution with the seawater used as the feed solution for the RO process. The energy consumption of the RO subsystem was 2 $kWhm^{-3}$ with 30% of recovery. Their model [120] specified the minimum net specific energy of 1.2 $kWhm^{-3}$ for 50% of RO recovery. For energy consumption of 2 $kWhm^{-3}$, the modeled PRO subsystem can achieve 40% energy reduction.

A feasibility study and thermodynamic analysis for an RO-PRO system investigated by He et al (Figure 2.12) [121]. A feasible condition (FC) number was used to

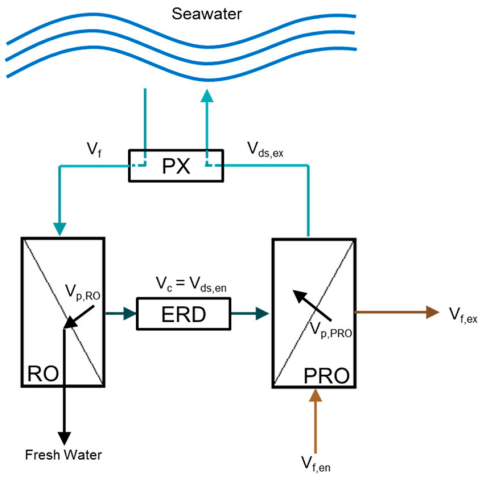

Figure 2.11: A schematic of an RO-PRO system. V_f is the volume flow of the RO feed solution, and V_c is the concentrated brine waste stream exiting from RO subsystem. $V_{p,RO}$ and $V_{p,PRO}$ are freshwater permeate in RO and PRO subsystems, respectively. In PRO subsystem $V_{ds,en}$ is the draw solution stream and $V_{f,en}$ is the feed solution stream. $V_{f,ex}$ and $V_{ds,ex}$ are exiting concentrated feed and diluted draw solutions from PRO subsystem, respectively. ERD and PX denote energy recovery device and pressure exchanger, respectively. [120].

study the feasibility using the efficiency of all components in the RO-PRO system.

$$FC = \frac{\Delta P\big[(1-Y)(\eta_{HT} - \frac{\eta_{ERD}}{\eta_{HP}}) + Y_P\big]}{\Delta P\big[\frac{1-\eta_{ERD}(1-Y)}{\eta_{HP}}\big]}, \tag{2.13}$$

where η_{HP}, η_{ERD}, and η_{HT} are the efficiencies of HP, ERD, and HT, respectively. Y is the RO water recovery. The higher FC number means the higher feasibility. The study showed that lower RO water recovery and higher dimensionless flow rate (volumetric feed to the volumetric combined feed and draw flow rates) increased the FC number. For the PRO subsystem the optimum FC number was attained when a higher hydraulic pressure applied to a lower membrane area. However, the study neglected the effect of concentration polarization and reverse salt flux on the performance of the RO-PRO hybrid system.

A model-based comparison of open-loop and close-loop RO-PRO systems was done by Wang et al [122] regarding normalized specific energy consumption. The closed-loop RO-PRO system showed better energy recovery than the open-loop system due to energy saving and cost reduction. However, the closed-loop configuration was more sensitive to the variation of operational conditions and degradation of the membrane.

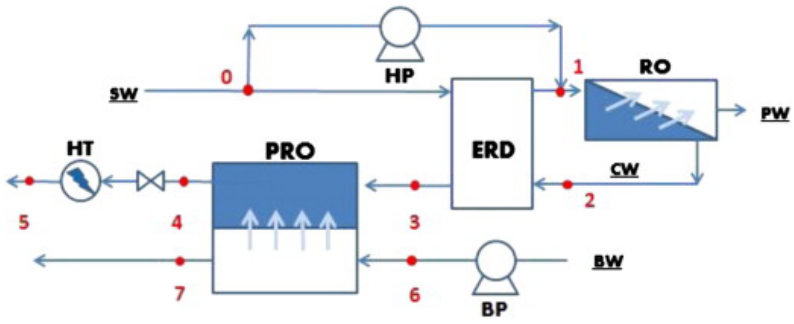

Figure 2.12: A schematic of stand-alone salinity power driven RO desalination system. HP: Hydro pump, BP: Booster pump, HT: Hydro turbine, ERD: Energy recovery device, SW: Seawater, PW: Pure water, CW: Concentrated water, BW: Brackish water [121].

2.8.2 MD-PRO hybrid systems

When a direct utilization of low-grade heat at the source is not accessible, the only option is converting it to the electricity. MD-PRO hybrid system is a candidate with the advantages of high efficiency and low-grade heat sources $< 80°C$. This range is hardly achievable by organic Rankine cycle heat engines due to limitations of working streams. A closed-loop hybrid of membrane distillation (MD) and PRO system was investigated by Lin et al [123](Figure 2.13). In this system, MD is used to generate concentrated and diluted water using low-grade heat for thermal separation. The draw and feed supplies enter to a PRO system for energy production. Theoretically, this system can achieve the energy efficiency of 9-10% (73-83% of Carnot efficiency) with the working solution source of 1-4 M NaCl and the operating temperatures of hot and cold 60 and 20°C, respectively. However, the practical energy efficiency will be lower due to mass and heat transfer limitations.

An MD-PRO hybrid system was also investigated by Han et al. [124]. The study was conducted by employing 2 M NaCl solution and fresh water for the draw and feed solutions, respectively and TFC membrane to produce 31 Wm^{-2} power. A multi stage vacuum membrane distillation (MVMD) with PRO subsystem were studied to generate power and to distillate fresh water [125]. As shown in the Figure 2.14 the MVMD system utilizes a recycling flow scheme (MVDM-R) for the continues production of fresh and concentrated brine streams. The draw solution for PRO subsystem is the brine from MVDM-R and the feed solution is river water. With the brine concentration of 1.9 M NaCl, the power density of 9.7 Wm^{-2} was produced under the conditions of hydraulic pressure 13 bar and feed to draw solution flow rate

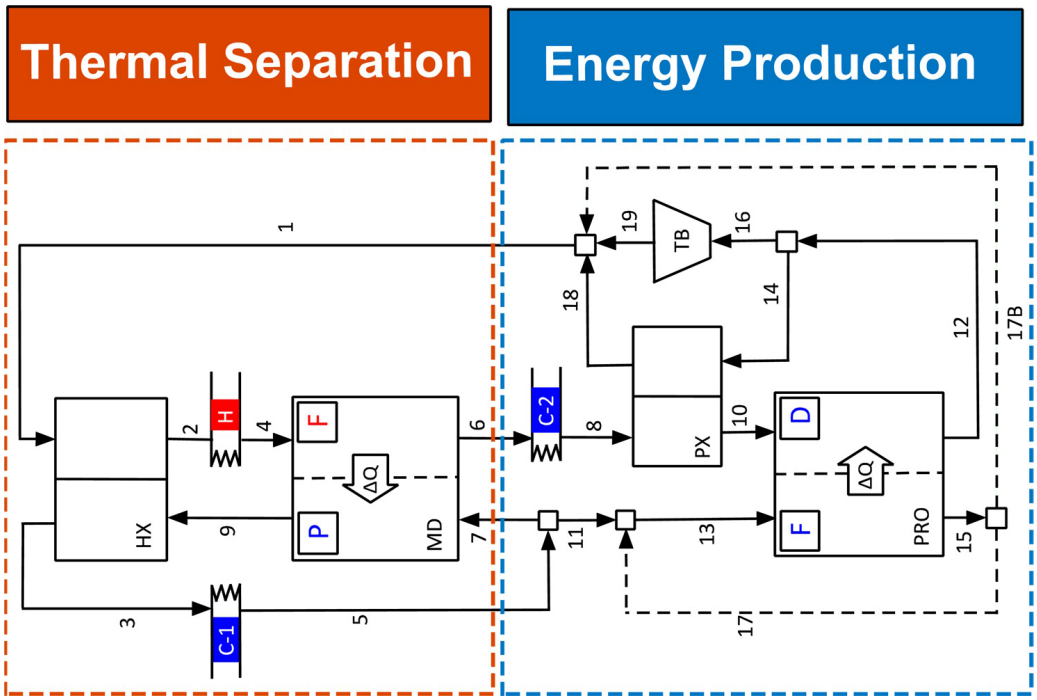

Figure 2.13: A schematic of the hybrid MD-PRO system for harvesting low-grade heat energy [123]. The system includes of a thermal separation and power generation components. Thermal separation consists a membrane distillation (MD) module and a heat exchanger (HX). Power generation component consists a pressure retarded osmosis (PRO) module, a pressure exchange (PX), and a turbine (TB). The numbers represent the streams. The H (in red) stands for an ideal constant temperature heat source, whereas the C1 and C2 (in blue) represent ideal constant-temperature heat sinks. The P and F in the MD module stand for the permeate (distillate) and feed channels, respectively. The F and D in the PRO module stand for the feed and draw solutions, respectively

of 0.5 kg/min.

2.8.3 FO-PRO hybrid systems

A hybrid system of FO-PRO was investigated for hypersaline solution treatment and power generation [126]. The FO subsystem if used for hypersaline solution treatment has the advantages of low fouling propensity, easy membrane cleaning and minimizing required external energy. Two configurations of FO-PRO and PRO-FO systems were compared using a hypersaline solution and wastewater effluent to harvest the maximum efficiency. The results showed that PRO-FO system has higher efficiency than FO-PRO system. It also was found that feed solution flow rate has a negligible

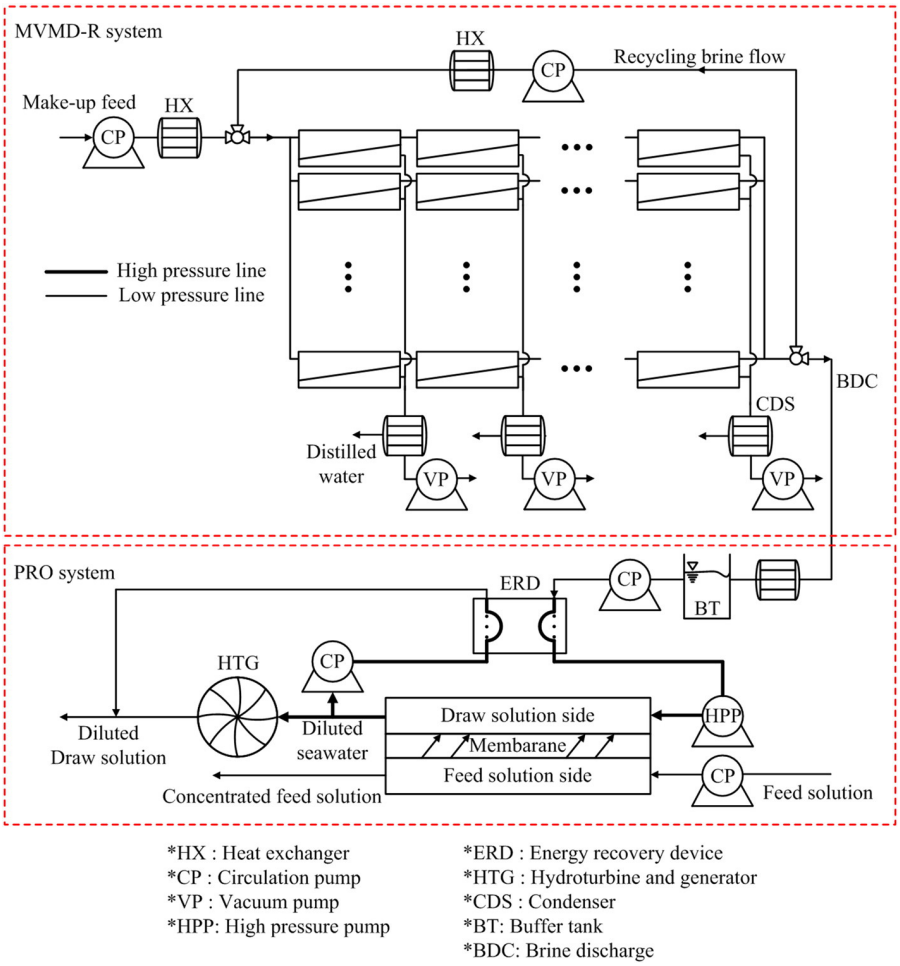

Figure 2.14: A schematic of the hybrid MVMD-R-PRO system [125].

effect on FO performance.

Cheng et al. [127] investigated model simulations of full-scale FO-PRO hybrid system by choosing the salinity of the inter-loop solution to PRO as 0.1 M (Figure 2.15). The study showed that with this hybrid, it is possible to reach a power density greater than 5 Wm^{-2} that makes the process economically feasible.

2.8.4 Dual stage PRO systems

Multi stage PRO configurations reduce the irreversible energy losses and increase the efficiency of power generation. Additional stages can rejuvenate the chemical potential difference along the membrane module and reduce the concentration polarization on the feed solution. They may utilize the advantages of flexibility in selection of membrane types, module configurations, and draw and feed solution sources. Further-

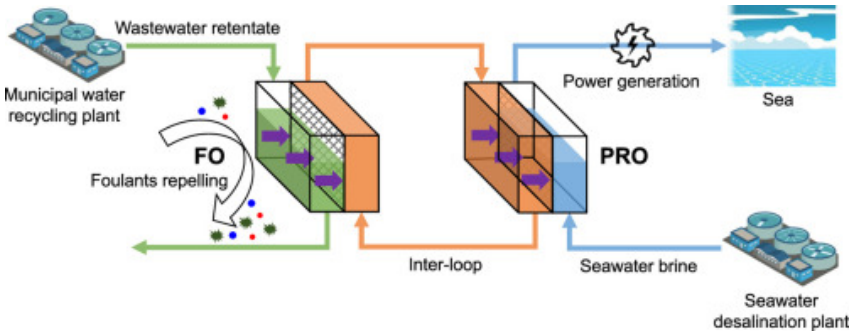

Figure 2.15: A schematic of the hybrid FO-PRO system [125].

more, low concentrated fresh water entering the second module may cause additional water permeation through the membrane, hence increasing power density. However, most of the improvement in multistage PRO systems occurs at low stage number (up to three-stage) [128]. Three- stage PRO systems are most likely not economically acceptable due to their high capital cost. Therefore, most of the studies are focused on dual stage PRO systems.

Shaheed et al. [25] introduced dual stage PRO system and conducted a thermodynamic analysis on it. In another study, they proposed four configurations of CDCF, DDDF, CDDF, and DDCF, either with the continuous or divided flow (C or D) of the draw and feed solution (D and F) (Figure 2.16) [129]. All configurations utilize energy recovery systems and pump-turbine (PT) pairs. The hydraulic pressure applied in the draw solution is constant, and the system is optimized to maximize the average power density. It is noted that the CDCF configuration operation highly depends on the dimensionless flow rate and the maximum energy can be reached at dimensionless flow rates of 0.5 and 0.6. In the DDDF configuration, the extractable energy of the dual stage PRO system with divided draw and feed streams for each module is less than the single stage PRO system. In the CDDF and DDCF configurations, there is one divided stream either in feed or draw solutions. Under fixed dimensionless flow rate, CDDF and DDCF have advantageous energy capacity over the single stage PRO system.

A schematic of the thermodynamic analysis of CDDF configuration is illustrated in Figure 2.16 [25]. The energy generated by each stage is presented by dashed rectangular area. Figure 2.17 represents a dual stage PRO system operating (a) at the optimum condition of each module separately and (b) at the conditions to obtain the total optimum energy. As can be seen in Figure 2.17, the optimum operating conditions for each module does not mean that the overall performance of the dual

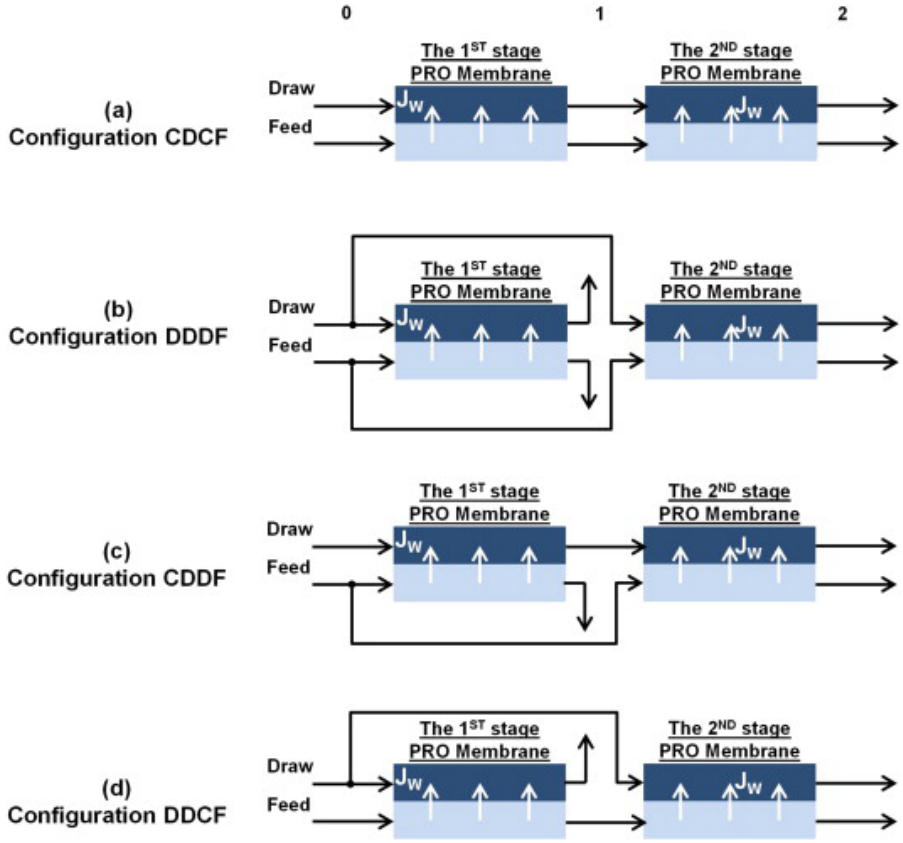

Figure 2.16: schematic diagram of the four possible configurations of dual stage PRO system proposed by [25].

stage PRO will be maximized. Rearranging the distribution of the energy between each module results in extra energy generation due to reducing frictional loss and unused energy compared to that of single stage PRO system [25].

The proposed configurations utilized co-current flow regime and did not consider concentration polarization effects and reverse salt flux. A Dual stage PRO system with counter-current flow was suggested by Altaee research group Figure 2.18(A) [26]. Unlike the other group which focused on river-sea pair, Altaee et al. used different feed sources to reduce membrane fouling and investigated the impact of feed salinity on maximum power density. The feed solution for the first module was brackish water (1-5 g/lit salinity) or freshwater (0.2 g/lit) and for the second module was wastewater effluent (0.2 g/lit). The best performance of the system was for the pair of brackish water and wastewater for first and second modules, respectively. The power generation in dual stage PRO system was more than the single stage one by the amount of generated power in the second module but it required more membrane

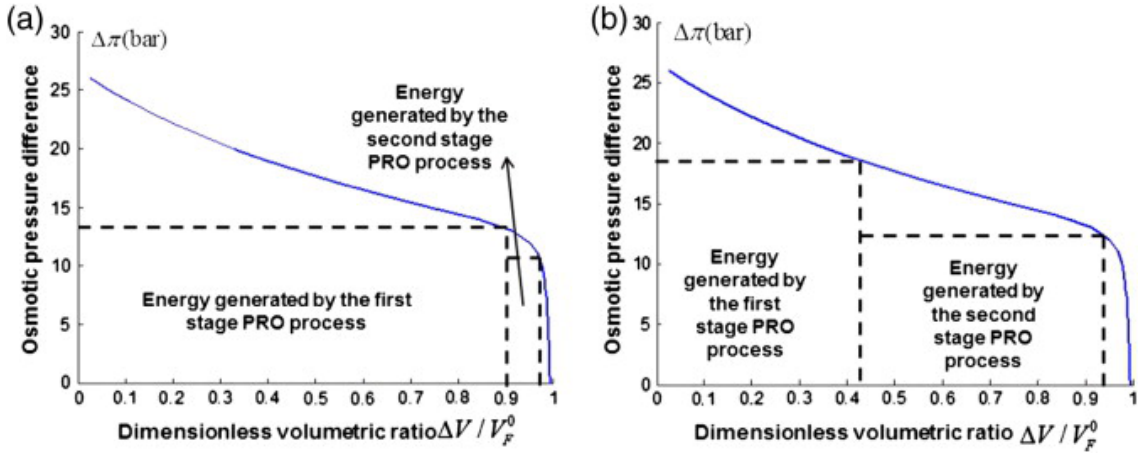

Figure 2.17: The illustration of thermodynamic analysis of dual stage PRO system that are a) operated at their optimal C-PRO b) operated at the condition to obtain the total optimum C-PRO [129].

area. In 2015, the presented dual stage configuration was compared to another design. As shown in Figure 2.18(B), in the new configuration all the seawater flow instead of going back to pressure exchanger enters the second module to increase the membrane flux [130]. The draw solution was seawater with salinities of 32 g/lit and 45 g/lit and the feed solution was wastewater effluent. Generally, the dual stage system performed better with higher draw salinities. The power density of the new design was 17.4% higher than the old one due to high membrane flux in the second module. The capital cost was also suggested to be less in the new design due to the need for less membrane elements. However, both studies ignored the effect of concentration polarization and hydraulic losses.

In 2017, they investigated dual stage PRO systems considering the effect of concentration polarization and reverse salt flux [131]. The system was modeled to maximize specific energy using different salinity gradients for the draw and feed solutions on the configuration proposed in Figure 2.18(A). The results showed maximum 13% increase of specific energy generation for dual stage PRO system while using the Dead Sea as draw solution and seawater as feed solution. For Dead Sea-RO brine as draw and feed solution, the performance of dual stage PRO system improved up to 16%. However, for the Dead Sea-wastewater and RO brine-wastewater, a neutral or negative impact was observed when a second stage PRO was added.

Altaee research group continued their investigation on dual stage PRO by studying on the effect of membrane orientation and proposing closed-loop dual stage systems.

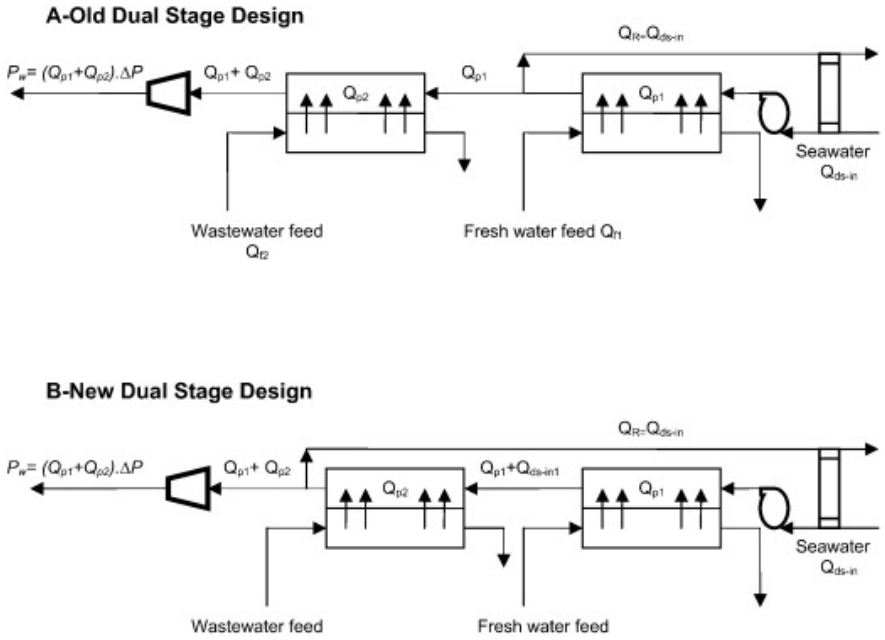

Figure 2.18: Schematic diagram of two proposed design for dual stage PRO system [130]. P_w: Power, Q_{ds-in}: Draw solution flow rate, Q_R: Recycle flow to PX, V_1: Permeate flow rate in first stage, V_2: Permeate flow rate in second stage, Q_{f-in}: Feed flow rate.

The impact of membrane orientation on the energy efficiency of the dual stage PRO system was investigated on PRO and FO operating modes [132]. Operating the PRO on the FO mode means the feed solution in PRO system is facing the active layer (FS-AL). Operating the PRO on the PRO mode means the draw solution in the PRO system is facing the active layer (DS-AL). The total power generation of the dual stage PRO on the PRO mode was 2.2-5 times higher than FO mode. On the FO mode, the effect of concentration polarization and reverse salt flux was more severe. The results indicated that at lower feed solution concentration the performance of dual stage PRO system was higher.

Single and dual stage closed-loop PRO systems were compared (Figure 2.19) [133]. The results showed that power generation improved 18% in dual stage closed-loop PRO (CLPRO) process compared to single stage CLPRO regardless of the regeneration processes. For regeneration of draw solution multi effect distillation (MED) was used. The power generation by the dual stage CLPRO was 95% higher than the power consumption of MED.

Dual stage PRO system coupled with the RO system was investigated to improve

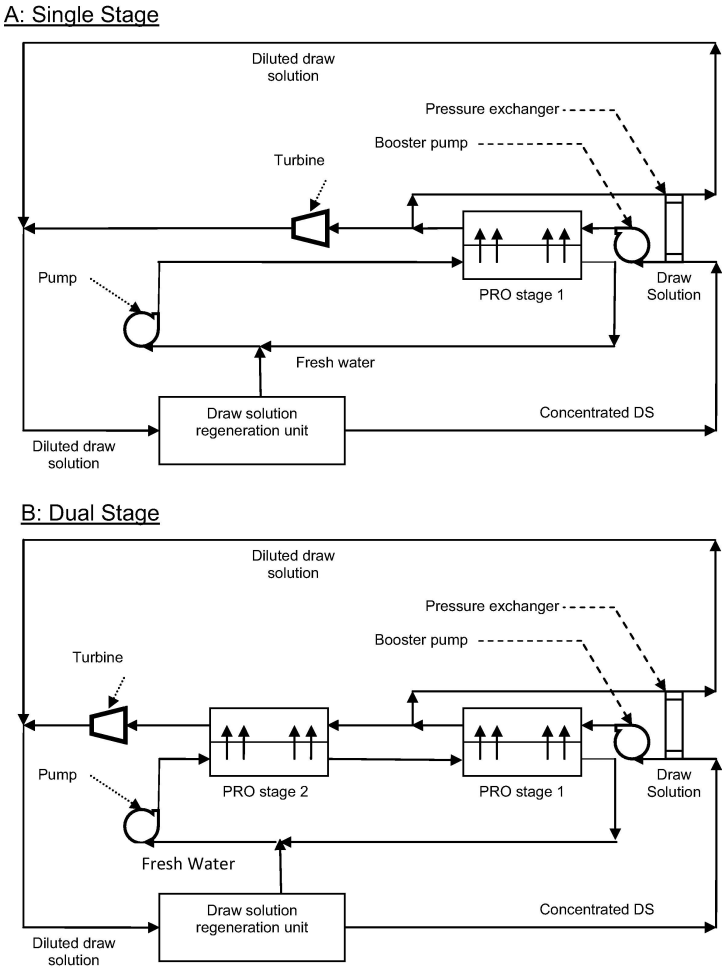

Figure 2.19: Schematic diagram of a closed-loop a) single stage b) dual stage PRO system [133].

the energy efficiency [134]. In a dual stage PRO system with a configuration like Figure 2.18(A), the feed solution was brine water coming out of the RO plant for the first module and wastewater effluent for the second module. The draw solution was seawater with concentrations of 45 g/lit and 73 g/lit. For 45 g/lit draw solution concentration, power density was 0.62 and 3.35 Wm^{-2} in the first and second modules, respectively. For 75 g/lit of draw solution concentration, the power density increased to 4 and 6.26 Wm^{-2} in the first and second module of the dual stage PRO subsystem. The PRO subsystem was able to reduce the volume of RO brine by 18% when the concentration of draw solution was 73 g/lit.

Dual stage PRO systems have also been studied as a hybrid system with RO plants to improve the energy efficiency of RO system. Touati et al. [135], investigated 2RO-

2PRO hybrid system. They compared 2RO-PRO and 2RO-2PRO systems in terms of energy recovery and changes of effluents. As can be seen in Figure 2.20, for the 2RO-PRO system the draw solution of PRO subsystem was the brine coming out of RO_1 and the feed solution was the brine coming out of RO_2. For the 2RO-2PRO system, the draw solution for PRO_1 was the RO_1 brine and the feed solution was seawater. The draw solution for PRO_2 was the seawater bleed coming out of PRO_1 and the feed solution was the brine coming out of RO_2. The results showed better performance of the proposed dual stage PRO. Optimizing the operation conditions showed that the increase in the feed concentration and the feed flow rate improve the performance of the PRO subsystem.

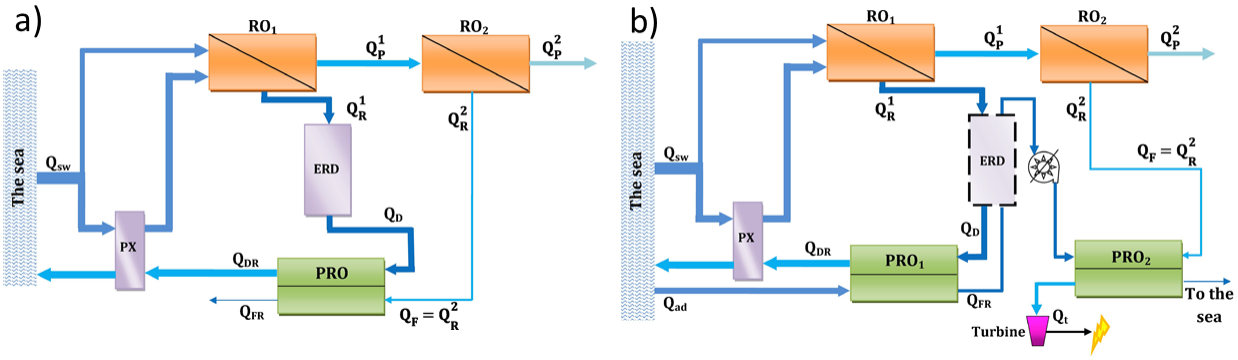

Figure 2.20: Schematic diagram of dual stage RO subsystem with a) single stage PRO subsystem b) dual stage PRO subsystem [135]. Darker colors correspond to more concentrated solutions and arrow thickness represents the approximate flow rate. Q_{sw} and Q_{DR} are the seawater flow and the diluted draw solution flows, respectively. Q_D and Q_F are the PRO entering draw and feed solution flows, respectively. Q_{FR} is the PRO feed solution bleed flow. Q_R^1 and Q_R^2 are the rejected flow of the RO first and second stages, respectively. Q_P^1 and Q_P^2 are the permeate flow of the RO first and second stages, respectively. Q_{ad} is the added seawater and Q_t is the flow that goes to turbine.

Another configuration of hybrid RO-RO-PRO-PRO process of is suggested for an energy efficient seawater desalination [136]. In this system, unlike the previous one, the PRO is utilized for energy recovery by means of several ERDs and there is no turbine in the design for power generation. The system was optimized for maximum specific energy subject to total membrane area and total water recovery. As shown in Figure 2.21, seawater was pressurized by several ERDs and a feed pump before entering the first RO. The RO brine from RO 1 was pressurized further by a booster pump and entered RO 2. The osmotic and hydraulic energies were then recovered

by PRO and ERDs, respectively. The feed solution for PRO systems was wastewater effluent. In this system, the second RO and PRO subsystems were added to increase

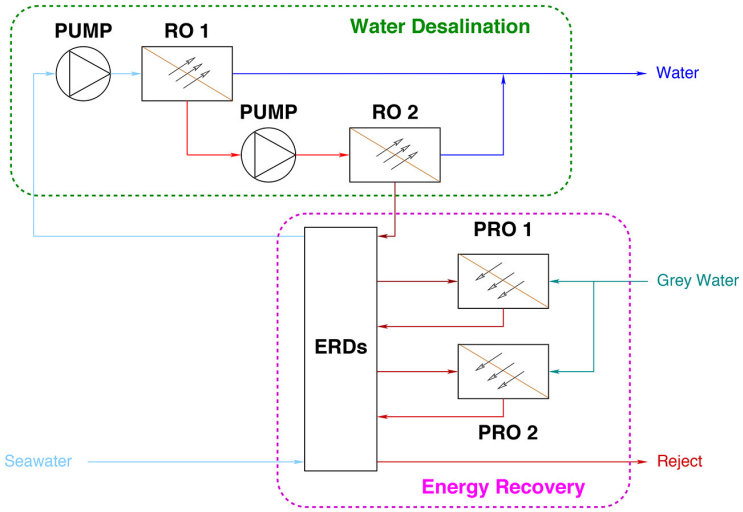

Figure 2.21: Schematic diagram of dual stage hybrid RO-PRO with dual stage RO and dual stage PRO subsystems connected in series [136].

the water recovery rate and osmotic energy recovery, respectively. However, the results showed that the energy recovery by PRO systems are not as drastic as adding ERDs unless a breakthrough in membrane technology makes it economically feasible.

Chapter 3

Methodology

3.1 General

In this chapter, large scale dual stage PRO systems with new configurations are presented and compared to a single stage system. Figure 3.1 presents several configurations of both single and dual stage PRO systems. Schematic diagrams of a simple single stage PRO system and a dual stage PRO both equipped with pumps and turbines are shown in Figures 3.1(a) and (b), respectively. These simple models are presented to be compared with PRO systems that employ pressure exchangers (PX) in order to obtain efficiency improvement, as shown in Figures 3.1(c) to (g).

Two configurations of dual stage PRO systems with PX and two Hydro-Turbines (HT) are proposed in Figures 3.1(d) and (e). The effects of applying various hydraulic pressures to each module are investigated after addition of the second hydro-turbine. Thermodynamically, depressurizing the draw solution before entering the second module may reduce the entropy generation by more even utilization of membrane through the channel.

To compare the dual stage systems with single stage ones Figure 3.1(c) and to find out the effect of adding the second turbine Figure 3.1(g) are presented. To find out the effect of exchanging the high pressure pump with the second PX, the configuration of Figure 3.1(f) is also proposed.

Many different configurations for dual stage PRO employing pressure exchangers, pumps and turbines are possible, and a detailed analysis based on thermodynamic modeling is required to evaluate the merits and failures of the different configurations. It is noted that more complex models might increase the capital cost, while providing

savings in operation. For the subsequent analysis, optimization based on operating cost, not capital cost, is considered.

The length of the membrane for the single stage module is twice the length for each module in the dual stage system; i.e., $L_1 = L_2 = L/2$, where L is membrane length for the single stage module, and L_1 and L_2 are membrane length of first and second modules in a dual stage system, respectively. In terms of capital cost, dual stage PRO modules may need more membrane area in comparison with the single stage PRO systems. However, the same membrane area is used for all configurations presented in the current research.

In the counter-current flow through a module, draw and feed solutions have the opposite flow directions. As elaborated by van der Zwan et al. [137], the counter-current flow gives an approximately 15% higher power output compared to co-current flow. The higher production of power under counter-current flows in PRO systems is due to the more even distribution of salinity. Considering this, all suggested PRO configurations in this research have been studied in the counter-current flow direction.

The efficiency study of the basic single stage and dual stage PRO systems (Figures 3.1(a) and (b)) is followed by evaluation of the other proposed configurations, as shown in Figures 3.1(c) to (g). The proposed configurations employ high pressure pumps (HP), booster pumps (BP), PRO membrane modules, hydro-turbines (HT), and in the case of Figures 3.1(c) to (g) pressure exchangers (PX). The efficiencies of these pumps, turbines and PX play an important role for the overall system performance.

For an ideal pump and turbine system, the isentropic efficiencies are $\eta_P = \eta_T = 1$, where η_P and η_T denote pump and turbine efficiencies, respectively. In practice, these values are typically around 0.9. The current study is conducted assuming realistic efficiencies for all pumps and turbines.

For pressure exchangers, as explained by Bharadwaj et al. [128], in the relevant pressure ranges of PRO systems, pressure losses for high pressure stream ($\delta \mathrm{P}_H$) and low pressure stream ($\delta \mathrm{P}_L$) are approximately $\delta \mathrm{P}_H = \delta \mathrm{P}_L = \delta \mathrm{P} = 0.5$ bar. These pressure losses are atoned by booster pumps in the configurations of Figure 3.1.

In the dual stage system of Figure 3.1(b), the entering volumetric flow of the draw solution ($Q_{D,in}$) has environmental pressure at P_0. After pressurizing to P_{D1}, the flow runs along a semipermeable membrane drawing the fresh water flux $Q_{drawn1} = \int J_{wr1} dL_1$. In this equation, J_{wr1} is fresh water drawn through the membrane from feed to draw solution. The outlet flow from the module 1 (Q_{DL}) is equal to $Q_{D,in}$ +

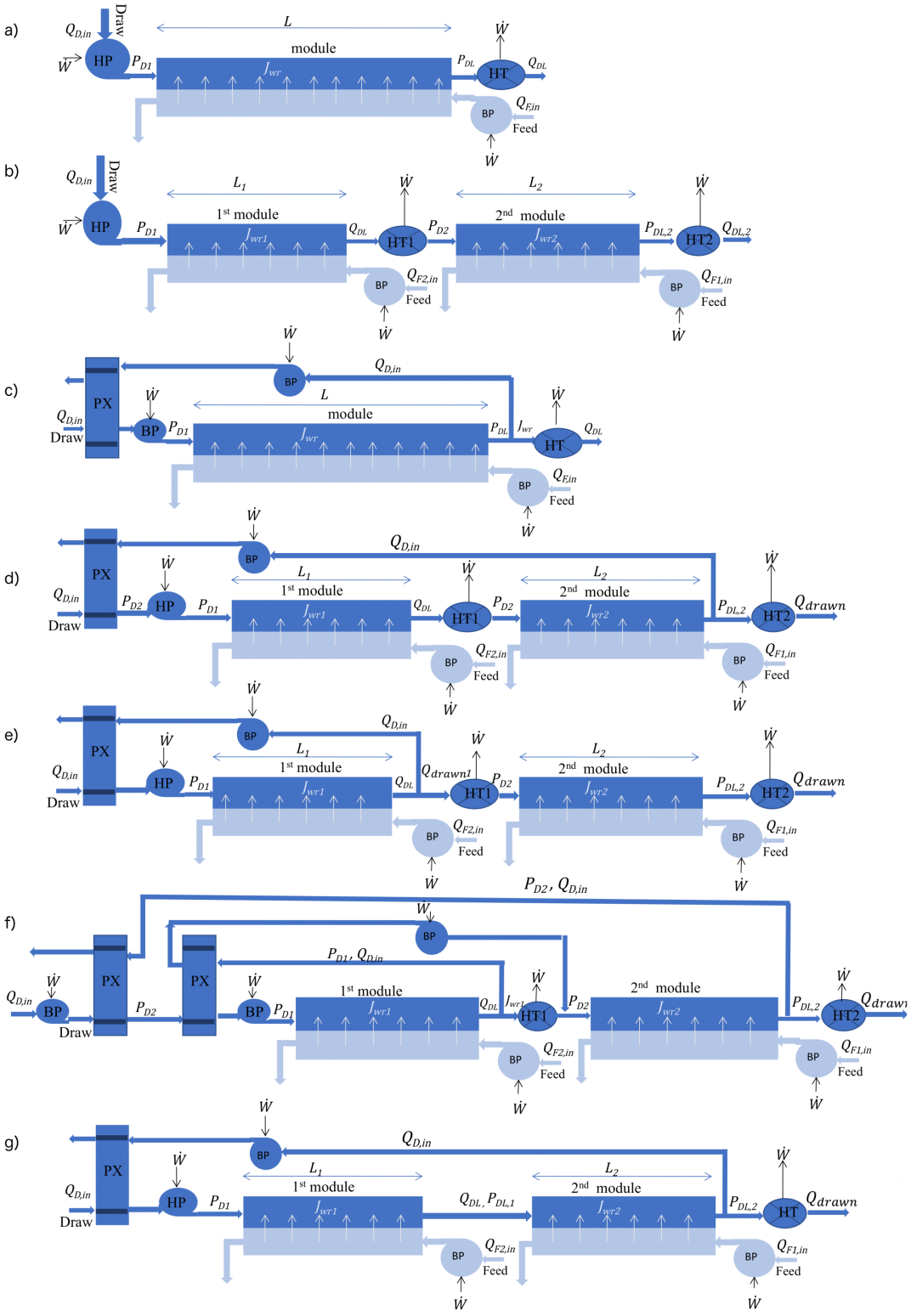

Figure 3.1: Schematic of single and dual stages PRO systems with the same membrane area: (a) Single stage with P-T; (b) dual stage with P-T; (c) single stage with PX; (d) dual stage with 1PX; (e) dual stage PRO with $Q_{D,in}$ back to PX before the HT1; (f) dual stage with 2PX; (g) dual stage system with 1HT

Q_{drawn1}. Due to friction and flow resistance along the membrane, the pressure will drop from P_{D1} to P_{DL} upon exiting the first module. The flow drives the first turbine (HT1) and depressurizes to P_{D2}. At this point, the flow enters the second module at pressure P_{D2} and volumetric flow Q_{DL}. The same procedure happens in module 2, resulting in the exiting volumetric flow $Q_{DL,2} = Q_{DL} + Q_{drawn2}$, with $Q_{drawn2} = \int J_{wr2} dL_2$, where J_{wr2} is defined for module 2 similar to J_{wr1}. Similar to the process in module 1, the pressure will decrease to $P_{DL,2}$. The flow will drive the second turbine (HT2) and discharge to the environmental pressure P_0.

A single stage PRO equipped with a PX is shown in Figure 3.1(c). The PX is added to improve the efficiency of the system. In this configuration, a PX is used to pressurize the draw solution with the flow rate of $Q_{D,in}$ from P_0 to P_{D1} - δP. The internal head loss δP in PX and the frictional pressure drop in the membrane modules are compensated by booster pumps (BP) before the flow enters the module and on the way back to PX, respectively. At the end of the module, the flow splits into Q_{drawn} which runs the HT, and $Q_{D,in}$, which is sent back to the PX, where it is depressurized.

A dual stage PRO system equipped with a PX is shown in Figure 3.1(d). The PX pressurizes the inlet flow from P_0 to P_{D2}. Following this stage, an HP pressurizes the flow to P_{D1}. Then, the flow enters the first module and exits with volumetric flow Q_{DL}. The fluid is depressurized to P_{D2} following the passage through HT1 and then enters to module 2. The outlet fluid from module 2 is divided into two parts. The first part returns to PX with volumetric flow $Q_{D,in}$. The second part enters to HT2 with volumetric flow $Q_{Drawn}(= Q_{Drawn1} + Q_{Drawn2})$.

In a dual stage PRO, the flow returning to the PX can be deviated after the second module or the first module, as shown in Figures 3.1(d) and (e), respectively. In the latter case (Figure 3.1(e)), a PX pressurizes the draw solution from P_0 to P_{D1} - δP to enter the first module. The exiting flow from the first module is divided into $Q_{D,in}$ (back to PX) and Q_{drawn1} (entering to the second module). Q_{drawn1} runs HT1 while depressurizing to P_{D2} and enters the second module. The exiting flow from the second module Q_{drawn} runs the HT2 while depressurizing to P_0. The booster pumps compensate the internal head loss δP in PX and the frictional pressure drop in the membrane modules.

A considerable improvement in system efficiency is anticipated after replacing the HP from Figures 3.1(a) and (b) with PX in Figures 3.1(d) and (e). In Figures 3.1(d) and (e) the difference in the applied pressure between two modules (P_{D1} and P_{D2})

is provided by a HP. If the difference between P_{D1} and P_{D2} is sufficiently large, this HP can also be replaced with a second PX. In order to investigate the efficiency of adding another PX instead of the HP, the configuration shown in Figure 3.1(f) is proposed. In this configuration, the HP is substituted by the second PX. The first PX pressurizes the flow from P_0 to P_{D2}, and the second one pressurizes it from P_{D2} to P_{D1}. The exit flow from the module 1 splits into the two streams of $Q_{D,in}$ and Q_{drawn1}. The $Q_{D,in}$ returns to the second PX at pressure P_{D1} and leaves at P_{D2}. The flow at volumetric rate Q_{drawn1} drives the first turbine. Following the combination with the depressurized flow $Q_{D,in}$, the flow enters the second module at pressure P_{D2}. After the second module, the diluted draw solution is divided into the flows at volumetric flow rates $Q_{D,in}$ and Q_{drawn}. The former returns to the first PX and the latter drives the second turbine.

The last configuration is shown in Figure 3.1(g). The effect of having two counter-current feed flows for each module is investigated [130]. In this configuration, the draw flow after the first module is not depressurized - i.e., there is no HT1. The draw solution with a volumetric rate of $Q_{D,in}$ at pressure of P_0 is pressurized by a PX to P_{D1} and enters module 1. Then it runs into the second module at the pressure of $P_{DL,1}$. The exiting flow is split between $Q_{D,in}$ and Q_{drawn}. $Q_{D,in}$ returns to PX. The remaining flow at Q_{drawn} drives the HT.

3.2 Mass balances of water and solutes in membrane

The study of flow through a membrane is achieved by application of conservation laws. Assuming a constant temperature, thermal effects can be ignored. Therefore, we consider only the conservation laws for mass and momentum.

As shown in Figure 3.2, the volume of a slice of salt water with thickness dx is $V = \int HZdx$, where height of the channel (H) and width of the channel (Z) are given values. Integration of flow over the volume of a slice of salt water will have the compact form

$$\frac{dQ_D}{dx} = -\frac{dQ_F}{dx} = J_{wr}, \tag{3.1}$$

where J_{wr} is the water flux passing through the membrane, and dQ_D and dQ_F are the flow rate differential in the draw and feed solutions, respectively. The difference

in signs is related to the difference in current direction.

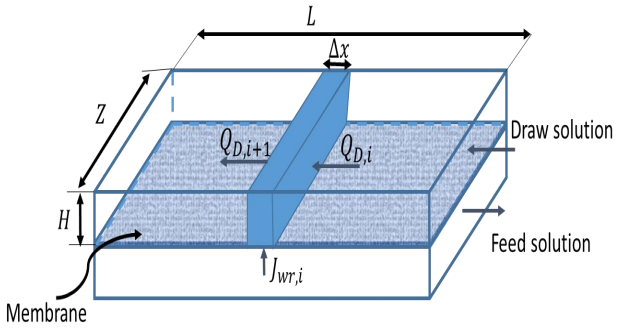

Figure 3.2: Volumetric slice of the draw channel with thickness of Δx, height of the channel (H) and width of the channel (Z)

Mass conservation law for reverse salt flux (molar flux) is the change of salt flow ($d(Q_c)$) in the element of dx, where c_F and c_D is the concentration of dissolved salt in feed and draw solutions, respectively,

$$J_s = \frac{d(Q_F c_F)}{dx} = -\frac{d(Q_D c_D)}{dx}. \tag{3.2}$$

As described in chapter 2 section 2.3.1, the water and salt flux along the active layer are

$$J_{wr} = A(\Delta\pi - \Delta P) = A(\pi_D - \pi_F - \Delta P), \tag{3.3}$$

$$J_s = B(c_{D,m} - c_{F,m}). \tag{3.4}$$

3.2.1 Mass transfer in the feed side

A schematic of mass transfer profile in a membrane module is presented in Figure 3.3. The membranes are not ideal, the solute pass through the active layer and build up within the porous support. The support layer acts as an unstirred boundary layer, resulting internal concentration polarization (ICP). At the surface of the support layer, the concentration of the solute is more than its concentration in the feed solution resulting the external concentration polarization (ECP). Reverse salt flux in feed side is the sum of diffusive and convective components. Diffusion of solute occurs due to salt concentration gradient from the active layer to the boundary layer in the feed side

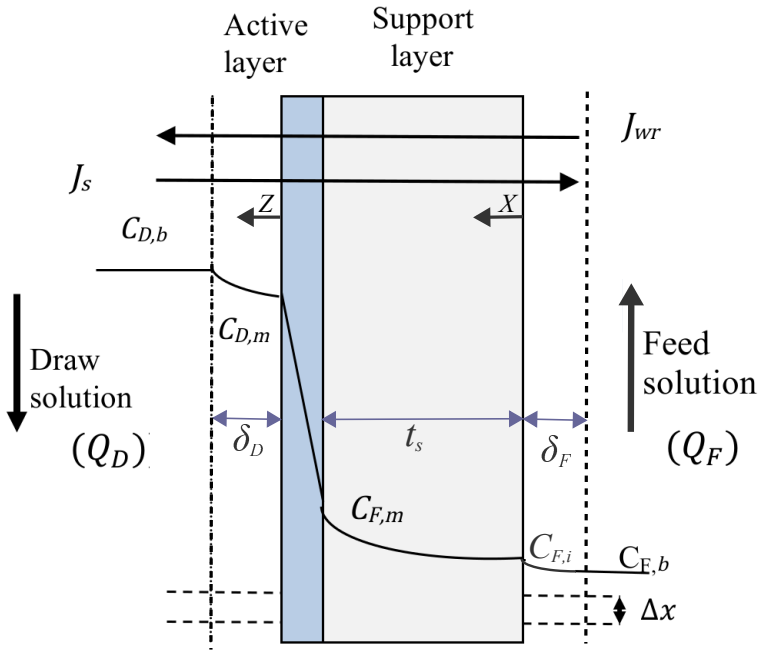

Figure 3.3: A schematic of salt concentration profile in a membrane module.

and the convection happens due to permeation of the water across the membrane,

$$J_s^f = D^s \frac{dc(x)}{dx} - J_{wr} c(x), \tag{3.5}$$

Where J_s^f is the salt flux in the porous support to the feed solution, D^s is the effective diffusion coefficient of the solute that may vary at the support layer and the boundary layer of the feed side. At steady state $J_s = J_s^f$, so that

$$B(c_{D,m} - c_{F,m}) = D^s \frac{dc(x)}{dx} - J_{wr} c(x). \tag{3.6}$$

Boundary conditions are

$$\begin{bmatrix} x = 0, c(x) = c_{F,i} \\ x = t_s, c(x) = c_{F,m}, D^s = \dfrac{D\varepsilon}{\tau} \\ x = -\delta_F, c(x) = c_{F,b}, D^s = D \end{bmatrix} \tag{3.7}$$

Assuming the same diffusion coefficient of draw and feed solutions, t_s is the thickness of support layer, δ_F is the boundary layer in feed solution, D is the bulk diffusion coefficient, ε is the porosity and τ is the tortuosity of the support layer. Also,

$\frac{t_s}{D} = \frac{S(\frac{\varepsilon}{\tau})}{D(\frac{\varepsilon}{\tau})} = \frac{S}{D}$ and $\frac{\delta_F}{D_F} = \frac{1}{k_F}$, where k_F is the mass transfer coefficient in feed solution.

Integrating Eq. (3.6) and substituting boundary conditions,

$$c_{F,m} = c_{F,b}e^{J_{wr}(\frac{1}{k_F}+\frac{S}{D})} + \frac{B(c_{D,m}-c_{F,m})}{J_{wr}}(e^{J_{wr}(\frac{1}{k_F}+\frac{S}{D})}-1), \tag{3.8}$$

3.2.2 Mass transfer in the draw side

As water permeates through the membrane and reaches the draw side, the fresh water needs to be mixed with the draw solution. The salt concentration of solution right after the active layer varies from the bulk draw solution, resulting in ECP. Similar to the feed side, the salt flux equation in the draw solution is composed of diffusive and convective components.

$$J_s^d = D^s\frac{dc(z)}{dz} - J_{wr}c(z), \tag{3.9}$$

At steady state, $J_s = J_s^f$, so that

$$B(c_{D,m}-c_{F,m}) = D^s\frac{dc(z)}{dz} - J_{wr}c(z), \tag{3.10}$$

In the draw side $\delta_D = \frac{D}{k_D}$, where k_D is the mass transfer coefficient in draw solution and the boundary conditions are

$$\begin{bmatrix} z=0, c(z)=c_{D,i} \\ z=\delta_D, c(z)=c_{D,b} \end{bmatrix} \tag{3.11}$$

Integrating Eq. (3.10) and applying boundary conditions

$$c_{D,m} = c_{D,b}e^{(-\frac{J_{wr}}{k_D})} - \frac{B(c_{D,m}-c_{F,m})}{J_{wr}}(1-e^{(-\frac{J_{wr}}{k_D})}), \tag{3.12}$$

Subtracting Eq. (3.8) from Eq. (3.12), the difference of local interfacial concentrations is

$$c_{D,m}-c_{F,m} = c_{D,b}e^{(-\frac{J_{wr}}{k_D})} - c_{F,b}e^{J_{wr}(\frac{1}{k_F}+\frac{S}{D})} + \frac{B(c_{D,m}-c_{F,m})}{J_{wr}}[e^{(-\frac{J_{wr}}{k_D})} - e^{J_{wr}(\frac{1}{k_F}+\frac{S}{D})}],$$

or

$$c_{D,m} - c_{F,m} = \Delta c_m = \frac{c_{D,b} e^{(-\frac{J_{wr}}{k_D})} - c_{F,b} e^{J_{wr}(\frac{1}{k_F}+\frac{S}{D})}}{1 + \frac{B}{J_{wr}}[e^{J_{wr}(\frac{1}{k_F}+\frac{S}{D})} - e^{(\frac{J_{wr}}{k_D})}]}, \tag{3.13}$$

Assuming the validation of the van't Hoff equation, osmotic pressure is linearly proportional to the salt concentration. Substituting Eq. (3.13) in Eq. (3.3) the expression for the water flux considering ECP and ICP effects is

$$J_{wr} = A \left\{ \frac{\pi_D e^{\frac{-J_{wr}}{k_D}} - \pi_F e^{J_{wr}(\frac{1}{k_F}+\frac{S}{D})}}{1 + \frac{B}{J_{wr}}[e^{J_{wr}(\frac{1}{k_F}+\frac{S}{D})} - e^{-\frac{J_{wr}}{k_D}}]} - \Delta P \right\}, \tag{3.14}$$

and substituting Eq. (3.13) in Eq. (3.4) the salt flux is

$$J_S = B \left\{ \frac{c_D e^{\frac{-J_{wr}}{k_D}} - c_F e^{J_{wr}(\frac{1}{k_F}+\frac{S}{D})}}{1 + \frac{B}{J_{wr}}[e^{J_{wr}(\frac{1}{k_F}+\frac{S}{D})} - e^{\frac{-J_{wr}S}{k_D}}]} \right\}. \tag{3.15}$$

In this study, the mass transfer coefficient of draw and feed solution are assumed to be the same $k_F = k_D$. The model is considered to be relatively accurate and has been validated by experiments for flat sheet membranes [138, 139, 140]. As an example, a comparison by Altaee et al. [140] showed 6% deviation of the model and the experimental data from [58]. In PRO modules, the model has been validated for both spiral wound [141] and hollow fiber membrane modules [142, 95]. The model, accepted to be valid, has also been used in experimental studies to find the structural parameter in spiral wound membrane modules [143].

3.3 Momentum balance

The pressure losses in the membrane modules are determined from the balance of momentum. Pressure loss is caused by friction in the channel and is related to the size of the channel, the flow rates, and the friction factor. Similar to mass balance, diffusion due to composition variation of the solution is ignored and thermal effects are ignored. Integration over a slice of salty water of volume dV, the momentum balance equation assumes the form

$$\int_V \frac{\partial(\rho v_i v_k + P\delta_{ik} - \sigma_{ik})}{\partial x_k} dV = 0, \tag{3.16}$$

where ρ is the mass density of the flow, v_i is the flow velocity, P is the pressure, and σ_{ik} are viscous stresses. Considering $V = HZdx$ (see Figure 3.2) and applying the Gauss theorem, Eq. (3.16) assumes the form

$$\int_{\partial V} \partial(\rho v_i v_k + P\delta_{ik} - \sigma_{ik}) n_k dA = 0, \tag{3.17}$$

where ∂V is the surface of V, and n_k is the outward normal. Since there are no boundary effects along z direction, the longitudinal component for the momentum equation is

$$\begin{aligned} Z \int_{-H/2}^{H/2} [\rho(x+dx,y)v_x^2(x+dx,y) - \rho(x,y)v_x^2(x,y)dy]dy \\ +HZ[P(x+dx) - P(x)] - \int_{\partial V} \sigma_{xk} n_k dA = 0, \end{aligned} \tag{3.18}$$

In Eq. (3.18), considering a plug flow condition, the volumetric flow rate in x direction is $Q = \frac{\dot{V}}{HZ}$, where Q is the average volumetric flow along the membrane and $\dot{V}$ is the flow rate. By averaging the first term, Eq. (3.18) turns to

$$\frac{1}{HZ}\frac{d(\rho Q^2)}{dx}dx + HZ\frac{d\Delta P}{dx}dx = \int_{\partial V} \sigma_{xk} n_k dA, \tag{3.19}$$

Integrating the above equation over the surface Zdx when side forces are ignored, gives

$$\frac{1}{HZ}\frac{d(\rho Q^2)}{dx} + HZ\frac{d\Delta P}{dx} = Z\sigma_{xy}^w, \tag{3.20}$$

where σ_{xy}^w is the average surface stress at the membrane. The Darcy friction factor f is defined as

$$f = \frac{8\left|\sigma_{xy}^w\right|}{\rho v^2}, \tag{3.21}$$

so the momentum equation can be written as:

$$\frac{d(\rho Q^2)}{dx} + (HZ)^2\frac{d\Delta P}{dx} = -\frac{f_{mix}}{8}\frac{\rho Q^2}{H}, \tag{3.22}$$

f_{mix} is the modified friction factor in the presence of spacers [144].

3.4 Mass transfer and frictional pressure drop

As discussed in section 2.3.2, the thickness of polarization boundary layer in draw and feed solutions (δ_D and δ_F) affect the effective osmotic pressure and the driving force for water permeation. To minimize the effect of ICP and ECP and accordingly for proper operation of the system, it is essential that the permeated freshwater entering the draw side is effectively mixed with the saltwater. If the permeated freshwater is not mixed effectively, the local osmotic pressure will decrease drastically. Hence, successful mixing is imperative for proper operation.

The effective mixing can be achieved by introducing spacers into the channel. Indeed, spacers have a dual function of providing mechanical support for the membranes and being vortex promoters in channels. Spacers induce more flow resistance due to the increased friction. CFD studies on flow patterns near obstacles show spiral and erratic motions [145, 146].

In comparison to laminar flow, the existing flow regime has more flow resistance, due to an additional irreversibility. In this condition, there is an interaction between the pressure drop due to friction and an improvement of mass transportation (mixing). The former decreases the net work, while the latter increases it. To find the best performance, it is necessary to optimize the spacers' configuration. Schock and Miquel [147] measured mass transfer and flow resistance in flat channels and spiral wound modules filled with various commercial spacers. In the current study, a simple geometry of non-woven net spacers is considered. The relation between the mass transfer and power dissipation (in terms of pressure losses) is attained by using the results obtained from Li et al. [148].

The spacer geometrical parameters include the distance between spacer filaments $l_1 = l_2$, where $l = l_1 + l_2$, angle between the spacer filaments β, channel height H, and flow attack angle α as in Figure 3.4.

Li et al. [148] found the optimum geometrical values as $H/l = 4$, $\alpha = 30°$, and $\beta = 120°$. They introduced a dimensionless power number P_n which is the normalized value of pressure drop in the channel which is correlated with Reynolds number (Re). Moreover, it can be related to the Sherwood number (Sh) which is related to effective diffusion coefficient (d). Considering the relations between the aforementioned parameters, it is possible to show the effect of changes in Reynolds number as a turbulence factor and the trade-off between pressure drop due to friction and enhancing mass transport.

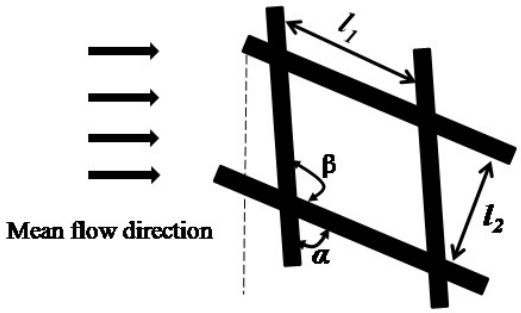

Figure 3.4: The geometric parameters of a non-woven spacer

For a wide channel, where side effects can be ignored ($Z \gg H$), the hydraulic diameter is $D_H = 2H$, and the Reynolds number is

$$Re = \frac{D_H \rho v}{\eta} = \frac{2H_\rho v}{\eta} = \frac{2Q}{\nu}, \tag{3.23}$$

where ν= 1.57 $\times$ 10^{-6} m^2/s is the kinematic viscosity. In [148], the following contributions are found,
Power number as

$$P_n = 5Re^{2.6}, \tag{3.24}$$

Sherwood number as

$$Sh = 2.5P_n^{0.25}. \tag{3.25}$$

By definition Sherwood number is

$$Sh = \frac{kH}{d}, \tag{3.26}$$

k is the mass transfer coefficient for the membrane and d is the effective diffusion coefficient. The friction factor is given as [148]

$$f_{mix} = \frac{p_n}{Re^3} = 5Re^{-0.4}, \tag{3.27}$$

Considering Eqs. (3.24) to (3.27) and Eq. (3.22) the pressure drop along the channel is known and the balance of momentum becomes

$$\frac{(\rho Q^2)}{dx} + (HZ)^2 \frac{d\Delta P}{dx} = -\frac{Pn}{8Re^3} \frac{\rho Q^2}{H}. \tag{3.28}$$

The mass transfer is updated along the module by updating d value.

3.5 PRO modeling

The inlet volumetric flow of draw (Q_D) and feed solutions (Q_F), as well as hydraulic pressures of the first (P_{D1}) and the second (P_{D2}) module are variable parameters which must be optimized in order to find the maximum power output.

The selection of membrane parameters appropriate for PRO was studied in detail by Wang et al. [149]. However, most PRO membranes are on laboratory scale and still need to be tested on larger scales.

The selected parameters in this paper are listed in Table 3.1. Some of the selected parameters are based on the values presented by Wei et al. [150].

Table 3.1: Parameters used in PRO model

Model parameters	Values
Water permeability, A [m s $^{-1}$Pa^{-1}]	4.86×10^{-12} [150]
Salt permeability, B [m s^{-1}]	4.44×10^{-8} [150]
Structural parameter, S [m]	307×10^{-6} [150]
Temperature, $T[K]$	298
Diffusion coefficient of salt, D [m^2 s^{-1}]	1.49×10^{-9} [150]
Draw solution concentration, c_D [mol m^{-3}]	600
Feed solution concentration, c_F [mol m^{-3}]	0
Mass transfer coefficient, k [m s^{-1}]	3.85×10^{-5} [150]
Membrane length, L [m]	15 for single module, 7.5 for dual stage modules
Membrane width, Z [m]	1
Flow channel height, H [m]	0.001
Pump, turbine efficiency	0.9

The mass transfer of water and salt fluxes in Eqs. (3.14) and (3.15) need to be solved for a differential element. Then, the results need to be related to changes in water flow rates and solute concentrations based on mass balance in Eqs. (3.1) and (3.2). Hence, on both, the draw and feed sides, water flux (J_{wr}) is obtained from Eqs. (3.1) and (3.14) and the reverse salt flux (J_s) equations are drrivedas expressed in Eqs. (3.2) and (3.15). The updates for the pressure drop is obtained from Eq. (3.28) and the mass transfer coefficient is updated by updating Eqs. (3.14) and (3.15) with Eq. (3.26).

The volumetric flow rates, osmotic and hydraulic pressures, salt concentrations and mass transfer in both draw and feed solutions are updated by marching along the membrane with $\Delta x = \frac{L}{n}$ where n is the number of grid points. The marching is at the same direction in both draw and feed channels.

3.6 Quantifying the system performance

For the system with pump and turbine, the general power equations for pump and turbine are

$$\dot{W}_P = \frac{1}{\eta_P} Q(P_{in} - P_{out}) < 0, \tag{3.29}$$

$$\dot{W}_T = \eta_T Q(P_{in} - P_{out}) > 0, \tag{3.30}$$

where $\dot{W}_P$ and $\dot{W}_T$ are the power required to pressurize or obtained from depressurizing in pump and turbine, respectively, and Q is the volumetric flow rate. P_{in} and P_{out} are input and output pressures, respectively. Net power output is the sum of pump and turbine powers,

$$\dot{W}_{net} = \dot{W}_T + \dot{W}_P. \tag{3.31}$$

As shown in Figure 3.1, seven different configurations are suggested. Power outputs corresponding to each configuration are presented in Eqs. 3.32 to 3.39:

For the single stage system equipped with pump and turbine (Figure 3.1(a)), the power output is

$$\dot{W}_{net} = \eta_T Q_{DL}(P_{DL} - P_0) - \frac{1}{\eta_P} Q_{D,in}[(P_{D1} - P_{DL}) + Q_{F,in}(P_{F1} - P_0)], \tag{3.32}$$

For the dual stage system equipped with pump and turbine (Figure 3.1(b)), the power output is

$$\begin{aligned} \dot{W}_{net} = {} & \eta_T[Q_{DL}(P_{DL} - P_{D2}) + Q_{DL,2}(P_{DL,2} - P_0)] - \frac{1}{\eta_P}[Q_{D,in}(P_{D1} - P_0 \\ & + Q_{F1,in}(P_{F1} - P_0) + Q_{F2,in}(P_{F2} - P_0)], \end{aligned} \tag{3.33}$$

In the presence of PX, the required work for booster pumps to compensate the pressure loss of PX ($\delta \dot{W}_{PX}$) is

$$\dot{W}_{PX} = Q_{D,in}(\delta P_H + \delta P_L) = 2Q_{D,in}\delta P, \tag{3.34}$$

For the single stage system with the pressure exchanger (Figure 3.1(c)), the power output is

$$\dot{W}_{net} = \eta_T Q_{drawn}(P_{DL} - P_0) - \frac{1}{\eta_P}[Q_{D,in}(2\delta P + (P_{D1} - P_0)) + Q_{F,in}(P_F - P_0)], \quad (3.35)$$

For the dual stage system with 1 pressure exchanger (1PX) shown in Figure 3.1(d), the power output is

$$\dot{W}_{net} = \eta_T[Q_{DL}(P_{DL} - P_{D2}) + Q_{drawn}(P_{DL,2} - P0)] - \frac{1}{\eta_P}[Q_{D,in}((P_{D1} - P_{DL2}) + 2\delta P) + Q_{F1,in}(P_{F1} - P_0) + Q_{F2,in}(P_{F2} - P_0)], \quad (3.36)$$

For the dual stage system with (1PX) that drives back to the PX before the first HT (Figure 3.1(e)), the power output is

$$\dot{W}_{net} = \eta_T[Q_{Drawn1}(P_{DL} - P_{D2}) + Q_{drawn}(P_{DL,2} - P0)] - \frac{1}{\eta_P}[Q_{D,in}((P_{D1} - P_{DL}) + 2\delta P) + Q_{F1,in}(P_{F1} - P_0) + Q_{F2,in}(P_{F2} - P_0)], \quad (3.37)$$

For the dual stage system with 2 pressure exchangers (2PX) showed in Figure 3.1(f), the power output is

$$\dot{W}_{net} = \eta_T[Q_{Drawn1}(P_{DL} - P_{D2}) + Q_{drawn}(P_{DL,2} - P_0)] - \frac{1}{\eta_P}[Q_{D,in}(P_{D1} - P_{DL} + P_{D2} - P_{DL2} + 4\delta P) + +Q_{F1,in}(P_{F1} - P_0) + Q_{F2,in}(P_{F2} - P_0)], \quad (3.38)$$

Finally, for the dual stage system with 1PX and 1HT (Figure. 3.1(g)), the power output is

$$\dot{W}_{net} = \eta_T[Q_{Drawn}(P_{DL2} - P_0)] - \frac{1}{\eta_P}[Q_{D,in}((P_{D1} - P_{DL2}) + 2\delta P) + Q_{F1,in}(P_{F1} - P_0) + Q_{F2,in}(P_{F2} - P_0)], \quad (3.39)$$

3.7 Target functions for optimization

Considering Eqs. (3.29) and (3.30), power output depends on pressures and volumetric flow rates. Therefore, they have to be chosen in order to achieve an optimum system performance. Based on the application, there are several methods to optimize the system performance. Note that the goal of all these methods is to make PRO economically feasible. To achieve this goal, most previous research has focused on optimizing for power density (PD) or specific energy (SE).

Power density is defined as the extractable work per membrane area [46],

$$PD = \frac{\dot{W}_{net}}{A_m}, \tag{3.40}$$

where $\dot{W}_{net}$ is the system power output and A_m is the total membrane area. Power density reflects the importance of membranes in PRO systems. Consideration of capital cost for the membrane and its partial maintenance cost are the rationale behind the consideration of the PD. Hence, the efficiency and utilization of membrane area is of great importance. Optimizing the PD results in smaller membrane area and obtaining higher power output per area.

The second target function is specific energy (SE) which is defined as extracted energy per inlet flow rates of draw and feed solutions.

$$SE = \frac{\dot{W}_{net}}{Q_{F,in} + Q_{D,in}}, \tag{3.41}$$

$Q_{F,in}$ and $Q_{D,in}$ are inlet volumetric flow rates of feed and draw solutions, respectively. For dual stage PRO systems, $Q_{F,in} = Q_{F1,in} + Q_{F2,in}$, where $Q_{F1,in}$ and $Q_{F2,in}$ are inlet flow rates of feed solutions in the first and second module, respectively. Specific energy should be considered when the energetic costs of pumping and water pretreatment are important or the accessible amounts of draw and fresh water are restricted. The cost of pretreatment and pumping will increase with increasing the flow of water on each side of the membrane. SE can be used as an indicator of energy efficiency for the system.

Since optimization is based on the availability of fresh water rather than salt water, the optimization process can also be conducted based on drawn freshwater along the

module. Hence, the extracted work per liter of drawn fresh water is defined as

$$W_{drawn} = \frac{\dot{W}_{net}}{Q_{drawn}}, \tag{3.42}$$

Each of the above descriptions are used as a target function for optimization, while P_{D1}, P_{D2}, $Q_{F1,in}$ and $Q_{F2,in}$ are variable parameters.

3.8 Thermodynamic analysis of PRO system

The Gibbs free energy of mixing is the thermodynamic upper bound of the energy. The maximum extractable energy of mixing two solutions with different salinities can be attained via a thermodynamically reversible process. A thermodynamically reversible process in the PRO system can be conducted by keeping the applied hydraulic pressure infinitesimally below the osmotic pressure.

In general, the work supplied to the plant can be obtained from the Gibbs free energy of mixing, $\Delta\dot{G}$,

$$\dot{W} = -T\dot{S}_{gen} - \Delta\dot{G}, \tag{3.43}$$

where T is temperature, $\dot{S}_{gen}$ is entropy generation, and $\Delta\dot{G}$ is the Gibbs free energy per unit time. Any generation of entropy due to irreversible process reduces the work output.

Assuming an ideal mixture, the Gibbs free energy of mixing is

$$\Delta\dot{G} = \bar{R}T\sum_{out}\dot{n}_\alpha X_\alpha \ln(X_\alpha) - \sum_{in}\dot{n}_\alpha X_\alpha \ln(X_\alpha), \tag{3.44}$$

where $\bar{R}$ is the universal gas constant, $\dot{n}_\alpha$ is the mole flow of component α, X_α is the corresponding mole fraction. For reversible work, $\dot{S}_{gen} = 0$ and considering draw and feed solution Eq. (3.44) turns to

$$\begin{aligned}\dot{W}_{rev} = -\Delta\dot{G} = \bar{R}T[&\dot{n}_D^{in}X_D^{in}\ln(X_D^{in}) + \dot{n}_D^{in}(1-X_D^{in})\ln(1-X_D^{in}) \\ &+ \dot{n}_F^{in}X_F^{in}\ln(X_F^{in}) - (\dot{n}_D^{out}X_D^{out}\ln(X_D^{out}) + \dot{n}_D^{out}(1-X_D^{out})\ln(1-X_D^{out}) \\ &+ \dot{n}_F^{out}X_F^{out}\ln(X_F^{out}) + \dot{n}_F^{out}(1-X_F^{out})\ln(1-X_F^{out}))],\end{aligned} \tag{3.45}$$

where D and F indicate draw and feed solutions, respectively. Since $X_F^{in} = X_F^{out} = 1$, and assuming a dilute solution at both the draw and feed sides, Eq. (3.45) can be

simplified to

$$\dot{W}_{rev} = -\Delta\dot{G} = i\bar{R}T[\dot{n}_{D^{in}} X_D^{in} \ln(X_D^{in}) - \dot{n}_{D^{out}} X_D^{out} \ln(X_D^{out}) - \dot{n}_{F^{out}} X_F^{out} \ln(X_F^{out})], \tag{3.46}$$

Assuming negligible contribution of solute to the volume of the solution and dividing Eq. (3.46) to the volume of mixed solution, the Gibbs free energy per volume of total mixed solution is achieved. The resulting quantity is obtained as a function of molar concentrations of the draw and feed solutions (C_D and C_F), as well as volumetric flow of salt and water in the draw and feed solutions (Q_D and Q_F),

$$\Delta\dot{G} = i\bar{R}T[Q_{D,in}c_{D,in} \ln(c_{D,in}) - Q_{D,out}c_{D,out} \ln(c_{D,out}) - Q_{F,out}c_{F,out} \ln(c_{F,out})], \tag{3.47}$$

The total work loss then can be expressed as

$$\dot{W}_{loss} = \dot{W}_{rev} - \dot{W}_{net}. \tag{3.48}$$

The sources for irreversible energy loss in a PRO system with PX, pump and turbine can be listed as follows

1. water and salt transfer through the membrane;
2. Pressure drop in pressure exchanger;
3. Pressure drop along the membrane in both sides;
4. in pump; and
5. in turbine.

Considering the water quality in British Columbian rivers, the work loss related to pretreatment of the feed solution, which is considerable (estimated around 0.1-0.4 kWhm^{-3} [14]), is ignored in this study.

Work loss of water transfer in the module is

$$\dot{W}_{loss}^{water} = T\dot{S}_{gen}^{water}, \tag{3.49}$$

where T is the temperature and $\dot{S}_{gen}^{water}$ is the entropy generation due to water transfer. The entropy generation is

$$\dot{S}_{gen}^{water} = \int \sigma_{gen}^{water} dA, \tag{3.50}$$

where A is the membrane area and σ_{gen}^{water} is the entropy generation per membrane area, as

$$\sigma_{gen}^{water} = \frac{\dot{n}_v}{T}(\bar{\mu}_v^D - \bar{\mu}_v^F), \tag{3.51}$$

$\dot{n}_v$ is the mole flow of water, $\bar{\mu}_v^D$ and $\bar{\mu}_v^F$ are the chemical potential of water at draw and feed side, respectively.

$$(\bar{\mu}_v^D - \bar{\mu}_v^F) = \bar{V}_w(\Delta_P - \Delta\pi), \tag{3.52}$$

and,

$$\dot{n}_v = \int J_v dA, \tag{3.53}$$

where J_v is the mole flux which has the relation of $J_v = \frac{J_{wr}}{\bar{v}_w}$. Considering the equations (3.49 -3.53) the work loss for water is

$$\dot{W}_{loss}^{water} = \sum_{i=1}^{n} J_{wr}(\Delta P - \Delta\pi)\Delta x. \tag{3.54}$$

For the salt transfer through the membrane

$$\dot{W}_{loss}^{salt} = \sum_{i=1}^{n} J_s R \ln(\frac{c_D}{c_F})\Delta x. \tag{3.55}$$

Work loss of pressure exchanger is

$$\dot{W}_{loss}^{PX} = Q_{D,in} 2\delta P. \tag{3.56}$$

Work loss of pressure drop in the membrane considering both draw and feed solutions is

$$\dot{W}_{loss}^{mem} = \frac{Q_{F,in} + Q_{F,out}}{2}(P_{F,in} - P_0) + \frac{Q_{D,in} + Q_{D,out}}{2}(P_{D,in} - P_{D,out}). \tag{3.57}$$

Work loss of pump is

$$\dot{W}_{loss}^{P} = \dot{W}_{irr}^{P} - \dot{W}_{rev}^{P} = (\frac{1}{\eta_P} - 1)\dot{W}_{rev}^{P}. \tag{3.58}$$

$$\dot{W}^{P}_{loss} = (\frac{1}{\eta_P} - 1)[Q_{D,in}(2\delta_P + (P_{D,in} - P_{D,out})) + Q_{F,in}(P_{F,in} - P_0)]. \quad (3.59)$$

Work loss of turbine is

$$\dot{W}^{T}_{loss} = (1 - \eta_T)Q_{drawn}(P_{D,out} - P_0). \quad (3.60)$$

Total work loss is the sum of all work losses

$$\dot{W}_{loss} = \dot{W}^{water}_{loss} + \dot{W}^{salt}_{loss} + \dot{W}^{PX}_{loss} + \dot{W}^{mem}_{loss} + \dot{W}^{P}_{loss} + \dot{W}^{T}_{loss}. \quad (3.61)$$

Equations 3.43 to 3.61 will be used in chapter 4 section ... for thermodynamic analysis of the system performance.

3.9 Optimization of PRO modules

Applying target functions on all configurations leads to choose the best operative target function on presented dual stage PRO configurations. This target function upon with related configurations will be used to optimize the PRO module in terms of membrane length and characteristics, and draw and feed solution sources.

3.9.1 Arrangement of membrane module

The driving force for water permeation decreases along the membrane module. Based on the selected configuration, the optimum length for each module may vary. There is a point that the amount of water permeation cannot compensate for the losses in the module anymore. To avoid the losses due to unnecessary flow in the module, the membrane has to be cut at this point. To harvest maximum specific energy, the optimum length of the membrane may alter for each configuration due to the variation of inlet draw solution. To find the optimum length of each configuration, the length of the membrane varied from 1-10 m in each module in the model. The maximum obtained SE for each configuration then compared to the single stage PRO system with the same membrane length.

3.9.2 Membrane characteristics

Efficiency in the PRO process highly depends on developing membranes with high water permeability while minimizing the reverse salt flux and accumulation of the salt in boundary and support layer of the membrane. The highly porous support layer will minimize internal concentration polarization that enhances PRO performance. In addition to the minimal structural parameter (S), an ideal membrane for PRO application should have high water permeability of active layer (A) coupled with low salt permeability (B). In reality, there is a trade-off between A and B, since as the membrane becomes more permeable to water, an increase in the salt permeability accompanies it. In this study, hypothetical membranes are assumed to identify the effect of each membrane parameter on the performance of the presented configurations. As shown in Table 3.2, the membrane that is used in the model is assumed as the reference membrane. Each parameter is improved 4 times offering a new membrane and the best values for A, B, and S are used as the best-case scenario (M2-M5). It should be noted that membrane characteristics have been applied on optimized membrane length obtained from the previous section.

Table 3.2: Proposed membrane characteristics

Membrane	A [10^{-9} m s $^{-1}$Pa^{-1}]	B [10^{-7}m s^{-1}]	S [10^{-6} m]
M1 (Ref.)	4.86	0.44	307
M2	20	0.44	307
M3	4.86	0.10	307
M4	4.86	0.44	75
M5	20	0.10	75

3.9.3 Draw and feed solution sources

At a given hydraulic pressure, power output can be increased by increasing the osmotic pressure gradient across the PRO membrane. Therefore, salinity gradient resource should be given more attention in the design of the osmotic power plant. The higher the osmotic pressure gradient across the PRO membrane is, the higher the power generated by the PRO process.

Dual stage PRO modules have the advantage of selecting various feed solution entering each module. As for draw solution source, RO brine has been intensively

used for PRO systems [121, 120, 151, 114, 152]. Therefore, the effect of selecting RO brine as draw solution source is investigated. The selected sources are RO brine and seawater as draw solution and sea water, and fresh water as feed solutions. The salt consecration of RO brine and fresh water as draw and feed solution sources are 1300 and 0 $\frac{mol}{m^3}$, respectively.

Chapter 4

Results and Discussions

4.1 Variations along the membrane length in PRO

To gain a detailed insight into the membrane module and find out what happens to each parameter along the membrane length, some spatial variations are studied. It will result in monitoring the water and salt permeation behavior along the membrane and corresponding volumetric flows in draw and feed solutions. The membrane length for single stage scaled-up PRO module is assumed to be 15 m. For single stage PRO Figure 3.1 (c), spatial variations of osmotic pressures (π_D and π_F), applied hydraulic pressures (P_D and P_F), and concentrations (c_D and c_F) between the membrane inlet at $x = 0$ and the membrane outlet at $x = 15$ m are illustrated in Figure 4.1 for draw and feed solution sides. The configuration is in the counter-current flow which draw and feed solutions have the opposite directions. Therefore, as can be seen in Figure 4.1 in the feed solution the x direction is the opposite of the draw solution.

Permeated water flux J_{wr} dilutes the bulk draw solution along the membrane as fresh water is added from the feed solution, hence the draw solution concentration (c_D) drops along the membrane (Figure 4.1(a)). Reverse salt flux (J_s) from the draw solution makes the bulk feed solution concentration (c_F) to increase along the membrane module (Figure 4.1(b)). The changes in c_D and c_F along the module is obtained from Eq. (3.2). It is assumed that the densities remain constant along the membrane length.

A drop in the draw solution concentration (c_D) causes the related osmotic pressure (π_D) to drop accordingly based on the van't Hoff equation (Eq. (2.1)). As can be seen in Figure 4.1(d), the same trend occurs in the feed solution when the osmotic pressure

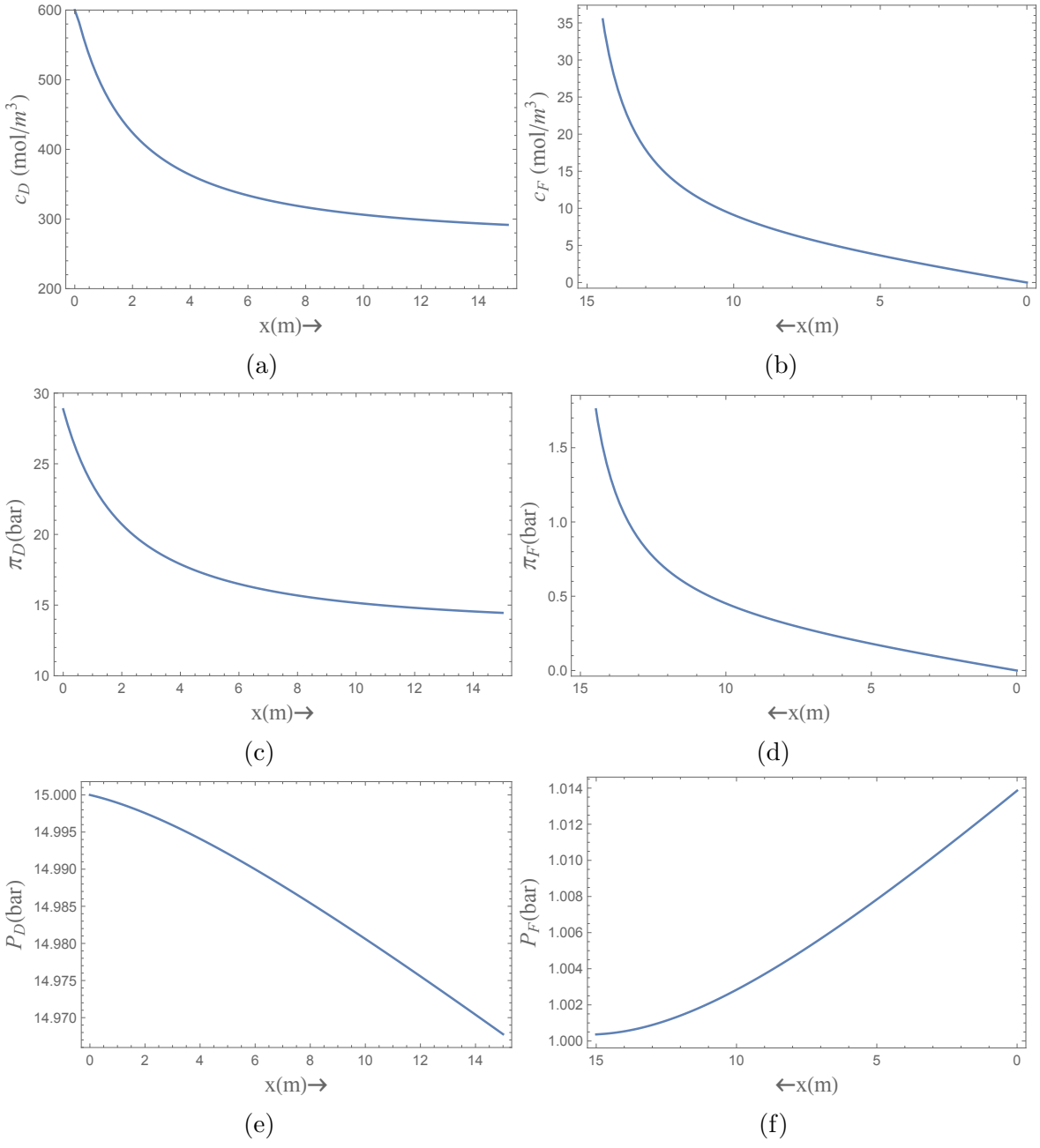

Figure 4.1: (a) and (b) Salt concentration of draw and feed solutions (c_D, c_F); (c) and (d) Osmotic pressure of draw and feed solutions (π_D, π_F); (e) and (f) Hydraulic pressure of draw and feed solutions (P_D, P_F) in the case of optimal power production in single stage PRO systems with PX (configuration (c)) for the counter-current flow.

inclines with the increase of the feed solution concentration along the membrane. The effective osmotic pressure difference ($\Delta\pi_{eff} = \pi_D - \pi_F$) drop along the membrane has a detrimental effect on the driving force of the fresh water permeation through the membrane.

The concentration difference drop along the membrane leads to a reduction in the power output due to the drop in osmotic pressure gradient. This drop can be more severe in co-current draw and feed flows since concentration drop in the draw solution is synchronized with concentration incline in the feed solution. However, in the counter-current flow scheme the concentration gradient is kept in maximum possible. Counter-current flow of draw and feed solutions helps to hinder the drop in effective osmotic pressure.

Pressure drop along the module affects the power output and often is ignored since most of the studies are in laboratory scale and the pressure loss is negligible in them. However, in a scaled-up module, the pressure drop is more significant and needs to be studied. As can be seen in Figure 4.1(e) and (f), the pressure drop along the membrane due to the frictional loss in the channel is more significant in the draw solution side than the feed solution side. The pressure loss depends on the size of the channel, the flow rates and the friction factor. The flow rate in the draw side is more than the feed side causing more pressure loss. It means that as flow rates increase so will parasitic pressure losses. The updates for the P_D and P_F in each interval are obtained from Eq. 3.28.

When all the variations along the membrane length are taken to account, the fundamental water and reverse salt flow rate equations (Eqs. 3.14 and 3.15) will also change with the position of x along the membrane length. This update can be achieved by inputting the updated values of concentrations, osmotic pressures, and pressure losses in Eqs. 3.14 and 3.15. The result will be diminishing the freshwater flux along the membrane as the driving force for water permeation ($\Delta\pi_{eff} - \Delta P$) will drop along the module and reverse salt flux will incline at the same time (see Figure 4.2 (a) and (b)). As clearly can be seen in Figure 4.2 (a), more than 80% of the water permeation happens only in the first half of the membrane length. It implies that the membrane is unevenly used in terms of freshwater flux though the membrane. More even utilization of the membrane is our main motivation toward proposing dual stage systems that rejuvenates the water permeation by depressurizing the draw solution after the first module.

The freshwater permeation from the feed solution to the draw solution causes the

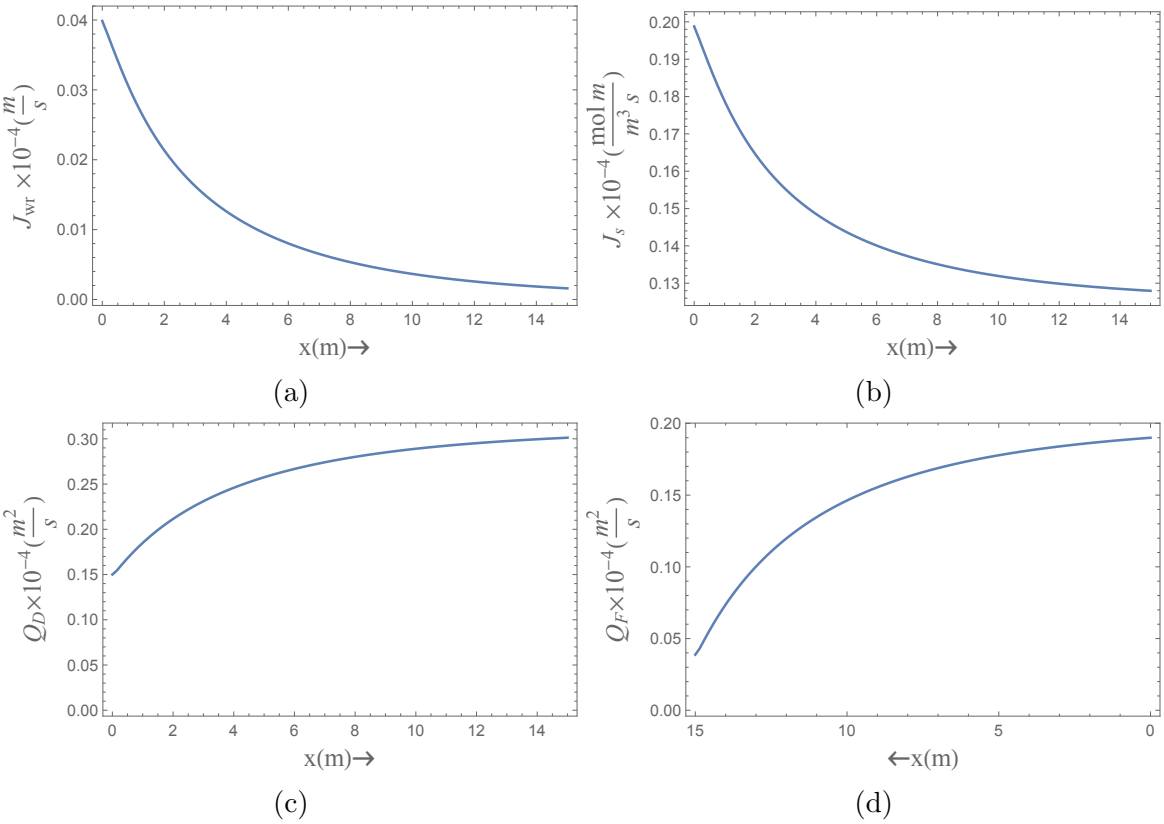

Figure 4.2: (a) and (b) Permeated water (J_{wr}) and reverse salt flux (J_s); (c) and (d) Volumetric flow rate of draw and feed solutions (Q_D, Q_F) in the case of optimal power production in single stage PRO systems with PX (configuration (c)) for the counter-current flow.

feed flow rate to decrease along the membrane and the draw solution to increase as it flows along the membrane (figure 4.2 (c) and (d)). The draw and feed solutions flow rate (Q_D and Q_F) in each interval is obtained from Eq. 3.1. The curves will be flatter along the membrane due to diminishing freshwater flux.

The draw and feed flux changes along the module also affect the thickness of the polarization boundary layers. As the draw flow rate increases along the module, the mixing improves and the boundary layer in draw solution (δ_D) (Figure 3.3) shrinks. On the contrary, the feed boundary layer (δ_F) increases due to the flow rate drop along the module. As a result, the concentration polarization becomes more significant in the feed side while it becomes more relaxed in the draw solution. This effect is also ignored in the bench scale studies since the permeated freshwater flux is relatively negligible compared to the input draw and feed flow rates in scaled-up modules [31, 58, 59, 153]. In scaled-up modules, the total permeated water flow rate along the

membrane (Q_{drawn}) is a significant ratio of the inlet feed solution. As an example, in the configuration (c) the total drawn fresh water is 80% of the inlet feed solution flow rate to maximize the SE value. In our model, the effective mass transfer is also updated considering the mixing effect (not illustrated in Figure 4.1) and applying the ECP on the feed side in Eqs. 3.14 and 3.15.

Whether the active layer of membrane facing the draw or feed solution affects the variation of the parameters studied in Figures 4.1 and 4.2. It is investigated that in both single [154] and dual stage [132] PRO systems the performance of membrane is superior when the active layer faces the draw solution (PRO mode). When the active layer (FO mode) is facing the feed solution, concentration polarization and reverse salt diffusion increase and reduce the system performance. It is claimed that in FO mode even adding the second stage does not improve the PRO performance [132]. In this study, we have modeled our configurations on PRO mode membrane orientation.

4.2 Single stage versus dual stage PRO System

Some dual stage PRO configurations have been studied previously [25, 130]. However, to our best knowledge, none of these has considered the effect of changing hydraulic pressures after each module. Tables 4.1 -4.3 compare maximum work values for target functions with their inlet draw and feed solution pressures and flow rates. The values for the applied hydraulic pressures (P_{D1} and P_{D2}) and inlet draw and feed flow rates ($Q_{D,in}$, $Q_{F,in}$, and $Q_{F2,in}$) were changed so that the maximum value for each target function is obtained.

4.2.1 Power Density (PD)

Optimization for the maximum amount of power density (PD) for each configuration, results in the optimal values for pressures and flow rates shown in Table 4.1. The dual stage system with pump and turbine (2PT) has slightly higher PD compared to single stage 1PT. However, this amount is less than PD in single stage system with PX, since the lower efficiency of the pump has canceled the advantage of the dual stage system. The dual stage system with 1HT and 1PX configuration has the maximum PD and shows a 36 % improvement compared to the single stage PT, 34 % over dual stage 2PT, and 3.8 % over single stage PX. The improvement from the dual stage to the single stage systems derives from separated feed flows which

maximize the difference in salt concentration. However, adding the second HT and depressurizing the draw flow after the first module is not effective and the system tends to minimize the pressure difference between the two modules. The 0.5 bar difference in the applied pressure between two modules seen in Table 4.1 is due to the selected pressure discretization step in the model. When this step size vanishes, as in the dual stage with 1HT, PD value improves. To investigate the losses and their effects on the system performance, a thermodynamic analysis of the system is presented in section 4.3, see Table 4.4.

Looking at flow rates for dual stage systems, the feed flow rates have been optimized separately for each stream. For PD, $Q_{F,in}$ is almost equally distributed between the two modules and $Q_{D,in}$ is equal or less than $Q_{F,in}$. The molar concentration of salt in the draw solution is $c_D = 600\ \frac{mol}{m^3}$. At a temperature of 298 K, the osmotic pressure of the draw solution is $\pi_D = 29.7$ bar [43]. Since the concentration of salt in the incoming feed solution is considered zero, the osmotic pressure of the incoming feed solution is $\pi_F = 0$. For all dual stage systems with 1PX, the optimum applied hydraulic pressure approaches the value at $\frac{\Delta\pi_D}{2}$.

Table 4.1: Optimization results for single and dual stage modules for maximum power density (PD)

	Single stage	Dual stage	Single stage	Dual stage with 2 HT			Dual stage with 1 HT
	1PT (a)	2PT (b)	1PX (c)	1PX (d)	1PX (e)	2PX (f)	1PX (g)
PD ($\mathbf{Wm^{-2}}$)	**2.19**	**2.22**	**2.87**	**2.96**	**2.78**	**2.56**	**2.98**
SE (KJ L^{-1})	0.25	1.12	0.27	0.15	0.15	0.14	0.15
W_{drawn} (KJ L^{-1})	0.65	0.59	0.96	0.92	0.87	0.79	0.94
P_{D1} (bar)*	12	12.5	15	15	15	17.5	15
P_{D2} (bar)	—	11.5	—	14.5	11	12	—
$Q_{D,in}\times10^{-4}$ (m^2s^{-1})	0.6	0.8	0.8	0.9	0.9	0.8	0.9
$Q_{F,in}\times10^{-4}$ (m^2s^{-1})	0.7	1	0.7	1	1.2	1	1.1
$Q_{F2,in}\times10^{-4}$ (m^2s^{-1})	—	1	—	1	0.7	1	0.1

*The presented P_{D1}, P_{D2}, $Q_{D,in}$, $Q_{F,in}$ and $Q_{F2,in}$ are the optimized values for PD.

4.2.2 Specific Energy (SE)

As shown in Table 4.2, maximum specific energy (SE) is found for the dual stage 1PX design (e). This configuration shows an improvement of about 8 % with respect to

the single stage 1PX, 12 % to the dual stage 2PT and 25 % to the single stage 1PT. Generally, in the dual stage PRO systems, the optimum pressure for the first module is above $\frac{\Delta\pi}{2}$ and for the second module is below $\frac{\Delta\pi}{2}$. This means that the maximum SE is obtained for individual optimum pressures for each module. It implies that depressurizing before the second module is helpful and reduces the irreversibility. This will be proved by thermodynamic analysis provided for SE as shown in section 4.3, see Table 4.5.

Table 4.2: Optimization results for single and dual- stage modules for maximum specific energy (SE)

	Single stage	Dual stage	Single stage	Dual stage with 2 HT			Dual stage with 1 HT
	1PT (a)	2PT (b)	1PX (c)	1PX (d)	1PX (e)	2PX (f)	1PX (g)
PD (Wm^{-2})	1.06	0.82	1.15	0.84	0.87	0.96	1.13
SE (KJ L^{-1})	**0.44**	**0.49**	**0.51**	**0.53**	**0.55**	**0.52**	**0.46**
W_{drawn} (KJ L^{-1})	0.88	0.95	1.14	1.04	1.09	1.02	1.14
P_{D1} (bar)*	13.0	16.5	15.0	17.5	16.0	18.5	15.0
P_{D2} (bar)	—	11.0	—	11.5	10.5	11	—
$Q_{D,in}\times10^{-4}$ (m^2s^{-1})	0.14	0.08	0.15	0.08	0.09	0.09	0.15
$Q_{F,in}\times10^{-4}$ (m^2s^{-1})	0.22	0.08	0.19	0.07	0.09	0.07	0.15
$Q_{F2,in}\times10^{-4}$ (m^2s^{-1})	—	0.09	—	0.09	0.06	0.11	0.07

*The presented P_{D1}, P_{D2}, $Q_{D,in}$, $Q_{F,in}$ and $Q_{F2,in}$ are the optimized values for SE.

4.2.3 Work per Fresh Water Drawn (W_{drawn})

As shown in Table 4.3, in the case of the dual stage system with 1PX, work per fresh water drawn shows a 61 % improvement with respect to the single stage PT, 47 % compared to dual stage 2PT, and 2 % compared to single stage PX. Similar to PD, depressurizing the flow after the first module does not have any benefit and the improvement is only related to the individual feed flows for each module.

It is worthwhile to note that using multi stage systems with additional stages will facilitate more energy recovery as discussed in [14]. However, it may not be economically feasible. As shown in Tables 4.1 - 4.3, achieving one optimized target function requires sacrificing the other. Therefore, the designer should be precisely aware of what the most important issue in each power plant is. For instance, the optimization for W_{drawn} requires high applied pressures which are far from the optimum values for

PD or SE. Hence, the results for these target functions are very low, and might not be acceptable.

Table 4.3: Optimization results for single and dual stage modules for maximum work per drawn water (W_{drawn})

	Single stage	Dual stage	Single stage	Dual stage with 2 HT			Dual stage with 1 HT
	1PT (a)	2PT (b)	1PX (c)	1PX (d)	1PX (e)	2PX (f)	1PX (g)
PD (Wm^{-2})	0.73	0.63	0.72	0.69	1.36	0.65	0.74
SE (KJ L^{-1})	0.32	0.18	0.22	0.96	0.19	0.95	0.11
W_{drawn} (KJ L^{-1})	**1.0**	**1.1**	**1.59**	**1.61**	**1.49**	**1.44**	**1.62**
P_{D1} (bar)*	17.0	19.5	24.0	24.0	22.0	24.5	24.0
P_{D2} (bar)	—	11.0	—	11.5	10.5	11	—
$Q_{D,in}\times10^{-4}$ (m^2s^{-1})	0.14	0.1	0.27	0.23	0.33	0.15	0.27
$Q_{F,in}\times10^{-4}$ (m^2s^{-1})	0.2	0.23	0.22	0.36	0.64	0.44	0.31
$Q_{F2,in}\times10^{-4}$ (m^2s^{-1})	—	0.23	—	0.46	0.06	0.44	0.42

*The presented P_{D1}, P_{D2}, $Q_{D,in}$, $Q_{F,in}$ and $Q_{F2,in}$ are the optimized values for W_{drawn}.

For all target functions, the values for dual stage 1PX 2HT are higher than the single stage. In the presence of incoming fresh water drawn through the membrane, the osmotic pressure in draw solution (π_D) decreases. Hence, according to Eq. (3.3), J_{wr} decreases along the module. One advantage of the dual stage configurations is that by dropping the hydraulic pressure to a specific value half way, the pressure difference ($\Delta\pi$ - ΔP) will remain almost the same and the flux across the membrane (J_{wr}) will not change drastically, hence the membrane will be utilized better. Another advantage of dual stage systems is that two separate fresh water streams for each module are used instead of one long stream. According to Eq. (3.3), the osmotic pressure of the feed solution (π_F) will decrease along the module due to the contamination with the salt flow (J_s). Therefore, the fresh water inlet in the second module will increase the osmotic pressure difference. This increase in driving force helps to take more water in and may also increase the power output. This effect is more tangible with longer modules, where the fresh water is more concentrated at the terminal part of module.

In Figure 3.1 (c) to (g), all configurations with PX produce more work than PT configurations which is predictable due to the higher efficiency of PX. However, for all target functions, the power produced with 2PX is equal or even less than the single stage PRO with 1PX. This means the addition of the second PX in Figure 3.1(e), does not improve efficiency. As discussed in [14], the best operation condition for PX is

when it works for higher pressure differences. For smaller pressure differences similar to the case of the dual stage PRO systems, pressure exchangers lose the advantage against pump-turbine pairs. Therefore, in the configuration of Figure 3.1(e) the pressure increase from P_{D1} to P_{D2} is not high enough to take advantage of the second PX. The pressure difference can better be obtained by a booster pump.

Interestingly, in cases where the difference between P_{D1} and P_{D2} is significant, the optimum applied hydraulic pressures for all target functions in single stage systems lie between the two optimum values of pressures in dual stage systems. This implies that in the dual stage systems, the application of optimal conditions of single stage module in the operation conditions will not meet the global maximum of the dual stage system.

4.3 Thermodynamic Analysis of the PRO Systems

Thermodynamic analysis is conducted based on the equations presented in section 3.8. For each target function, the percentage of net work and total work loss is presented in Tables 4.4 to 4.6. As observed in the tables, except for PD, the percentile of the net work for the dual stage systems is more than for single stage systems. The reversible work in a dual stage system is expected to be more than a single stage system. For this reason, even though the amount of net work or power density in a dual stage system is more than a single stage in the case of PD, the losses of dual stage system exceed the improvement in net work. This results in decrease of percentile of net work in dual stage systems.

The maximum net work percentage of all target functions belongs to SE in the dual stage 1PX system where Q_{Din} is drawn back to PX before the first turbine Figure 3.1(e). This system also has the maximum improvement with respect to the single stage system. In this case, the pressure drop is significant and confirms that depressurizing the draw solution before the second module is beneficial. Drawing the Q_{Din} back to the PX after the first module causes more net work percentage in SE and W_{drawn} target functions. This is expected since Q_{Din} will eventually be send back to the PX and does not contribute to power production. The unnecessary losses resulting from Q_{Din} flow into the second module are avoided. However, the amount of W_{drawn} is larger in dual stage 1PX Figure 3.1(e) and Table 4.3) rather than the single stage 1PX system where Q_{Din} is drawn back to PX after the first module. This can be explained by the fact that, by the definition of W_{drawn}, the division of the

amount of net work to the inlet flow rate (which is more in the latter case) does not compensate the excess amount of net work in dual stage configuration (e).

Table 4.4: Thermodynamic analysis for single and dual stage modules for net work and losses percentages for PD

	Single stage	Dual stage	Single stage	Dual stage with 2 HT			Dual stage with 1 HT
	1PT (a)	2PT (b)	1PX (c)	1PX (d)	1PX (e)	2PX (f)	1PX (g)
Net Work %	29.61	25.33	39.6	37.16	35.22	33	38.01
Total Work Loss %	**70.39**	**74.66**	**60.4**	**62.84**	**64.78**	**66.97**	**61.99**
Water and Salt Transfer %	50.71	52.26	42.88	44.25	44.04	43.86	44.03
Pressure Exchanger %	—	—	8.2	8.38	8.43	14.51	8.51
Turbine %	10.72	11.46	5.78	5.87	4.99	5.62	5.51
Membrane Module %	2.33	3.16	3.55	3.91	3.93	2.98	3.94
Pump %	6.63	7.78	—	0.42	3.37	—	—

As expected, the losses of pump and turbine in 1PT and 2PT systems are more than the sum of pump, turbine and PX in PX systems, which makes the use of PX advantageous. However, adding the second PX to the system, despite eliminating the pump loss, makes the 2PX system less efficient. That is because the sum of pump and PX losses in the dual stage system with 1PX is less than PX losses in a 2PX system. This is in accordance with our previous findings, as discussed before.

Table 4.5: Thermodynamic analysis for single and dual stage modules for net work and losses percentages for SE

	Single stage	Dual stage	Single stage	Dual stage with 2 HT			Dual stage with 1 HT
	1PT (a)	2PT (b)	1PX (c)	1PX (d)	1PX (e)	2PX (f)	1PX (g)
Net Work %	44.96	51.67	53.77	55.45	56.70	56.08	52.85
Total Work Loss %	**55.04**	**48.33**	**43.92**	**46.23**	**44.62**	**43.30**	**47.15**
Water and Salt Transfer %	38.67	30.27	29.31	34.15	29.01	29.72	35.18
Pressure Exchanger %	—	—	7.39	5.19	3.89	4.30	5.19
Turbine %	10.82	12.17	7.10	6.58	9.20	6.78	6.47
Membrane Module %	0.32	0.11	0.12	0.31	0.10	0.11	0.30
Pump %	5.23	5.78	—	2.33	2.37	—	—

As shown in Tables 4.4-4.6, the addition of the second hydro turbine between the modules does not increase the PD and W_{drawn} target functions. Addition of the

second turbine and depressurizing the draw flow between modules only adds to work loss rather than net work. However, in all dual stage systems, net work for SE with 2HT is more than 1HT.

Table 4.6: Thermodynamic analysis for single and dual stage modules for net work and losses percentages for W_{drawn}

	Single stage	Dual stage	Single stage	Dual stage with 2 HT			Dual stage with 1 HT
	1PT (a)	2PT (b)	1PX (c)	1PX (d)	1PX (e)	2PX (f)	1PX (g)
Net Work %	42.1 4	44.1	51.15	48.08	53.14	46.96	48.60
Total Work Loss %	**57.86**	**55.90**	**48.85**	**51.92**	**46.59**	**53.04**	**51.04**
Water and Salt Transfer %	32.59	30.71	26.32	31.36	24.69	30.53	30.52
Pressure Exchanger %	—	—	14.22	11.94	9.67	15.22	13.18
Turbine %	15.35	15.49	7.38	7.39	7.05	7.02	6.93
Membrane Module %	0.33	0.18	0.93	0.63	0.35	0.27	0.76
Pump %	9.59	9.52	—	0.6	4.83	—	—

4.4 Internal Performance of Modules for Single and Dual Stage Systems

To better understand what takes place in membrane modules and where the improvements occur in dual stage system, changes in some parameters along the membrane are investigated and illustrated in Figure 4.3. As indicated earlier, membrane length in the single stage module is the same as the total membrane length in dual stage PRO. The input values for pressures and flow rates are chosen such that maximum specific energy (SE) is obtained and the comparison is illustrated between single stage 1PX (c), dual stage with 2HT- 1PX configuration (e), and dual stage 1HT (g) as shown in Table 4.2.

Figure 4.3 shows the change of osmotic pressures in draw and feed solutions (π_D and π_F) (Figure 4.3(a) and (b)) and volumetric flow rates of the draw and feed solutions (Q_D and Q_F) along the membrane coordinate (Figure 4.3(c) and (d)). It also illustrates the local water (J_{wr}) and salt transfer flow through the membrane Figure 4.3 (e) and (f). All diagrams show the difference between the single stage system with PX (c) (green solid line), the dual stage system configuration (e) (blue line for module 1, and red line for module 2) and the dual stage system with 1HT

configuration (g) (blue dashed line for module 1, and black dashed line for module 2).

The osmotic pressure difference between the draw and feed solutions along with hydraulic pressure difference (π_D - π_F - ΔP) induces the driving force of fresh water passing through the membrane, see Eq. 3.3. At the upstream, the osmotic pressure for the draw solution (π_D) is at its highest value. As the drawn fresh water is added to the draw solution, the concentration of salt in the bulk reduces; hence, the osmotic pressure drops along the membrane. As illustrated in Figure 4.3(a), the osmotic pressure in the draw solution (π_D) for single stage and dual stage with 1HT (g), are almost the same. However, for dual stage system configuration (e), the π_D is less than others, specifically at the second module since the drawn fresh water added to the second module in this system is more than the others. This means that the draw solution is more diluted which results in less π_D.

On the feed side, osmotic pressure π_F increases along the membrane due to the loss of some fresh water passing through the membrane, as well as, salt being added due to reverse salt flux (notice that the flow is counter current). This increase drops J_{wr} according to Eq. (3.3).

As shown in Figure 4.3(c), draw solution flow rate (Q_D) increases gradually due to the addition of fresh water intake. At the end of each module, this additional flow drives the turbine to produce power (in the case of dual stage configuration (e)). However, drawn fresh water (J_{wr}) decreases along the membrane length because of smaller driving force at the downstream. Therefore, the rate of increase in Q_D drops. The optimum Q_D for dual stage configuration (e), is less than the single stage and dual stage with 1HT. This results in the major advantage of this system having higher SE value. As can be seen in Figure 4.3(e), J_{wr} is higher at the second module due to introducing fresh water at the second module and depressurizing the draw flow after the first module. The salt flow rate (J_s) in the feed solution drops along the membrane due to the dilution of the draw solution. The overall value of J_s is less in dual stage compared to single stage. There is a breakpoint at the beginning of the second module because of new fresh water entering the module between the first and second modules in Figure 4.3(f).

The trends for the dual stage 1HT system configuration (g) are almost similar to the single stage system. However, as can be seen in Figure 4.3(f). J_s is less than the single stage due to addition of fresh water flow to the second module. As can be seen in Figure 4.3 (e) and (d), J_{wr} and the sum of Q_f in both modules are less than single

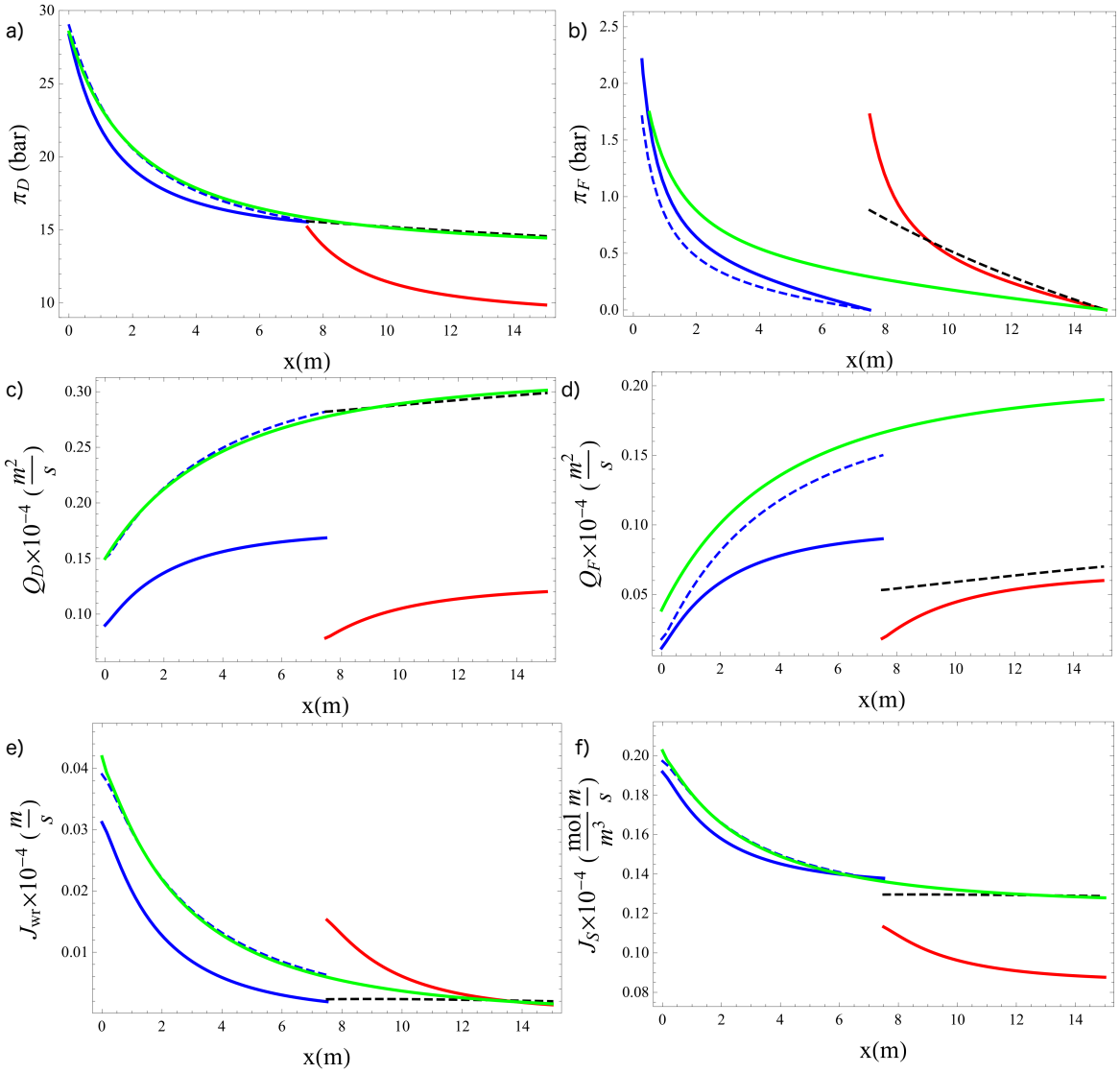

Figure 4.3: Osmotic pressure of draw and feed solutions (a) and (b)(π_D,π_F); (c) and (d) volumetric flow rate of draw and feed solutions (Q_D,Q_F); (e) permeated water flux (J_{wr}) and (f) reverse salt flux (J_s), for single stage PRO configuration (C) (green solid line), dual stage configuration (e) (blue solid line for module 1, and red solid line for module 2) and dual stage 1HT configuration (g) (blue dashed line for module 1, and black dashed line for module 2) optimized for specific energy (SE).

stage ones which results in lower SE values. The improvement for dual stage system with 2HT can be higher depending on the membrane characteristics and membrane length in each module to confer the most advantage from the system.

After investigating the proposed configurations of single and dual stage PRO system, it can be concluded that generally, the systems with pressure exchangers will operate with higher efficiency than the pump-turbine pair. For the further study configurations of dual stage PRO systems (d) and (e) are selected since they showed the best performance compared to the other configurations. Single stage system of configuration (c) and dual stage PRO with 1HT (g) are also studied for comparison. As concluded in section 4.2 the proposed dual stage PRO systems of (d) and (e) demonstrated their superior performance with specific energy (SE) as target function. In the power density and work per drawn fresh water target functions, the systems attempt to eliminate the applied pressure difference between the first and second module. Therefore, for further studies only specific energy will be investigated in selected configurations.

4.5 Effect of membrane area on PRO performance

As discussed in section 4.1 the water permeation flux starts with the maximum value at the entrance of the draw channel and then gradually decreases along the membrane length. At some point, water permeation becomes nearly constant and very small and adding more membrane area does not benefit the performance. In this study, the height and width of the membrane are supposed to stay constant at $H = 0.001$ and $Z = 1$ m, respectively, and the length of the membrane is considered as a variable. Figure 4.4 shows the change of fresh water permeation along the selected membrane areas of 5, 15, 30, and 40 m^2 in single stage PRO. For each membrane area, the operating conditions are optimized for the maximum SE value. As can be seen in Figure 4.4, freshwater permeation flux varies continuously along the membrane with the membrane areas of 5 and 15 m^2. However, the changes at 20 m^2 become less significant and after 30 m^2, the curve tends to be flat and eventually 'zero'. Therefore, the membrane area needs to be optimized in the PRO system since at a certain point the capital cost of the system due to additional membrane area,inlet flows, and hydraulic pump overcomes the generated power.

Previously, we assumed a fixed membrane length of L=15 m in the single stage PRO that has been divided equally in dual stage PRO as L_1=L_2=7.5 m. However,

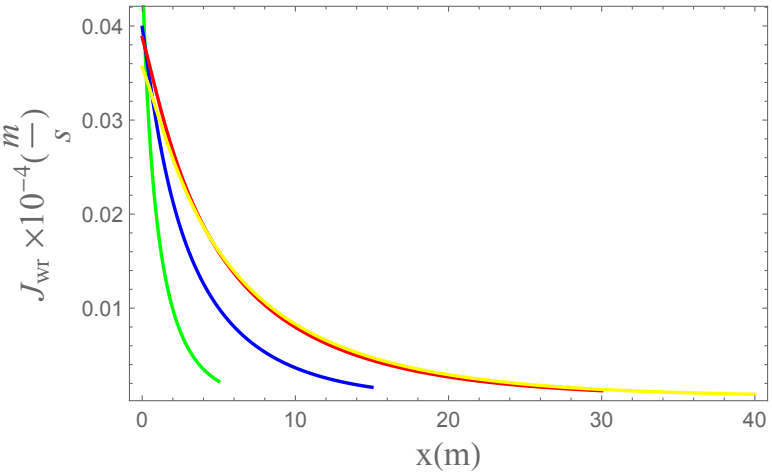

Figure 4.4: Fresh water permeation flux through the membrane in single stage PRO with various membrane area of 5 (green line), 15 (blue line), 30 (red line), and 40 (yellow line) m^2

the membrane area and distribution of it in each module may change if the system is optimized for membrane area. In dual stage PRO systems, we added two other variables of L_1 and L_2 changing from 1 to 15 m individually in each module to optimize the dual stage PRO system for maximum SE value. The SE normalizes the power output based on the total inlet flow rates of draw and feed solutions. Utilization of more membrane length increases the permeated flux along the membrane (J_{wr}) which increases SE but needs more inlet flow rate that decreases the SE value. Therefore, there is a trade-off between the two factors. Two configurations of dual stage PRO in Figure 3.1 (d) and (e) are selected for optimization of membrane area. The optimized membrane area is used in single stage PRO in Figure 3.1 (c) as (L=L_1+L_2) and dual stage PRO with 1HT in Figure 3.1 (g) for comparison. The optimized values for all variables in different configurations are shown in Table 4.7.

In the dual stage configuration (e) the optimum membrane length for each module is L_1=9 and L_2=6 m. The SE value is the same as the equally distributed membrane length (L_1=L_2=7.5 m). However, the distribution of the membrane length is such that it uses more membrane area at the first module and less at the second module. The distribution of the draw solution flow in this configuration is such that just the drawn fresh water from the first module enters the second one. Therefore, with less available draw solution the second module needs less membrane area to operate in optimum condition.

In the dual stage configuration (d) the optimum membrane length is obtained at

Table 4.7: Optimization results for single and dual stage modules for maximum specific energy (SE) with optimum membrane length

	Single stage		Dual stage with 2 HT		Dual stage with 1 HT	
	1PX (c)		1PX (d)	1PX $_{\text{before T1}}$ (e)		1PX (g)
L (m)	12	15	12	15	12	15
L_1 (m)	—	—	5	9	5	9
L_2 (m)	—	—	7	6	7	6
SE (KJ L^{-1})	**0.50**	**0.51**	**0.53**	**0.55**	**0.49**	**0.49**
P_{D1} (bar)*	14.0	15	17.5	17.0	14.0	14.5
P_{D2} (bar)	—	—	11.5	11.0	—	—
$Q_{D,in}\times10^{-4}$ (m^2s^{-1})	0.11	0.15	0.07	0.11	0.17	0.17
$Q_{F,in}\times10^{-4}$ (m^2s^{-1})	0.16	0.19	0.06	0.10	0.14	0.17
$Q_{F2,in}\times10^{-4}$ (m^2s^{-1})	—	—	0.08	0.06	0.17	0.05

* The presented P_{D1}, P_{D2}, $Q_{D,in}$, $Q_{F,in}$ and $Q_{F2,in}$ are the optimized values for SE.

L_1= 5 and L_2=7m. The SE value for this configuration is the same as the dual stage PRO with L_1=L_2=7.5 m. However, the new distribution uses less membrane area by saving 3 m^2 of membrane area to obtain the same SE value. The distribution of the membrane length, unlike the previous configuration, uses less membrane area at the first module rather than the second one. This is due to the design of this configuration which applies more draw solution in the second module than the first one.

Interestingly, the distribution of the membrane area for each module highly depends on the selected configuration and consequently the entering flow rate in each module. It is reported [155] that there is an optimal draw solution flow rate needed for a given membrane area not to reach the equilibrium state. As can be seen in Table 4.7 the flow rate of the feed and draw solution increase in the first module for configuration (e) since it utilizes more membrane area at the first module rather than the one with equally distributed membrane area (see Table 4.2 for comparison).

As can be seen in the bar chart provided in Figure 4.6, the effect of optimizing the membrane area is more noticeable for the dual stage PRO with 1HT configuration; as the SE value improves up to 7% compared to the equally distributed membrane area in the same configuration. Furthermore, the same SE values obtained for both L=12 and 15 m in configuration (d) that means membrane area can be saved with no change in SE results.

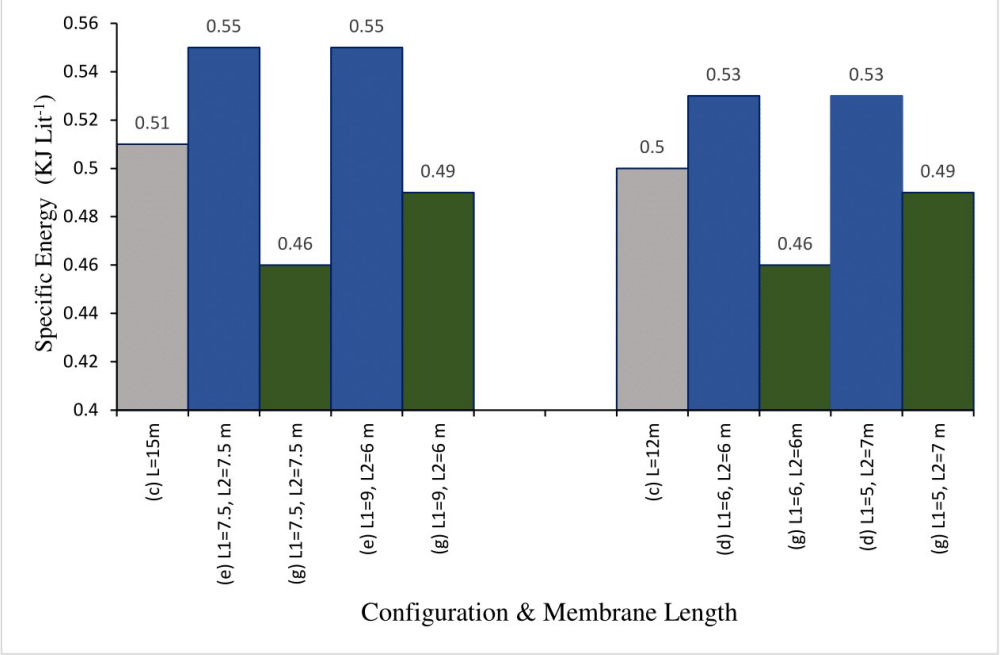

Figure 4.5: The effect of membrane length on specific energy of single and dual stage PRO configurations

The variation of water permeation flux (J_{wr}) along the membrane module is illustrated in Figure 4.6 for the dual stage PRO configuration (e) with two distributions of L_1=9 and L_2=6 m (solid line) and L_1=L_2=7.5 m (dashed line). As can be seen in Figure 4.6 , the water permeation in the optimized membrane area is more than equally distributed one in both modules. This improvement is more significant in the second module which means better utilization of the membrane area.

4.6 Effect of the membrane characteristics on PRO performance

As discussed in section 2.6, for best operation of membrane in PRO, it needs to have the high water permeation coefficient (A) along with low salt permeation coefficient (B). The structural parameter (S) of the membrane also needs to be kept as minimum as possible. To evaluate the effect of membrane characteristics, four hypothetical membranes are proposed in Table 4.8. The amount of water and salt permeability coefficients (A and B), and structural parameter (S) improved four times from our reference membrane (M1) indicating M2 to M4, respectively, and M5 exploits all the

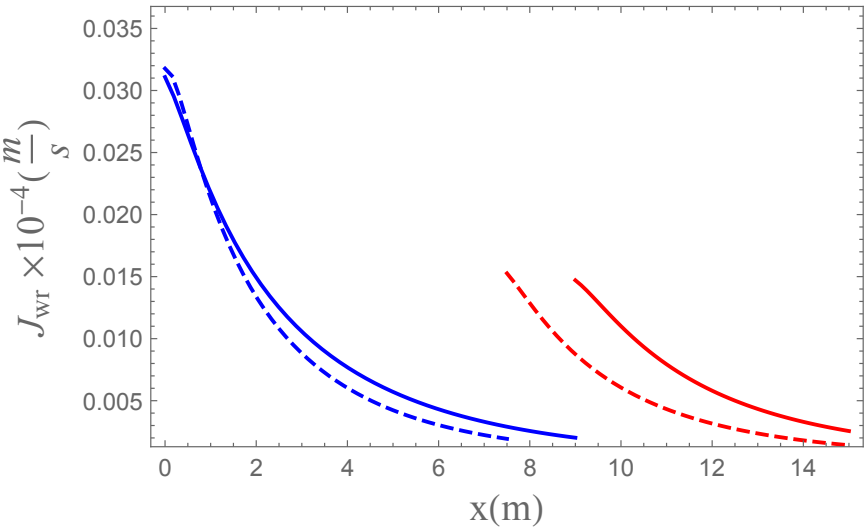

Figure 4.6: The variation of water permeation flux (J_{wr}) along the membrane module for dual stage PRO configuration (e) with optimized membrane distribution of L_1=9 and L_2=6 m (solid line) and equally distributed membrane of L_1=L_2=7.5 m (dashed line).

Table 4.8: Proposed membrane characteristics

Membrane	A [10^{-9} m s $^{-1}$Pa^{-1}]	B [10^{-7}m s^{-1}]	S [10^{-6} m]
M1 (Ref.)	4.86	0.44	307
M2	20	0.44	307
M3	4.86	0.10	307
M4	4.86	0.44	75
M5	20	0.10	75

improvements. The results for dual stage configuration (d) and (e) are compared to the single stage (c) and dual stage 1HT (g) PRO systems and illustrated in Table 4.9.

As stated in Eq. 3.3, water flux in PRO is equal to the difference of applied hydraulic pressure and the effective osmotic pressure multiplied by the membrane intrinsic water permeability (A). Therefore, high value of A enhances the water flux across the membrane which prompts increased power generation (see Eq. 3.14). The improvement of SE by increasing A value from M1 to M2 in dual stage systems is up to 5% and the improvement from single stage to dual stage within M2 itself is 9.5 %.

Salt passage through the membrane enhances both internal and external Concentration polarization effect that results in a drop in the water flux. When the solute permeates from the concentrated draw solution to the diluted feed solution,

the leaked solute accumulates in the porous support layer and reduces the effective osmotic pressure. It also enhances the salt flux through the membrane that has an adverse effect on power output. The negative effects of this coupling between reverse salt permeation and ICP are reflected in the denominator of Eq. 3.14. To alleviate this adverse effect, the salt permeation factor (B) has to be minimized. In our systems reducing B value improves the dual stage system from M1 to M3 by 13 % and the improvement from single to dual stage in M3 is 13%.

Table 4.9: Optimization results for single and dual stage modules for maximum specific energy (SE) with improved membrane characteristics

Membrane	Configuration	SE (KJ L^{-1})	P_{D1} (bar)	P_{D2} (bar)	$Q_{D,in}\times10^{-4}$ (m^2s^{-1})	$Q_{F,in}\times10^{-4}$ (m^2s^{-1})	$Q_{F2,in}\times10^{-4}$ (m^2s^{-1})
	(c)	**0.51**	15.0	—	0.15	—	0.19
M1	(d)	**0.53**	17.5	11.5	0.08	0.07	0.09
(Reference)	(e)	**0.55**	16.0	10.5	0.09	0.09	0.06
	(g)	**0.46**	15.0	—	0.15	0.15	0.07
	(c)	**0.53**	14.0	—	0.19	—	0.28
M2	(d)	**0.57**	17.0	11.5	0.12	0.11	0.14
(Increased A)	(e)	**0.58**	16.0	10.5	0.19	0.20	0.12
	(g)	**0.52**	15.0	—	0.34	0.34	0.08
	(c)	**0.55**	16.0	—	0.15	—	0.16
M3	(d)	**0.62**	18.0	13	0.05	0.04	0.04
(Smaller B)	(e)	**0.62**	16.0	10.5	0.07	0.07	0.04
	(g)	**0.55**	14.5	—	0.17	0.17	0.03
	(c)	**0.51**	15.0	—	0.15	—	0.19
M4	(d)	**0.54**	16.0	11.0	0.06	0.06	0.07
(Smaller S)	(e)	**0.55**	16.0	11.0	0.11	0.11	0.07
	(g)	**0.50**	14.0	—	0.17	0.18	0.05
	(c)	**0.57**	15.0	—	0.15	—	0.21
M5	(d)	**0.65**	16.0	12.0	0.09	0.19	0.07
(A,B, and S)	(e)	**0.65**	17.0	11.5	0.15	0.13	0.07
	(g)	**0.57**	15.5	—	0.35	0.34	0.19

* The presented P_{D1}, P_{D2}, $Q_{D,in}$, $Q_{F,in}$ and $Q_{F2,in}$ are the optimized values for SE.

A contour plot of the SE values of the dual stage PRO configuration (e) under various amounts of water and salt permeability coefficients is illustrated in Figure 4.7. As can be seen in Figure 4.7, the enhancement obtained from applying low salt permeation factor (B) is more than increasing the water permeation factor (A) in our configurations. The higher values of SE assigned to lower B can be related to the input draw and feed water flow for SE optimization. Since prompting water permeation

with increasing A value, means that the system needs more input draw and feed flow rates to maximize the power generation. Therefore, even though improved water permeation increases the SE value, but it is not as compelling as the improvement in salt rejection drop due to higher input flow rates (see Table 4.9).

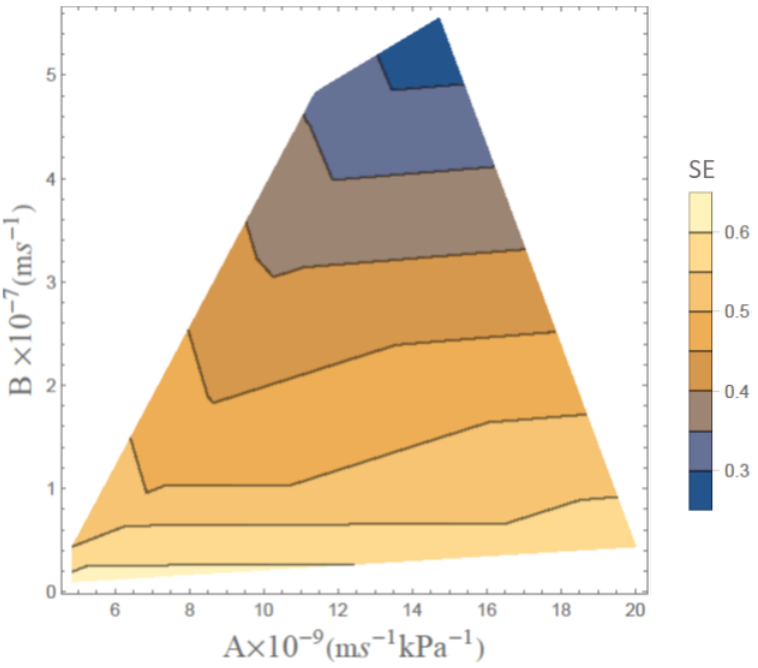

Figure 4.7: Contour plot of SE values changing with water and salt permeation coefficient (A and B) in membranes in dual stage configuration (e)

The structural parameter of the support layer (S) is determined by the microstructure of the membrane in this layer. As defined, S has a unit of length and is related to the thickness, tortuosity, and porosity of the support layer. It is regarded as the effective distance a solute particle has to diffuse from the active layer interface to reach the bulk feed solution. Hence, the shorter the distance, the more effective is the support layer.

Reducing S can be achieved by reducing the support layer in the membrane as well as achieving high porosity and low tortuosity. It can improve the system performance by limiting internal concentration polarization and effective directing the water flux through the membrane. In a recent study on the economic viability of PRO system, it is concluded that since only the high salinity sources will be viable for a stand-alone PRO system, the future membranes have to focus on reducing the structural parameters rather than water and salt permeability [156].

As can be seen in Table 4.9 minimizing S value does not have a significant impact on the system performance in our presented configurations. As an instant in single stage PRO, the SE value in reference membrane (M1) is 0.506 and for the improved S in (M4) is 0.513 (KJ L^{-1}). This change is beyond the accuracy of the presentation of the results and is not noticeable in Table 4.9. Such a small improvement in SE values can be related to the fact that both B and S need to be low enough to reduce the negative effect of reverse salt flux. A membrane with a large salt rejection parameter will limit the performance of the system by the effects of reverse salt flux, even if it has a relatively low structural parameter. Furthermore, the expression related to the S changes in J_{wr} and J_s equations (Eqs 3.14 and 3.15) is exp $(\frac{J_{wr}S}{d})$ which in the case of single stage PRO with S=307 μm changes along the membrane from 1.61 to 1.02 and for S=75 μm changes from 1.18 to 1.01. It implies that the S value in this membrane is optimized enough for our configurations so that a further decrease in S value does not have a significant impact on the resulted SE values.

As expected, the best performance belongs to the improvement in all membrane characteristics. The SE values improve in the dual stage from M1 to M5 by 18% and the improvement from single to dual stage in M5 is 14%. This membrane takes advantage of high A and low B and S values while improves the power generation with previously described methods. With the improvement of the membrane characteristics, the proposed dual stage configurations become more efficient than the single stage PRO system since the improvement from M5 in the single stage and dual stage PRO is 18% compared to 8% improvement in M1.

The applied hydraulic pressure differences between the first and second modules stays almost the same at 5 to 5.5 bar for all membranes and the draw and feed solutions flow rates increase with changing the water permeation coefficient (A).

As studied earlier, it is demonstrated that in order to maximize the PRO performance, the membrane should have the maximum water permeation and salt rejection. This ideal situation is studied with hypothetical membranes presented above. However, the PRO performance is limited due to the trade-off between water permeation and salt rejection, where an increase in water permeability is accompanied by a contributing increase in salt permeation [157, 158]. Water/salt permeability selectivity can be determined by [157, 159]

$$\frac{P_w}{P_s} = \frac{\lambda}{(P_W)^{\beta}}, \tag{4.1}$$

where P_w is the membrane permeability to water, P_s is the membrane permeability to salt, λ and β are empirical fitting parameters. The water and salt permeability coefficients A and B can be related to the bulk transport properties of the membrane by [157, 159]

$$A = \frac{P_w}{L}\frac{M_w}{\rho RT}, \tag{4.2}$$

and

$$B = \frac{P_s}{L}, \tag{4.3}$$

where L is the thickness of the active layer, M_w is the molar mass of water, ρ is the density of water, R is the gas constant, and T is the absolute temperature. Substitution of Eqs. 4.2 and 4.3 into Eq. 4.1 links the water and salt permeability coefficients and the permeability-selectivity trade-off relationship can be presented as

$$B = \frac{L^{\beta}}{\lambda}(\frac{\rho RT}{M_w})^{\beta+1}A^{\beta+1}. \tag{4.4}$$

For PRO application β is evaluated to be 2 [157, 159]. Maximum PRO performance can be obtained by balancing the trade-off between the permeability and selectivity of the membrane active layer.

4.7 Effect of the draw solution source on PRO performance

Several types of draw and feed solutions can be used in PRO systems as long as they provide sufficient osmotic pressure difference to generate economically viable power output. One advantage of the dual stage PRO system is providing more flexibility in the draw and feed source selection in each module. Other than the most common ,and mostly abandoned, river-sea pair, RO brine is the best option for draw solution since it increases the osmotic pressure gradient due to its high solute concentration. Hence, the byproduct of RO plant can be used to recover some of the energy consumption, and the diluted brine with PRO alleviates the environmental effect of RO brine disposal to the sea. The results of RO brine-Freshwater pair as draw and feed solutions for suggested configurations with their optimum membrane length is illustrated in Table 4.10. The molar concentration of the salt in the RO brine is about 1300 $\frac{mol}{m^3}$. At the temperature of 298 K, the osmotic pressure of the RO draw solution is 64.42 bar.

Considering fresh water as the feed solution, the theoretical optimum applied pressure to achieve maximum power output is $\Delta P = \frac{\Delta\pi}{2} = 32.21$ bar. As can be seen in Table 4.10, the optimum applied pressure in single stage PRO is 31 bar which is close to the theoretical optimum. In the dual stage 1HT configuration (g), the optimum applied pressure is less than expected. In other dual stage configurations with 2HT (e) and (g), the applied pressure is higher than the optimum in the first stage while in the second stage is lower. The difference between the hydraulic pressure in the first and second stage is up to 13 bar. This difference for seawater-freshwater pair was up to 6 bar. It implies that in the presence of the RO brine as draw solution source, the depressurizing before the second module is more critical since there is no need of high pressures in the second module while the ultimate result will be the improvement of system performance.

Table 4.10: Optimization results for single and dual stage modules for maximum specific energy (SE) with RO brine as a draw solution source

	Single stage		Dual stage with 2 HT		Dual stage with 1 HT	
	1PX (c)		1PX (d)	1PX $_{\text{before T1}}$ (e)		1PX (g)
L (m)	12	15	12	15	12	15
L_1 (m)	—	—	5	9	5	9
L_2 (m)	—	—	7	6	7	6
SE (KJ L^{-1})	**1.21**	**1.21**	**1.26**	**1.29**	**1.18**	**1.17**
P_{D1} (bar)*	31	30	39	36	30	30
P_{D2} (bar)	—	—	27	23	—	—
$Q_{D,in}\times10^{-4}$ (m^2s^{-1})	0.18	0.18	0.13	0.19	0.22	0.31
$Q_{F,in}\times10^{-4}$ (m^2s^{-1})	0.24	0.23	0.10	0.17	0.20	0.31
$Q_{F2,in}\times10^{-4}$ (m^2s^{-1})	—	—	0.12	0.10	0.08	0.07

* The presented P_{D1}, P_{D2}, $Q_{D,in}$, $Q_{F,in}$ and $Q_{F2,in}$ are the optimized values for SE.

Exchanging seawater with the RO brine as the draw solution improved the SE values in PRO systems more than 134%. Draw solutions with high concentration cause the water flux and the power output to increase significantly. As can be seen in Table 4.10, the SE values using RO brine-Freshwater pair increases up to 7% from single stage to dual stage PRO. Table 4.10 shows that the improvement of dual stage systems by adding the second turbine is more obvious moving toward the high concentration draw solutions.

Interestingly, the SE values in dual stage PRO with 1HT (g) is less than the

single stage one.However, the results are slightly better for 12 m of membrane length than the 15 m. This is in contrary with the results from the literature that indicates more improvements in the dual stage when uses RO brine [131]. The distribution of membrane area is chosen based on the optimum values for configurations (d) and (e). Therefore, it does not mean that the overall performance of dual stage PRO with 1HT configuration (g) is worse than single stage PRO. The results show that PRO systems with higher concentration draw solution sources are more sensitive to membrane distribution since the permeated flow rate as well as inlet draw and feed flows are higher in those systems.

As can be seen in Table 4.9 and Table 4.10, the improvement in SE even with the best theoretical membranes studied here which is far from commercially available membranes is minor compared to the improvements obtained from changing the concentration of draw solution toward higher salt concentrations. This implies that the development of membranes that is mentioned as the main restriction for PRO development in researches [149, 44] needs to be modified to be suitable for high solute concentrations. The membranes suitable for high concentration sources require mechanical strength at high applied pressure and low salt permeation coefficient (B) as well as the modified structural parameter (S). In these applications, membranes with low structural parameters that have high porosity or thin support layer may not withstand the high applied pressures that are needed for high salinity gradient PRO systems. In flat sheet membranes the spacers have to be designed so that they allow water permeation and do not alleviate the fouling effect in both membranes and spacers. In the presence of not properly tailored membranes and spacers, water permeation will be severely dropped due to the deformation and shallow effects in the membrane. Hollow fiber membranes that are self-supported and do not need spacers as other membrane modules may be more effective for these kind of applications.

Chapter 5

Conclusions and recommendations

The research presented in this dissertation aims to introduce and examine large scale dual stage PRO systems. The production of sustainable energy by means of PRO is studied by concentrating on increasing the efficiency of the system by optimizing the operating conditions and by introducing several dual PRO configurations.

The theoretical background was discussed, introducing the basic concepts of PRO and the development of the various models with the evolution of the process. The thermodynamic limitations and PRO integration in other systems were presented and discussed. Previous studies of multi stage PRO were compared with this work.

A mathematical model was developed to consider all effective parameters and their influence on dual stage PRO performance. A thermodynamic analysis performed to evaluate the contribution of irreversible losses in the module. The effect of the changes in membrane area, membrane characteristics and draw solution sources on the suggested dual stage PRO systems were investigated and compared to the single stage PRO. To address the objective and scope of this dissertation, the following closures were achieved.

5.1 Mathematical model of PRO system

Improving power generation by PRO is about the reducing the irreversible losses around the semi permeable membrane in the PRO power plant. This is achievable by optimizing the operational conditions and proposing state-of-the-art configurations. The detailed mathematical model for PRO power generation considers the effects of

- Internal concentration polarization across the membrane support layer (ICP),

- External concentration polarization across the draw and feed side boundary layers (ECP),
- Reverse salt flux from draw solution to the feed solution,
- Spatial variations along the membrane length due to water and salt flux through the membrane,
- Pressure drop along the membrane length due to the frictional losses,
- Pressure drop in pressure exchanger,
- Efficiency of the mechanical components like pumps and turbines,
- Counter-current flow system in draw and feed channels,
- Active layer of the membrane facing the draw side (PRO mode).

The trade-off between the mass transfer and pressure loss introduced by the spacers along the membrane was modeled. The pressure loss along the module was obtained by momentum balance and frictional loss, and the mass transfer improvement was obtained by updating the mass transfer coefficient value along the module.

The optimum operating conditions were obtained for several suggested configurations. The operational conditions included inlet pressures and volumetric flow rates in the draw and feed solutions which were optimized such that the target functions were maximized. It was found that the best operational conditions depend on the investigated system configuration and the selected target function.

To investigate the cause of the losses and their contribution in each configuration and target function in the PRO system, a thermodynamic model was used to determine the irreversible energy losses. The thermodynamic model predicted the loss sources and their relative contribution to work loss in each configuration.

5.2 Dual stage PRO system configurations

The dual stage PRO system studies were concentrated on depressurizing the draw solution flow after the first module by adding a second turbine between the modules. It was expected that, better use of the membrane was an advantage of multi staging, which is quite unevenly used along the module in standard PRO. This aspect

was investigated by offering several dual stage configurations. Another advantage of multi staging of the PRO was improving the efficiency of the system by introducing individual freshwater streams in each module which causes less spoiled freshwater and increases the driving force of water permeation. The membrane area of the dual stage was kept constant at half the membrane length of single stage for each module. Target functions of power density (PD), specific energy (SE) and work per drawn freshwater (W_{drawn}) were studied.

We found that exchanging hydro pump with pressure exchanger (PX) improved the system performance in all target functions due to the higher efficiency of the pressure exchanger. However, adding the second pressure exchanger instead of the booster pump in dual stage PRO lost the advantage due to the lower efficiency of the PX in small pressure differences of P_{D1} and P_{D2}.

In general, the dual stage system was more efficient than the single stage system. In terms of specific energy, the dual stage system showed up to 8% improvement from the single stage. The improvements for PD and W_{drawn} were up to 3% which were below our expectations. Moreover, in those target functions the system tended to eliminate the pressure difference between the first and second module which implied that depressurizing was not beneficial.

A thermodynamic analysis was conducted to investigate the losses in the module. It was found that in PD and W_{drawn}, the contribution of loses outweighed the improvement from dual staging leading results that were below our expectations.

PRO power plants should be designed based on the desired target function because operational conditions change for each target function. For example, SE are useful when the accessible amount of draw and feed solutions are restricted like in energy storage applications.

5.3 Optimizing PRO modules

5.3.1 Effect of membrane area

At a specific membrane area in PRO system, water permeation eventually becomes constant and adding more membrane area does not increase the system performance. In dual stage systems, the distribution of membrane area were modified for each module. The membrane distribution depended on the selected configuration and the inlet flow rate of draw solution in each module.Despite the fact that commercially

available modules have standard size, more research could be done into whether one might prefer different sizes, depending on system configurations.

5.3.2 Effect of membrane characteristics

The effect of improving of membrane characteristics on dual stage PRO performance, was investigated. Increasing water permeation coefficient (A) increased the system performance by allowing more freshwater flux through the membrane. Reducing the salt permeation coefficient (B) improved the SE value by reducing the adverse salt flux, internal and external concentration polarizations due to the solute diffusion from the draw to feed solution. It was found that reducing B factor had more impact than increasing A factor in our configurations. However, minimizing the structural parameter (S) of the membrane did not have a significant effect on the SE values.

Improving all the membrane characteristics contemporaneously demonstrated an improvement of up to 14% in SE from single to dual stage configurations which was the maximum improvement achieved. It implied that dual staging of PRO systems with 2HT will likely be more beneficial for improved membranes and is promising for future developments in membrane technology.

5.3.3 Effect of draw solution

The increase of the draw solution concentration enhanced the PRO process by increasing the osmotic driving force. The dual stage system with RO brine demonstrated an improvement of up to 134% in SE values from the dual stage seawater-freshwater pair. In the RO brine-freshwater pair, the difference in hydraulic pressure between the first and second stage was significantly more than in the seawater-freshwater. It implied that the depressurizing of the system became more crucial with increasing draw solution concentration. The future membranes and configurations need to focus on higher salinity draw solution sources.

5.4 Implication and future directions

The overall performance of proposed dual stage PRO systems showed the superior results only when optimized for inlet flow rates of draw and feed solutions. Therefore, multi staging can be beneficial for applications where the inlet flow is limited such

as energy storage in remote locations. Impairing the PRO (single or dual stage) as a subsystem with other systems for energy recovery is another choice for improving system efficiency.

Dual stage PRO system will operate superior to single stage PRO with the improvement of membrane technology. Moreover, the striking improvements of SE with the high concentrated draw solution implied that future membranes and spacers need to be tailored to fulfill the requirements of high salinity sources like mechanical stability, salt rejection, scaling resistivity, and fouling resistivity. Hollow fiber membranes can be considered as an alternative solution and need to be developed to meet the new requirements.

Based on the obtained results, some recommendations can be improving the accuracy of the models and polishing the results with more detailed studies. Improvements in the mathematical model can be made by considering membrane fouling and membrane distortion.

Pre-treatment of the inlet solutions is another cause of losses in PRO systems that is neglected in our studies. This issue along with scaling and fouling need to be well studied and controlled in PRO systems to avoid pressure losses and performance drop.

Other sources of the feed and draw solutions can be applied for individual modules to find the best combination of draw and feed solutions in our suggested configurations. Different types of membrane are also applicable for each module and can be studied to find the optimum combination. This study was conducted on the flat sheet membranes and models. However, hollow fiber membranes are promising types of membranes for stand alone systems that need updated models considering the spatial effects in fibers.

Bibliography

[1] O. Ellabban, H. Abu-Rub, and F. Blaabjerg, "Renewable energy resources: Current status, future prospects and their enabling technology," *Renewable and Sustainable Energy Reviews*, vol. 39, pp. 748–764, 2014.

[2] P. A. Owusu and S. Asumadu-Sarkodie, "A review of renewable energy sources, sustainability issues and climate change mitigation," *Cogent Engineering*, vol. 3, no. 1, p. 1167990, 2016.

[3] K. Nijmeijer and S. Metz, "Salinity gradient energy," *Sustainability Science and Engineering*, vol. 2, pp. 95–139, 2010.

[4] B. E. Logan and M. Elimelech, "Membrane-based processes for sustainable power generation using water," *Nature*, vol. 488, no. 7411, p. 313, 2012.

[5] R. Pattle, "Production of electric power by mixing fresh and salt water in the hydroelectric pile," *Nature*, vol. 174, no. 4431, p. 660, 1954.

[6] F. La Mantia, M. Pasta, H. D. Deshazer, B. E. Logan, and Y. Cui, "Batteries for efficient energy extraction from a water salinity difference," *Nano Letters*, vol. 11, no. 4, pp. 1810–1813, 2011.

[7] R. S. Norman, "Water salination: a source of energy," *Science*, vol. 186, no. 4161, pp. 350–352, 1974.

[8] S. Loeb, F. Van Hessen, J. Levi, and M. Ventura, "The osmotic power plant," in *11th Intersociety Energy Conversion Engineering Conference*, pp. 51–57, 1976.

[9] S. Loeb, "Method and apparatus for generating power utilizing pressure-retarded-osmosis," Sept. 16 1975. US Patent 3,906,250.

[10] S. Loeb, "Production of energy from concentrated brines by pressure-retarded osmosis: I. preliminary technical and economic correlations," *Journal of Membrane Science*, vol. 1, pp. 49–63, 1976.

[11] S. Loeb, "Large-scale power production by pressure-retarded osmosis, using river water and sea water passing through spiral modules," *Desalination*, vol. 143, no. 2, pp. 115–122, 2002.

[12] K. Touati and F. Tadeo, "Green energy generation by pressure retarded osmosis: State of the art and technical advancement," *International Journal of Green Energy*, vol. 14, no. 4, pp. 337–360, 2017.

[13] A. Ali, R. A. Tufa, F. Macedonio, E. Curcio, and E. Drioli, "Membrane technology in renewable-energy-driven desalination," *Renewable and Sustainable Energy Reviews*, vol. 81, pp. 1–21, 2018.

[14] A. P. Straub, A. Deshmukh, and M. Elimelech, "Pressure-retarded osmosis for power generation from salinity gradients: is it viable?," *Energy & Environmental Science*, vol. 9, no. 1, pp. 31–48, 2016.

[15] G. O'Toole, L. Jones, C. Coutinho, C. Hayes, M. Napoles, and A. Achilli, "River-to-sea pressure retarded osmosis: Resource utilization in a full-scale facility," *Desalination*, vol. 89, pp. 39–51, 2016.

[16] S. E. Skilhagen, "Osmotic power? A new, renewable energy source," *Desalination and Water Treatment*, vol. 15, no. 1-3, pp. 271–278, 2010.

[17] S. Loeb, "Energy production at the dead sea by pressure-retarded osmosis: challenge or chimera?," *Desalination*, vol. 120, no. 3, pp. 247–262, 1998.

[18] S. Loeb, "One hundred and thirty benign and renewable megawatts from great salt lake? the possibilities of hydroelectric power by pressure-retarded osmosis," *Desalination*, vol. 141, no. 1, pp. 85–91, 2001.

[19] Y. Chen, C. H. Loh, L. Zhang, L. Setiawan, Q. She, W. Fang, X. Hu, and R. Wang, "Module scale-up and performance evaluation of thin film composite hollow fiber membranes for pressure retarded osmosis," *Journal of Membrane Science*, vol. 548, pp. 398–407, 2018.

[20] C. F. Wan, T. Yang, W. Gai, Y. De Lee, and T.-S. Chung, "Thin-film composite hollow fiber membrane with inorganic salt additives for high mechanical strength and high power density for pressure-retarded osmosis," *Journal of Membrane Science*, vol. 555, pp. 388–397, 2018.

[21] R. L. McGinnis, J. R. McCutcheon, and M. Elimelech, "A novel ammonia–carbon dioxide osmotic heat engine for power generation," *Journal of Membrane Science*, vol. 305, no. 1-2, pp. 13–19, 2007.

[22] J. R. McCutcheon, R. L. McGinnis, and M. Elimelech, "A novel ammonia-carbon dioxide forward (direct) osmosis desalination process," *Desalination*, vol. 174, no. 1, pp. 1–11, 2005.

[23] W. He, Y. Wang, and M. Shaheed, "Modelling and simulation of osmotic energy from salinity gradients: A case study from river thames," in *2013 International Conference on Renewable Energy Research and Applications (ICRERA)*, pp. 907–912, IEEE, 2013.

[24] D. D. Anastasio, J. T. Arena, E. A. Cole, and J. R. McCutcheon, "Impact of temperature on power density in closed-loop pressure retarded osmosis for grid storage," *Journal of Membrane Science*, vol. 479, pp. 240–245, 2015.

[25] W. He, Y. Wang, and M. H. Shaheed, "Energy and thermodynamic analysis of power generation using a natural salinity gradient based pressure retarded osmosis process," *Desalination*, vol. 350, pp. 86–94, 2014.

[26] A. Altaee, A. Sharif, G. Zaragoza, and N. Hilal, "Dual stage PRO process for power generation from different feed resources," *Desalination*, vol. 352, pp. 118–127, 2014.

[27] I. E. Agency, *World Energy Outlook 2010*. IEA, 2010.

[28] Food, A. O. of the United Nations, and London, *The State of the Worlds Land and Water Resources for Food and Agriculture (SOLAW)Managing Systems at Risk*. FAO, 2011.

[29] F. Helfer, C. Lemckert, and Y. G. Anissimov, "Osmotic power with pressure retarded osmosis: theory, performance and trends–a review," *Journal of Membrane Science*, vol. 453, pp. 337–358, 2014.

[30] T. Thorsen and T. Holt, "The potential for power production from salinity gradients by pressure retarded osmosis," *Journal of Membrane Science*, vol. 335, no. 1-2, pp. 103–110, 2009.

[31] G. Z. Ramon, B. J. Feinberg, and E. M. Hoek, "Membrane-based production of salinity-gradient power," *Energy & Environmental Science*, vol. 4, no. 11, pp. 4423–4434, 2011.

[32] R. A. Tufa, S. Pawlowski, J. Veerman, K. Bouzek, E. Fontananova, G. di Profio, S. Velizarov, J. G. Crespo, K. Nijmeijer, and E. Curcio, "Progress and prospects in reverse electrodialysis for salinity gradient energy conversion and storage," *Applied energy*, vol. 225, pp. 290–331, 2018.

[33] J. Veerman and D. Vermaas, "Reverse electrodialysis: fundamentals," in *Sustainable Energy from Salinity Gradients*, pp. 77–133, Elsevier, 2016.

[34] W. Finley and E. Pscheidt, "Hydrocratic generator," Nov. 6 2001. US Patent 6,313,545.

[35] A. Jones and W. Finley, "Recent development in salinity gradient power," in *Oceans 2003. Proceedings*, vol. 4, pp. 2284–2287, IEEE, 2003.

[36] D. Brogioli, "Extracting renewable energy from a salinity difference using a capacitor," *Physical Review Letters*, vol. 103, no. 5, p. 058501, 2009.

[37] D. Brogioli, R. Ziano, R. Rica, D. Salerno, and F. Mantegazza, "Capacitive mixing for the extraction of energy from salinity differences: survey of experimental results and electrochemical models," *Journal of Colloid and Interface Science*, vol. 407, pp. 457–466, 2013.

[38] F. La Mantia, D. Brogioli, and M. Pasta, "Capacitive mixing and mixing entropy battery," in *Sustainable Energy from Salinity Gradients*, pp. 181–218, Elsevier, 2016.

[39] X. Zhu, W. Yang, M. C. Hatzell, and B. E. Logan, "Energy recovery from solutions with different salinities based on swelling and shrinking of hydrogels," *Environmental Science & Technology*, vol. 48, no. 12, pp. 7157–7163, 2014.

[40] R. J. Seymour, *Ocean energy recovery: the state of the art*. ASCE Publications, 1992.

[41] V. K. Das and D. Ramaraju, "Estimation of salinity power potential in india," *Mahasagar*, vol. 19, no. 2, pp. 113–118, 1986.

[42] J. van't Hoff, "The function of osmotic pressure in the analogy between solutions and gases," *Proceedings of the Physical Society of London*, vol. 9, no. 1, p. 307, 1887.

[43] H. Struchtrup, *Thermodynamics and Energy Conversion*. Springer, 2014.

[44] I. Alsvik and M.-B. Hägg, "Pressure retarded osmosis and forward osmosis membranes: materials and methods," *Polymers*, vol. 5, no. 1, pp. 303–327, 2013.

[45] T. T. Tran, K. Park, and A. D. Smith, "System scaling approach and thermoeconomic analysis of a pressure retarded osmosis system for power production with hypersaline draw solution: A great salt lake case study," *Energy*, vol. 126, pp. 97–111, 2017.

[46] A. P. Straub, S. Lin, and M. Elimelech, "Module-scale analysis of pressure retarded osmosis: performance limitations and implications for full-scale operation," *Environmental Science & Technology*, vol. 48, no. 20, pp. 12435–12444, 2014.

[47] S. E. Skilhagen, J. E. Dugstad, and R. J. Aaberg, "Osmotic powerpower production based on the osmotic pressure difference between waters with varying salt gradients," *Desalination*, vol. 220, no. 1-3, pp. 476–482, 2008.

[48] A. D. Wilson and F. F. Stewart, "Deriving osmotic pressures of draw solutes used in osmotically driven membrane processes," *Journal of Membrane Science*, vol. 431, pp. 205–211, 2013.

[49] R. W. Baker, *Membrane Technology and Applications*. John Wiley & Sons, Ltd, 2004.

[50] W. A. Phillip, J. S. Yong, and M. Elimelech, "Reverse draw solute permeation in forward osmosis: modeling and experiments," *Environmental Science & Technology*, vol. 44, no. 13, pp. 5170–5176, 2010.

[51] N.-N. Bui, J. T. Arena, and J. R. McCutcheon, "Proper accounting of mass transfer resistances in forward osmosis: Improving the accuracy of model predictions of structural parameter," *Journal of Membrane Science*, vol. 492, pp. 289–302, 2015.

[52] C. H. Tan and H. Y. Ng, "Modified models to predict flux behavior in forward osmosis in consideration of external and internal concentration polarizations," *Journal of Membrane Science*, vol. 324, no. 1-2, pp. 209–219, 2008.

[53] G. D. Mehta and S. Loeb, "Internal polarization in the porous substructure of a semipermeable membrane under pressure-retarded osmosis," *Journal of Membrane Science*, vol. 4, pp. 261–265, 1978.

[54] J. R. McCutcheon and M. Elimelech, "Influence of concentrative and dilutive internal concentration polarization on flux behavior in forward osmosis," *Journal of Membrane Science*, vol. 284, no. 1-2, pp. 237–247, 2006.

[55] S. Chou, R. Wang, L. Shi, Q. She, C. Tang, and A. G. Fane, "Thin-film composite hollow fiber membranes for pressure retarded osmosis (PRO) process with high power density," *Journal of Membrane Science*, vol. 389, pp. 25–33, 2012.

[56] N. Y. Yip and M. Elimelech, "Performance limiting effects in power generation from salinity gradients by pressure retarded osmosis," *Environmental Science & Technology*, vol. 45, no. 23, pp. 10273–10282, 2011.

[57] K. Lee, R. Baker, and H. Lonsdale, "Membranes for power generation by pressure-retarded osmosis," *Journal of Membrane Science*, vol. 8, no. 2, pp. 141–171, 1981.

[58] A. Achilli, T. Y. Cath, and A. E. Childress, "Power generation with pressure retarded osmosis: An experimental and theoretical investigation," *Journal of Membrane Science*, vol. 343, no. 1-2, pp. 42–52, 2009.

[59] N. Y. Yip, A. Tiraferri, W. A. Phillip, J. D. Schiffman, L. A. Hoover, Y. C. Kim, and M. Elimelech, "Thin-film composite pressure retarded osmosis membranes for sustainable power generation from salinity gradients," *Environmental Science & Technology*, vol. 45, no. 10, pp. 4360–4369, 2011.

[60] K. Touati, F. Tadeo, C. Hänel, and T. Schiestel, "Effect of the operating temperature on hydrodynamics and membrane parameters in pressure retarded osmosis," *Desalination and Water Treatment*, vol. 57, no. 23, pp. 10477–10489, 2016.

[61] E. Nagy, "A general, resistance-in-series, salt-and water flux models for forward osmosis and pressure-retarded osmosis for energy generation," *Journal of Membrane Science*, vol. 460.

[62] E. Sivertsen, T. Holt, W. Thelin, and G. Brekke, "Modelling mass transport in hollow fibre membranes used for pressure retarded osmosis," *Journal of Membrane Science*, vol. 417, pp. 69–79, 2012.

[63] Z. L. Cheng and T.-S. Chung, "Mass transport of various membrane configurations in pressure retarded osmosis (PRO)," *Journal of Membrane Science*, vol. 537, pp. 160–176, 2017.

[64] N. Y. Yip and M. Elimelech, "Thermodynamic and energy efficiency analysis of power generation from natural salinity gradients by pressure retarded osmosis," *Environmental Science & Technology*, vol. 46, no. 9, pp. 5230–5239, 2012.

[65] S. Lin, A. P. Straub, and M. Elimelech, "Thermodynamic limits of extractable energy by pressure retarded osmosis," *Energy & Environmental Science*, vol. 7, no. 8, pp. 2706–2714, 2014.

[66] J. W. Post, H. V. Hamelers, and C. J. Buisman, "Energy recovery from controlled mixing salt and fresh water with a reverse electrodialysis system," *Environmental Science & Technology*, vol. 42, no. 15, pp. 5785–5790, 2008.

[67] R. Robinson, "Rh stokes, electrolyte solutions," *Butterworths Scientific Publications, London*, pp. 478–497, 1959.

[68] G. Han, S. Zhang, X. Li, and T.-S. Chung, "Progress in pressure retarded osmosis (PRO) membranes for osmotic power generation," *Progress in Polymer science*, vol. 51, pp. 1–27, 2015.

[69] K. Gerstandt, K.-V. Peinemann, S. E. Skilhagen, T. Thorsen, and T. Holt, "Membrane processes in energy supply for an osmotic power plant," *Desalination*, vol. 224, no. 1-3, pp. 64–70, 2008.

[70] X. Li, S. Zhang, F. Fu, and T.-S. Chung, "Deformation and reinforcement of thin-film composite (TFC) polyamide-imide (PAI) membranes for osmotic power generation," *Journal of Membrane Science*, vol. 434, pp. 204–217, 2013.

[71] G. Han, S. Zhang, X. Li, N. Widjojo, and T.-S. Chung, "Thin film composite forward osmosis membranes based on polydopamine modified polysulfone substrates with enhancements in both water flux and salt rejection," *Chemical Engineering Science*, vol. 80, pp. 219–231, 2012.

[72] G. Han, T.-S. Chung, M. Toriida, and S. Tamai, "Thin-film composite forward osmosis membranes with novel hydrophilic supports for desalination," *Journal of Membrane Science*, vol. 423, pp. 543–555, 2012.

[73] X. Wang, Z. Huang, L. Li, S. Huang, E. H. Yu, and K. Scott, "Energy generation from osmotic pressure difference between the low and high salinity water by pressure retarded osmosis," *Journal of Technology Innovations in Renewable Energy*, vol. 1, no. 2, pp. 122–130, 2013.

[74] S. Zhang and T.-S. Chung, "Minimizing the instant and accumulative effects of salt permeability to sustain ultrahigh osmotic power density," *Environmental Science & Technology*, vol. 47, no. 17, pp. 10085–10092, 2013.

[75] W. Xie, G. M. Geise, B. D. Freeman, H.-S. Lee, G. Byun, and J. E. McGrath, "Polyamide interfacial composite membranes prepared from m-phenylene diamine, trimesoyl chloride and a new disulfonated diamine," *Journal of Membrane Science*, vol. 403, pp. 152–161, 2012.

[76] Y. Cui, X.-Y. Liu, and T.-S. Chung, "Enhanced osmotic energy generation from salinity gradients by modifying thin film composite membranes," *Chemical Engineering Journal*, vol. 242, pp. 195–203, 2014.

[77] S. Zhang, F. Fu, and T.-S. Chung, "Substrate modifications and alcohol treatment on thin film composite membranes for osmotic power," *Chemical Engineering Science*, vol. 87, pp. 40–50, 2013.

[78] I. Farr, U. Bharwada, and T. Gullinkala, "Design and performance of hti's thin film composite membrane for forward osmosis and pressure retarded osmosis applications," *Procedia Engineering*, no. 44, p. 1271, 2012.

[79] J. A. Idarraga-Mora, D. A. Ladner, and S. M. Husson, "Thin-film composite membranes on polyester woven mesh with variable opening size for pressure-retarded osmosis," *Journal of Membrane Science*, vol. 549, pp. 251–259, 2018.

[80] N.-N. Bui and J. R. McCutcheon, "Hydrophilic nanofibers as new supports for thin film composite membranes for engineered osmosis," *Environmental Science & Technology*, vol. 47, no. 3, pp. 1761–1769, 2013.

[81] X. Song, Z. Liu, and D. D. Sun, "Energy recovery from concentrated seawater brine by thin-film nanofiber composite pressure retarded osmosis membranes with high power density," *Energy & Environmental Science*, vol. 6, no. 4, pp. 1199–1210, 2013.

[82] Y. C. Kim and M. Elimelech, "Adverse impact of feed channel spacers on the performance of pressure retarded osmosis," *Environmental Science & Technology*, vol. 46, no. 8, pp. 4673–4681, 2012.

[83] H. Zhang, S. Cheng, and F. Yang, "Use of a spacer to mitigate concentration polarization during forward osmosis process," *Desalination*, vol. 347, pp. 112–119, 2014.

[84] D. Attarde, M. Jain, and S. K. Gupta, "Modeling of a forward osmosis and a pressure-retarded osmosis spiral wound module using the spiegler-kedem model and experimental validation," *Separation and Purification Technology*, vol. 164, pp. 182–197, 2016.

[85] G. Han, S. Zhang, X. Li, and T.-S. Chung, "High performance thin film composite pressure retarded osmosis (PRO) membranes for renewable salinity-gradient energy generation," *Journal of Membrane Science*, vol. 440, pp. 108–121, 2013.

[86] Q. She, X. Jin, and C. Y. Tang, "Osmotic power production from salinity gradient resource by pressure retarded osmosis: effects of operating conditions and reverse solute diffusion," *Journal of Membrane Science*, vol. 401, pp. 262–273, 2012.

[87] Y. C. Kim and M. Elimelech, "Potential of osmotic power generation by pressure retarded osmosis using seawater as feed solution: Analysis and experiments," *Journal of Membrane Science*, vol. 429, pp. 330–337, 2013.

[88] N.-N. Bui and J. R. McCutcheon, "Nanofiber supported thin-film composite membrane for pressure-retarded osmosis," *Environmental Science & Technology*, vol. 48, no. 7, pp. 4129–4136, 2014.

[89] A. P. Straub, N. Y. Yip, and M. Elimelech, "Raising the bar: Increased hydraulic pressure allows unprecedented high power densities in pressure-retarded osmosis," *Environmental Science & Technology Letters*, vol. 1, no. 1, pp. 55–59, 2013.

[90] M. Sharma, P. Mondal, A. Chakraborty, J. Kuttippurath, and M. Purkait, "Effect of different molecular weight polyethylene glycol on flat sheet cellulose acetate membranes for evaluating power density performance in pressure retarded osmosis study," *Journal of Water Process Engineering*, 2018.

[91] J. H. Kim, S. J. Moon, S. H. Park, M. Cook, A. G. Livingston, and Y. M. Lee, "A robust thin film composite membrane incorporating thermally rearranged polymer support for organic solvent nanofiltration and pressure retarded osmosis," *Journal of Membrane Science*, vol. 550, pp. 322–331, 2018.

[92] N. Peng, N. Widjojo, P. Sukitpaneenit, M. M. Teoh, G. G. Lipscomb, T.-S. Chung, and J.-Y. Lai, "Evolution of polymeric hollow fibers as sustainable technologies: past, present, and future," *Progress in Polymer Science*, vol. 37, no. 10, pp. 1401–1424, 2012.

[93] S. Zhang, P. Sukitpaneenit, and T.-S. Chung, "Design of robust hollow fiber membranes with high power density for osmotic energy production," *Chemical Engineering Journal*, vol. 241, pp. 457–465, 2014.

[94] G. Han and T.-S. Chung, "Robust and high performance pressure retarded osmosis hollow fiber membranes for osmotic power generation," *AIChE Journal*, vol. 60, no. 3, pp. 1107–1119, 2014.

[95] Z. L. Cheng, X. Li, Y. Feng, C. F. Wan, and T.-S. Chung, "Tuning water content in polymer dopes to boost the performance of outer-selective thin-film composite (TFC) hollow fiber membranes for osmotic power generation," *Journal of Membrane Science*, vol. 524, pp. 97–107, 2017.

[96] S. Chou, R. Wang, and A. G. Fane, "Robust and high performance hollow fiber membranes for energy harvesting from salinity gradients by pressure retarded osmosis," *Journal of Membrane Science*, vol. 448, pp. 44–54, 2013.

[97] P. G. Ingole, W. Choi, K.-H. Kim, H.-D. Jo, W.-K. Choi, J.-S. Park, and H.-K. Lee, "Preparation, characterization and performance evaluations of thin film composite hollow fiber membrane for energy generation," *Desalination*, vol. 345, pp. 136–145, 2014.

[98] X. Li and T.-S. Chung, "Thin-film composite p84 co-polyimide hollow fiber membranes for osmotic power generation," *Applied Energy*, vol. 114, pp. 600–610, 2014.

[99] M. Zhang, D. Hou, Q. She, and C. Y. Tang, "Gypsum scaling in pressure retarded osmosis: experiments, mechanisms and implications," *Water research*, vol. 48, pp. 387–395, 2014.

[100] C. F. Wan and T.-S. Chung, "Osmotic power generation by pressure retarded osmosis using seawater brine as the draw solution and wastewater retentate as the feed," *Journal of Membrane Science*, vol. 479, pp. 148–158, 2015.

[101] Y. Li, S. Zhao, L. Setiawan, L. Zhang, and R. Wang, "Integral hollow fiber membrane with chemical cross-linking for pressure retarded osmosis operated in the orientation of active layer facing feed solution," *Journal of Membrane Science*, vol. 550, pp. 163–172, 2018.

[102] C. Fritzmann, J. Löwenberg, T. Wintgens, and T. Melin, "State-of-the-art of reverse osmosis desalination," *Desalination*, vol. 216, no. 1-3, pp. 1–76, 2007.

[103] B. Mi and M. Elimelech, "Organic fouling of forward osmosis membranes: fouling reversibility and cleaning without chemical reagents," *Journal of Membrane Science*, vol. 348, no. 1-2, pp. 337–345, 2010.

[104] Y. C. Kim, J. H. Lee, and S.-J. Park, "Novel crossflow membrane cell with asymmetric channels: Design and pressure-retarded osmosis performance test," *Journal of Membrane Science*, vol. 476, pp. 76–86, 2015.

[105] N. Y. Yip and M. Elimelech, "Influence of natural organic matter fouling and osmotic backwash on pressure retarded osmosis energy production from natu-

ral salinity gradients," *Environmental Science & Technology*, vol. 47, no. 21, pp. 12607–12616, 2013.

[106] Q. She, J. Wei, N. Ma, V. Sim, A. G. Fane, R. Wang, and C. Y. Tang, "Fabrication and characterization of fabric-reinforced pressure retarded osmosis membranes for osmotic power harvesting," *Journal of Membrane Science*, vol. 504, pp. 75–88, 2016.

[107] X. Zheng, M. Ernst, and M. Jekel, "Identification and quantification of major organic foulants in treated domestic wastewater affecting filterability in dead-end ultrafiltration," *Water research*, vol. 43, no. 1, pp. 238–244, 2009.

[108] X. Wei, Z. Wang, F. Fan, J. Wang, and S. Wang, "Advanced treatment of a complex pharmaceutical wastewater by nanofiltration: membrane foulant identification and cleaning," *Desalination*, vol. 251, no. 1-3, pp. 167–175, 2010.

[109] X. Li, T. Cai, and T.-S. Chung, "Anti-fouling behavior of hyperbranched polyglycerol-grafted poly (ether sulfone) hollow fiber membranes for osmotic power generation," *Environmental Science & Technology*, vol. 48, no. 16, pp. 9898–9907, 2014.

[110] S. Lim, M. J. Park, S. Phuntsho, A. Mai-Prochnow, A. B. Murphy, D. Seo, and H. Shon, "Dual-layered nanocomposite membrane incorporating graphene oxide and halloysite nanotube for high osmotic power density and fouling resistance," *Journal of Membrane Science*, vol. 564, pp. 382–393, 2018.

[111] B. Díez, G. Amariei, and R. Rosal, "Electrospun composite membranes for fouling and biofouling control," *Industrial & Engineering Chemistry Research*, vol. 57, no. 43, pp. 14561–14570, 2018.

[112] T. Cai, X. Li, C. Wan, and T.-S. Chung, "Zwitterionic polymers grafted poly (ether sulfone) hollow fiber membranes and their antifouling behaviors for osmotic power generation," *Journal of Membrane Science*, vol. 497, pp. 142–152, 2016.

[113] D. Rice, A. C. Barrios, Z. Xiao, A. Bogler, E. Bar-Zeev, and F. Perreault, "Development of anti-biofouling feed spacers to improve performance of reverse osmosis modules," *Water research*, vol. 145, pp. 599–607, 2018.

[114] J. L. Prante, J. A. Ruskowitz, A. E. Childress, and A. Achilli, "RO-PRO desalination: an integrated low-energy approach to seawater desalination," *Applied Energy*, vol. 120, pp. 104–114, 2014.

[115] A. Altaee, "Forward osmosis: potential use in desalination and water reuse," *Journal of Membrane and Separation Technology*, vol. 1, no. 2, pp. 79–93, 2012.

[116] Z. Li, A. Siddiqi, L. D. Anadon, and V. Narayanamurti, "Towards sustainability in water-energy nexus: Ocean energy for seawater desalination," *Renewable and Sustainable Energy Reviews*, vol. 82, pp. 3833–3847, 2018.

[117] K. Saito, M. Irie, S. Zaitsu, H. Sakai, H. Hayashi, and A. Tanioka, "Power generation with salinity gradient by pressure retarded osmosis using concentrated brine from swro system and treated sewage as pure water," *Desalination and Water Treatment*.

[118] M. Kurihara and M. Hanakawa, "Mega-ton water system: Japanese national research and development project on seawater desalination and wastewater reclamation," *Desalination*, vol. 308, pp. 131–137, 2013.

[119] M. Kurihara and H. Takeuchi, "SWRO-PRO system in mega-ton water system for energy reduction and low environmental impact," *Water*, vol. 10, no. 1, p. 48, 2018.

[120] A. Achilli, J. L. Prante, N. T. Hancock, E. B. Maxwell, and A. E. Childress, "Experimental results from RO-PRO: a next generation system for low-energy desalination," *Environmental Science & Technology*, vol. 48, no. 11, pp. 6437–6443, 2014.

[121] W. He, Y. Wang, A. Sharif, and M. H. Shaheed, "Thermodynamic analysis of a stand-alone reverse osmosis desalination system powered by pressure retarded osmosis," *Desalination*, vol. 352, pp. 27–37, 2014.

[122] S. Wang, Q. Zhu, C. He, B. Zhang, Q. Chen, and M. Pan, "Model-based optimization and comparative analysis of open-loop and closed-loop RO-PRO desalination systems," *Desalination*, vol. 446, pp. 83–93, 2018.

[123] S. Lin, N. Y. Yip, T. Y. Cath, C. O. Osuji, and M. Elimelech, "Hybrid pressure retarded osmosis–membrane distillation system for power generation from low-

grade heat: Thermodynamic analysis and energy efficiency," *Environmental Science & Technology*, vol. 48, no. 9, pp. 5306–5313, 2014.

[124] G. Han, J. Zuo, C. Wan, and T.-S. Chung, "Hybrid pressure retarded osmosis–membrane distillation (PRO–MD) process for osmotic power and clean water generation," *Environmental Science: Water Research & Technology*, vol. 1, no. 4, pp. 507–515, 2015.

[125] J.-G. Lee, Y.-D. Kim, S.-M. Shim, B.-G. Im, and W.-S. Kim, "Numerical study of a hybrid multi-stage vacuum membrane distillation and pressure-retarded osmosis system," *Desalination*, vol. 363, pp. 82–91, 2015.

[126] A. Altaee and N. Hilal, "Dual-stage forward osmosis/pressure retarded osmosis process for hypersaline solutions and fracking wastewater treatment," *Desalination*, vol. 350, pp. 79–85, 2014.

[127] Z. L. Cheng, X. Li, and T.-S. Chung, "The forward osmosis-pressure retarded osmosis (FO-PRO) hybrid system: A new process to mitigate membrane fouling for sustainable osmotic power generation," *Journal of Membrane Science*, vol. 559, pp. 63–74, 2018.

[128] D. Bharadwaj, T. M. Fyles, and H. Struchtrup, "Multistage pressure-retarded osmosis," *Journal of Non-Equilibrium Thermodynamics*, vol. 41, no. 4, pp. 327–347, 2016.

[129] W. He, Y. Wang, and M. H. Shaheed, "Enhanced energy generation and membrane performance by two-stage pressure retarded osmosis (PRO)," *Desalination*, vol. 359, pp. 186–199, 2015.

[130] A. Altaee and N. Hilal, "Design optimization of high performance dual stage pressure retarded osmosis," *Desalination*, vol. 355, pp. 217–224, 2015.

[131] A. Altaee, G. Zaragoza, E. Drioli, and J. Zhou, "Evaluation the potential and energy efficiency of dual stage pressure retarded osmosis process," *Applied Energy*, vol. 199, pp. 359–369, 2017.

[132] A. Altaee, J. Zhou, G. Zaragoza, and A. O. Sharif, "Impact of membrane orientation on the energy efficiency of dual stage pressure retarded osmosis," *Journal of Water Process Engineering*, 2018.

[133] A. Altaee, P. Palenzuela, G. Zaragoza, and A. A. AlAnezi, "Single and dual stage closed-loop pressure retarded osmosis for power generation: Feasibility and performance," *Applied energy*, vol. 191, pp. 328–345, 2017.

[134] A. Altaee and N. Hilal, "Dual stage PRO power generation from brackish water brine and wastewater effluent feeds," *Desalination*, vol. 389, pp. 68–77, 2016.

[135] K. Touati, F. Tadeo, and H. Elfil, "Osmotic energy recovery from reverse osmosis using two-stage pressure retarded osmosis," *Energy*, vol. 132, pp. 213–224, 2017.

[136] M. Li, "Optimization of multi-stage hybrid RO-PRO membrane processes at the water–energy nexus," *Chemical Engineering Research and Design*, vol. 137, pp. 1–9, 2018.

[137] S. van der Zwan, I. W. Pothof, B. Blankert, and J. I. Bara, "Feasibility of osmotic power from a hydrodynamic analysis at module and plant scale," *Journal of Membrane Science*, vol. 389, pp. 324–333, 2012.

[138] N. Y. Yip, A. Tiraferri, W. A. Phillip, J. D. Schiffman, and M. Elimelech, "High performance thin-film composite forward osmosis membrane," *Environmental Science & Technology*, vol. 44, no. 10, pp. 3812–3818, 2010.

[139] J. Kim, B. Kim, D. I. Kim, and S. Hong, "Evaluation of apparent membrane performance parameters in pressure retarded osmosis processes under varying draw pressures and with draw solutions containing organics," *Journal of Membrane Science*, vol. 493, pp. 636–644, 2015.

[140] A. Altaee, G. J. Millar, and G. Zaragoza, "Integration and optimization of pressure retarded osmosis with reverse osmosis for power generation and high efficiency desalination," *Energy*, vol. 103, pp. 110–118, 2016.

[141] S. Lee, Y. C. Kim, S.-J. Park, S.-K. Lee, and H.-C. Choi, "Experiment and modeling for performance of a spiral-wound pressure-retarded osmosis membrane module," *Desalination and Water Treatment*, vol. 57, no. 22, pp. 10101–10110, 2016.

[142] Y. Tanaka, M. Yasukawa, S. Goda, H. Sakurai, M. Shibuya, T. Takahashi, M. Kishimoto, M. Higa, and H. Matsuyama, "Experimental and simulation

studies of two types of 5-inch scale hollow fiber membrane modules for pressure-retarded osmosis," *Desalination*, vol. 447, pp. 133–146, 2018.

[143] H. T. Madsen, S. S. Nissen, J. Muff, and E. G. Søgaard, "Pressure retarded osmosis from hypersaline solutions: Investigating commercial fo membranes at high pressures," *Desalination*, vol. 420, pp. 183–190, 2017.

[144] C. Grace, "Static mixing and heat transfer," *Chemical and Process Engineering*, vol. 52, no. 7, p. 57, 1971.

[145] Z. Cao, D. Wiley, and A. Fane, "Cfd simulations of net-type turbulence promoters in a narrow channel," *Journal of Membrane Science*, vol. 185, no. 2, pp. 157–176, 2001.

[146] M. Park and J. H. Kim, "Numerical analysis of spacer impacts on forward osmosis membrane process using concentration polarization index," *Journal of Membrane Science*, vol. 427, pp. 10–20, 2013.

[147] G. Schock and A. Miquel, "Mass transfer and pressure loss in spiral wound modules," *Desalination*, vol. 64, pp. 339–352, 1987.

[148] F. Li, W. Meindersma, A. De Haan, and T. Reith, "Optimization of commercial net spacers in spiral wound membrane modules," *Journal of Membrane Science*, vol. 208, no. 1, pp. 289–302, 2002.

[149] J. Wang, D. S. Dlamini, A. K. Mishra, M. T. M. Pendergast, M. C. Wong, B. B. Mamba, V. Freger, A. R. Verliefde, and E. M. Hoek, "A critical review of transport through osmotic membranes," *Journal of Membrane Science*, vol. 454, pp. 516–537, 2014.

[150] W. He, Y. Wang, I. M. Mujtaba, and M. H. Shaheed, "An evaluation of membrane properties and process characteristics of a scaled-up pressure retarded osmosis (PRO) process," *Desalination*, vol. 378, pp. 1–13, 2016.

[151] L. G. Palacin, F. Tadeo, C. d. Prada, and K. Touati, "Evaluation of the recovery of osmotic energy in desalination plants by using pressure retarded osmosis," *Desalination and Water Treatment*, vol. 51, no. 1-3, pp. 360–365, 2013.

[152] M. H. Sharqawy, S. M. Zubair, *et al.*, "Second law analysis of reverse osmosis desalination plants: An alternative design using pressure retarded osmosis," *Energy*, vol. 36, no. 11, pp. 6617–6626, 2011.

[153] J. R. McCutcheon and M. Elimelech, "Modeling water flux in forward osmosis: implications for improved membrane design," *AIChE journal*, vol. 53, no. 7, pp. 1736–1744, 2007.

[154] Y. Oh, S. Lee, M. Elimelech, S. Lee, and S. Hong, "Effect of hydraulic pressure and membrane orientation on water flux and reverse solute flux in pressure assisted osmosis," *Journal of Membrane Science*, vol. 465, pp. 159–166, 2014.

[155] W. Yang, L. Song, J. Zhao, Y. Chen, and B. Hu, "Numerical analysis of performance of ideal counter-current flow pressure retarded osmosis," *Desalination*, vol. 433, pp. 41–47, 2018.

[156] H. W. Chung, L. D. Banchik, J. Swaminathan, *et al.*, "On the present and future economic viability of stand-alone pressure-retarded osmosis," *Desalination*, vol. 408, pp. 133–144, 2017.

[157] G. M. Geise, H. B. Park, A. C. Sagle, B. D. Freeman, and J. E. McGrath, "Water permeability and water/salt selectivity tradeoff in polymers for desalination," *Journal of Membrane Science*, vol. 369, no. 1-2, pp. 130–138, 2011.

[158] A. Mehta and A. L. Zydney, "Permeability and selectivity analysis for ultrafiltration membranes," *Journal of Membrane Science*, vol. 249, no. 1-2, pp. 245–249, 2005.

[159] H. Zhang and G. M. Geise, "Modeling the water permeability and water/salt selectivity tradeoff in polymer membranes," *Journal of Membrane Science*, vol. 520, pp. 790–800, 2016.